Establishment of Mammalian Cell Lines

for the Production of HIV-1 Virus-like Particles

Von der Naturwissenschaftlichen Fakultät der

Gottfried Wilhelm Leibniz Universität Hannover

zur Erlangung des Grades

Doktorin der Naturwissenschaften (Dr. rer. nat)

genehmigte Dissertation

von

Jamila Franca Rosengarten, M.Sc.

2024

Referent: Prof. Dr. rer. nat. Thomas Scheper

Korreferentin: Prof. Dr. rer. nat. Cornelia Lee-Thedieck

Korreferent: Prof. Dr. phil. nat. Jörn Stitz

Tag der Promotion: 11.10.2023

1. Abstract

Despite decades of research no vaccine against HIV-1 infection has proven sufficiently protective in humans to pass the mandatory market approval requirements. Mosaic HIV-1 antigens were recently utilized in the vaccine clinical trial, MOSAICO (NCT03964415). This trial involved the administration of adenovirus vectors encoding Gag-Pol and Env mosaic proteins together with soluble Env proteins used in the boost. The first part of this thesis aimed at the investigation, whether the mosaic Gag components of the entailed vaccine are capable to form HIV-1 virus-like particles (VLPs) as observed for naturally occurring Gag sequences upon expression in mammalian cells. The findings demonstrated that these mosaic antigens mediate HIV-1 VLP assembly. The mosaic Env protein was also shown to be incorporated on the surface of these VLPs. A remarkable feature of these Env proteins was the exposure of epitopes for the binding of broadly neutralizing antibodies (bNAbs). The induction of such bNAbs in vaccinees is a desired goal in HIV-1 vaccine development. As VLPs are commonly considered highly immunogenic, these results warrant further testing of the produced mosaic HIV-1 VLPs in preclinical studies as boost components in heterologous vaccine regimens.

The second part of this thesis focused on the establishment of a stable HIV-1 VLP producer cell line, which could serve as a tool in optimizing the VLP purification process using a fluorescence-based approach. Gag-GFP HIV-1 VLPs previously facilitated the quantification of VLPs in parallel to the discrimination from cell contaminants such as extracellular vesicles (EVs). This concept was expanded by the introduction of a second reporter protein dTomato harboring a membrane anchor. Resulting VLPs displayed double fluorescent signals while co-released EVs exhibited only red fluorescence. This should allow for the rapid detection, discrimination and quantification of both particle types employing fluorescence detectors. The obtained results provided initial prove of this principle, and thus offer future perspectives for the further development of purification and concentration protocols and methodologies to achieve HIV-1 VLP downstream optimization.

Key words: HIV-1 vaccines, p55-Gag virus-like particles, stable cell line establishment, suspension cells, transposon systems, bi-fluorescent VLPs, EVs

2. Kurzfassung

Die HIV-1 Impfstoffentwicklung hat bis heute keinen Kandidaten für die erforderliche Marktzulassung hervorgebracht. Kürzlich wurde ein Mosaikimpfstoff in der klinischen Studie MOSAICO (NCT03964415) getestet. Darin wurden u.a. adenovirale Vektoren für die Übertragung von Gag-Pol sowie Env Mosaikantigenen genutzt. Im ersten Teil dieser Arbeit wurde untersucht, ob die darin verwendeten Gag Mosaikantigene in der Lage sind sich zu sog. „virus-like particles" (VLPs) zu formieren. Die Beobachtung wird üblicherweise für Gag Proteine gemacht, die von natürlichen Primärsequenzen abgeleitet sind und in humanen Zellen exprimiert werden. Die Ergebnisse zeigen, dass auch die Gag Mosaikantigene in der Lage sind VLPs zu bilden. Darüber hinaus wurde demonstriert, dass das Env Mosaikprotein in der Oberfläche der VLPs inkorporiert wurde. Diese Env Proteine wiesen erstaunliche Eigenschaften auf, da sie Epitope für die Bindung breit neutralisierender Antikörper exponierten. Die Bildung dieser Antikörper im Impfling ist ein erwünschtes Ziel in der HIV-1 Impfstoffentwicklung. Die im Rahmen dieser Arbeit hergestellten Mosaik HIV-1 VLPs stellen daher vielversprechende Impfstoffkandidaten für die nachfolgende Testung in präklinischen Studien dar.

Der zweite Teil dieser Arbeit befasste sich mit der Etablierung einer stabilen HIV-1 VLP Produktionszelllinie als Werkzeug für die Optimierung des VLP Downstream-Prozesses. Fluoreszierende Gag-GFP HIV-1 VLPs wurden bereits für die Quantifizierung von VLPs sowie deren Unterscheidung von ko-sezernierten Kontaminanten wie extrazellulären Vesikeln (EVs) genutzt. Dieses Prinzip wurde um ein zweites Fluoreszenzfusionsprotein, dTomato, das membranständig ist, erweitert. Resultierende VLPs wiesen eine doppelte Fluoreszenz im Unterschied zu EVs mit nur roter Fluoreszenz auf. Dies sollte die schnelle Detektion, Diskriminierung und Quantifizierung beider Partikelklassen in hohem Durchsatz unter Verwendung von Fluoreszenzdetektoren ermöglichen. Die erhaltenen Ergebnisse bestätigen das grundlegende Prinzip und eröffnen daher neue Möglichkeiten für die Entwicklung von Reinigungs- und Konzentrierungsprotokollen und Methoden zur Optimierung des HIV-1 VLP Downstream-Prozesses.

Schlüsselwörter: HIV-1 Vakzine, p55-Gag VLPs, stabile Zelllinienentwicklung, Suspensionszellen, Transposon-Systeme, bi-fluoreszente VLPs, EVs

3.   **Table of Content**

4. List of Abbreviations

2v	bivalent
3v	trivalent
Ad26	adenovirus vector serotype 26
Ad35	adenovirus vector serotype 35
AEX	anion exchange chromatography
AIDS	acquired immunodeficiency syndrome
Alum	aluminum hydroxide suspension
α	alpha
APCs	antigen-presenting cells
app.	approximately
β	beta
bgH	bovine growth hormone
bNAbs	broadly neutralizing antibodies
BP	budding protein
CA	capsid
$CaCl_2$	calcium chloride
CCID50	cell culture infectious dose 50 %
cDNA	copy DNA
CFSN	cell-free supernatants
CHO	chinese hamster ovary
cm	centimeter
CRFs	circulating recombinant forms
CTLs	cytotoxic T lymphocytes
DCs	dendritic cells
° C	degree celsius
DEPC	diethyl pyrocarbonate
DF	diafiltration
dH_2O	distilled water
DNA	deoxyribonucleic acid
dNTP	nucleoside triphosphate
ds	double-stranded
DTT	dithiothreitol
ECFP	enhanced cyan fluorescent protein
EDTA	ethylenediaminetetraaceticacid
ELISA	enzyme-linked immunosorbent assay
Env	envelope
EVs	extracellular vesicles
FDA	food and drug administration
g	microgram
Gag	group specific antigen
gDNA	genomic DNA
GFP	green fluorescent protein
GMP	good manufacturing practice
GOI	gene of interest
gp	glycoprotein

gRNA	genomic ribonucleic acid
h	hour
HA	hemagglutinin
HAART	highly active antiretroviral therapy
HBV	hepatitis b virus
HCPs	host cell proteins
HEK	human embryonic kidney
HEV	hepatitis e virus
HIV	human immunodeficiency virus
HLA	human leukocyte antigen
HPV	human papilloma virus
HRP	horseradish peroxidase
IM	intramuscularly
IN	integrase
INT	intranasal
ITRs	inverted terminal repeats
kb	kilobase
kDa	kilodalton
L	litre
LB	luria broth
LTR	long terminal repeats
μ	micro
m	meter
MA	matrix
mAb	monoclonal antibody
MALS	multiangle light scattering
mg	milligram
$MgCl_2$	magnesium chloride
min	minute
mL	millilitre
$MnCl_2$	manganese(II) chloride
MOPS	3-(N-morpholino)propanesulfonic acid
mos	mosaic
MPER	membrane proximal external region
mRNA	messenger RNA
MVA	modified vaccinia Ankara
MVA-CMDR	modified vaccinia Ankara-Chiang Mai double recombinant
NA	neuraminidase
nAbs	neutralizing antibodies
NAD	nicotinamide adenine dinucleotide
NC	nucleocapsid
ng	nanogram
NHP	non-human primates
nm	nanometer
NNRTIs	non-nucleoside reverse transcriptase inhibitors
NRTIs	nucleoside reverse transcriptase inhibitors
NTA	nanoparticle tracking-analysis
Ø	diameter

OE-PCR	overlap-extension PCR
ORF	open reading frame
p(A)	polyadenylation signal
pAbs	polyclonal antibodies
PBS	phosphate-buffered saline
PCR	polymerae chain reaction
PDGFR β	platelet derived growth factor receptor-beta
PEG	polyethylene glycol
PEI	polyethylenimine
PEP	post-exposure prophylaxis
pfu	plaque forming units
POI	protein of interest
Pol	protease
Pr	precursor
PrEP	pre-exposure prophylaxis
PTM	posttranslational modifications
PVDF	polyvinylidene difluoride
RbCl	rubidium chloride
RNA	ribonucleic acid
rpm	rounds per minute
RT	reverse transcriptase
rTV	replicating competent Tiantan vaccinia vector
SARS	severe acute respiratory syndrome
SB100x	*Sleeping Beauty100X*
SDS-PAGE	sodium dodecyl sulfate-polyacrylamide gel electrophoresis
SEAP	secreted alkaline phosphatase
SEC	size-exclusion chromatography
sec	second
SHIV	simian-human immunodeficiency virus
SIV	simian immunodeficiency virus
SP1	spacer peptide 1
SP2	spacer peptide 2
ss	single-stranded
SU	surface unit
T_A	annealing temperature
TAR	trans-activation response
Tat	trans-activator of transcription
TEM	transmission electron microscopy
TFF	tangential flow filtration
TM	transmembrane unit
tr	truncated
trNGFR	truncated human nerve growth factor receptor
U	unit
URFs	unique recombinant forms
V	voltage
VLP	virus-like particle
vp	viral particle
WPRE	woodchuck hepatitis posttranscriptional regulatory element

5.   Introduction and Aim

Viral pathogens causing diseases in humans pose a threat to global health. The most recent example is the coronavirus pandemic starting in 2019 (COVID-19). COVID-19 not only lead to local temporary health system overload but also to worldwide economic consequences such as the second largest global recession [1]. The comparable rapid development of protective vaccines and following global immunization campaigns substantially affected the pandemic course resulting in millions of lives saved [2].

The basic concept of vaccines is to elicit immunity in the vaccinees against the microbial invader by training their immune system prior to pathogen contact. Since Edward Jenner pioneered this concept, several vaccines against different human pathogens were developed which accounted for the containment of numerous epidemics. Prominent examples are vaccines against the causative agents of Rabies, Cholera and Polio as well as against the Hepatitis viruses, Human Papilloma viruses and Rotaviruses [3]. However, there are some pathogenic viruses, which prove challenging in terms of developing vaccine countermeasures. These are, for example, the Human immunodeficiency virus (HIV), Herpes simplex virus (HSV) or the Middle east respiratory syndrome coronavirus (MERS) [4]. Among them, HIV is not only the most prominent but also the most challenging representative. The unique HIV biology severely hampers the search for a prophylactic vaccine. The major hurdle is the extremely high mutation rate connected to the emergence of virus variants that are capable of evading the host´s immune radar [5,6].

During HIV infection, both arms of the adaptive immunity are triggered. First, the activation of the T cell mediated immunity leads, amongst others, to the expansion of virus-specific cytotoxic T lymphocytes (CTLs), which are essential in the eradication of HIV infected cells. Second, the B cell mediated immunity involves the release of neutralizing antibodies (NAbs) that are crucial to impede virus entry into target cells. The design of preventive HIV vaccines therefore commonly targets those two pillars of the adaptive immunity [7–11].

Prophylactic HIV vaccines were recently tested in human efficacy trials (NCT03964415; NCT03060629) after receiving promising results of 67 % protection against a simian HIV infection in prior non-human primate studies [12–14]. The vaccines comprised adenovirus vectors conferring sequences encoding novel synthetic HIV antigens. These

antigens were designed using *in silico* shuffling of multiple sequence variants of global circulating HIV strains. Resulting so-called "mosaic" HIV antigens are supposed to induce a broader immune response in vaccinees than for example HIV antigens based on a randomly chosen global circulating HIV strain [15]. During pre-clinical studies, it was not investigated, whether mosaic HIV antigens, more specifically the synthetic mosaic Gag variants, facilitate formation of virus-like particles (VLPs). VLP formation is observed for naturally occurring Gag sequences upon expression in mammalian cells [16,17]. As VLPs are known to activate cellular and humoral immune responses [18–22], *in vitro* produced mosaic Gag HIV VLPs could act as vaccine candidates and as a booster component to other vaccine platforms.

Both potential applications would require VLPs of high purity, as impurities can impair efficacy and product safety. This prerequisite can pose a challenge in HIV VLP downstream processing, as VLPs are often in the presence of host cell contaminants with similar physicochemical properties, like extracellular vesicles (EVs). These are often co-secreted by the producer cells during the production of enveloped viruses and HIV VLPs and are difficult to differentiate and separate [23–25].

The aim of this work was directed at several steps in the upstream and downstream process:

- Assessing the functional HIV VLP formation in human cells, mediated by HIV mosaic Gag proteins
- Examining the functional expression of mosaic envelope proteins and proper incorporation into mosaic Gag-formed HIV VLPs
- Detection of broadly neutralization-sensitive epitopes in Mos2S.Env proteins using broadly neutralizing antibodies (bNAbs) in VLP capture assays
- Validating the concept of discriminating between HIV VLPs and EVs by marking HIV VLPs with the green fluorescence protein (GFP) while marking the membrane of both HIV VLPs and extracellular vesicles with dTomato, to simplify analysis and separation in the purification process

6. Theoretical Background

6.1. Retrovirus biology and pathogenesis
6.1.1. Human pathogenic RNA viruses and their epidemic potential

The global fight against human pathogenic RNA viruses poses challenges in the disease control since decades [26,27]. Among the retrovirus family, the genus lentivirus gained infamy since the 1980ies due to the emergence of a novel infectious disease associated with patterns of severe clinical symptoms such as Kaposi's sarcoma, pneumonia and candidiasis [28–30]. However, until 1982 this novel disease had no official name but was rather described by the diseases that were associated with the infection. In the same year, the term "Acquired Immunodeficiency Syndrome" (AIDS) was established, while the disease became increasingly a global health concern. In the following year, the causative agent of AIDS was first isolated and described by research groups around Françoise Barré-Sinoussi and Luc Montagnier and was named Human immunodeficiency virus (HIV) later on [31,32].

Like all RNA viruses, HIV packages genomic ribonucleic acid (gRNA) in the particles. HIV belongs to a unique family of RNA viruses, which are the retroviruses (*Retroviridae*). Retroviruses utilize the enzyme reverse transcriptase to transcribe an intermediate deoxyribonucleic acid (DNA) copy from their RNA genome [33]. This copy is then integrated into the genomic DNA (gDNA) of the infected host cell (Figure 1).

After integration of the viral genetic material into the host cell chromosome, the virus genome is referred to as the provirus. Once a provirus is established, the retroviral infection becomes life-long. The provirus can persist over a long period within the host genome while it remains transcriptionally silent. During this so-called latency, the provirus is able to evade the immune radar. However, and upon stimulation, the transcription and replication cycle of the provirus can be reactivated and the infection is perpetuated. As a result, new virions are released from the infected cell. The term "virion" hereby describes an infectious virus particle, which is present extracellular before infecting yet another host cell [34,35].
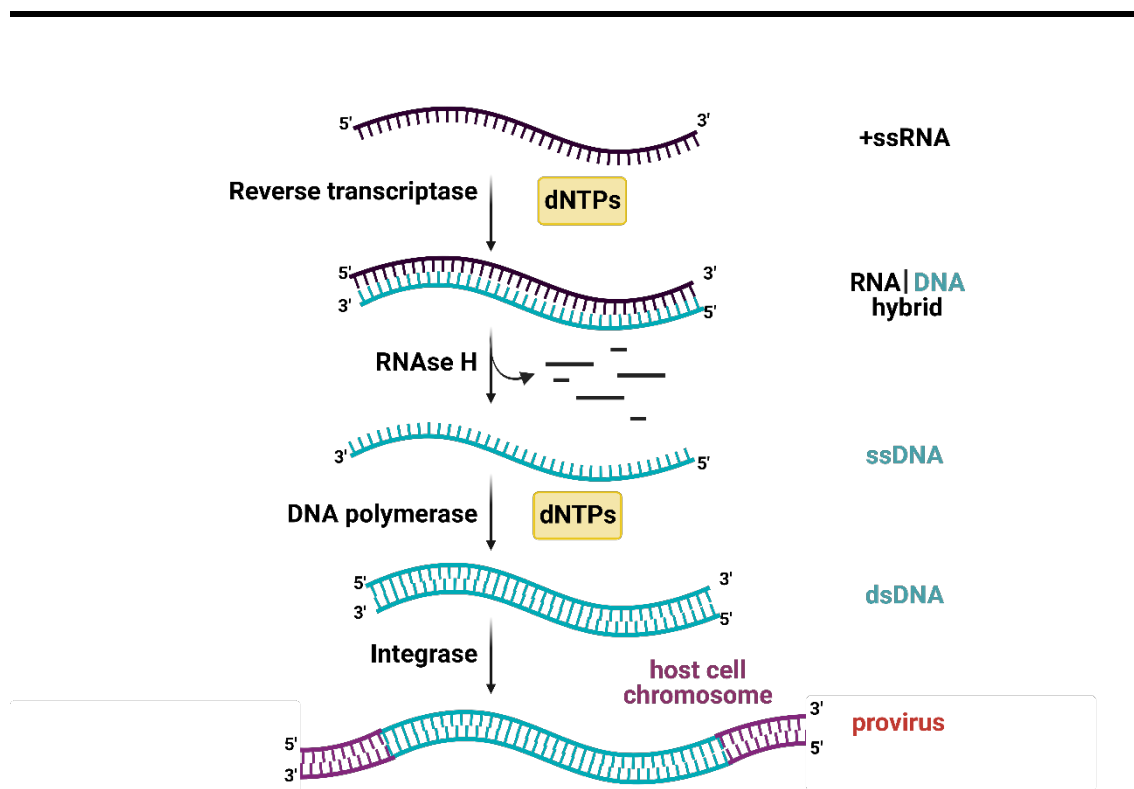
Figure 1. Schematic illustration of the reverse transcription. The reverse transcription of a complementary copy DNA (cDNA) strand from single-stranded (ss) viral RNA is catalyzed by the viral enzyme reverse transcriptase (RT) upon infection of the host cell. The RNA strand of the resulting RNA-DNA hybrid molecule is degraded by activity of the viral RNAse H. The remaining single-stranded cDNA is converted into double-stranded (ds) DNA by DNA dependent DNA polymerase activity. The integration of dsDNA into the host genome is catalyzed by the viral enzyme integrase. The resulting virus genome is termed provirus. This figure was adapted from [36].

6.1.2. The human immunodeficiency virus-1 (HIV-1) exhibits a huge phylogenetic diversity

Like other RNA viruses e.g. the Ebola virus or SARS-related coronaviruses, HIV is a result of zoonotic transmission. Zoonoses is generally defined as an event of disease transmission from vertebrate hosts to humans [37,38]. HIV originates from non-human primates (NHP) including Central African chimpanzees (HIV-1) and West African sooty mangabeys (HIV-2). Before zoonoses, these two parental viruses were described as the Simian immunodeficiency virus SIVcpz and SIVsmm, respectively [39]. HIV-1, which is the most prevalent and well-studied type of Human immunodeficiency viruses, is further divided into the groups M, N, O and P harboring multiple subtypes also referred to as clades (Figure 2). The term HIV-1 in this thesis is interchangeably used with the term HIV, as it is the predominant causative agent for infections.
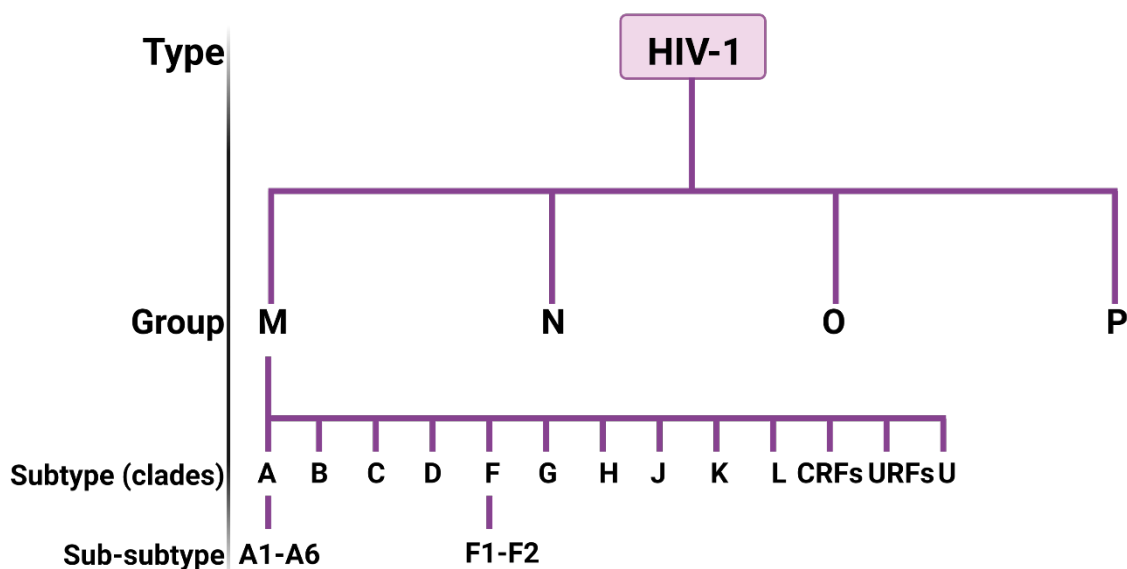
Figure 2. Schematic illustration of the phylogenetic relationships between HIV-1 groups, subtypes, sub-subtypes and recombinant forms. Subtype C accounts for approximately 50 % of all HIV-1 infections worldwide. Recombinant forms comprise circulating recombinant forms (CRFs) and unique recombinant forms (URFs). They emerge from genomic recombination events in viruses, which have previously acquired one gRNA strand from each of two different HIV-1 subtypes or strains. HIV-1 lineages for which virus genome sequences have not yet classified are listed as "U" for "untyped". This figure was adapted from [40].

Of these groups, group M spreads across the entire globe and is responsible for the majority of HIV-1 infections worldwide. Group O infections are less prevalent and mostly found in individuals in Cameroon and neighboring countries in West Central Africa [41]. Infections with group N is even less prevalent and its distribution restricted to Cameroon [42–44]. Lastly, group P, originating from gorillas, is the latest group identified and was only found in a few individuals worldwide [45,46].

The variety of HIV-1 groups is a result of independent cross-species transmission events from Simian immunodeficiency viruses [39]. In addition to cross-species events, the large variety of strains circulating nowadays can also be traced back to the constant molecular evolution of HIV-1. Several factors are commonly considered to contribute to this diversity: I) the error-prone activity of the reverse transcriptase leading to $4.1 \pm 1.7 \times 10^{-3}$ mutations per viral DNA base per cell II) the lack of 3' to 5' exonuclease activity required for correcting transcription errors; III) the high rate of viral replication; (IV) the propensity of genetic recombination events during HIV-1 replication and (V) the pressure of the host immune system that favors the emergence of virus escape mutants [5,40].

6.1.3. The genome structure and morphology of HIV-1 particles

To better understand and characterize the virus after its emergence, scientists isolated the circulating HIV strains and sequenced their genomes [47–49]. The HIV-1 genome was shown to be approximately 9 kb in length and encompasses nine genes encoding 15 mature viral proteins [50]. These genes are flanked by long terminal repeats (LTRs) at the 5' and 3' end both of the viral genomic RNA (gRNA) strand and of the provirus (Figure 3).
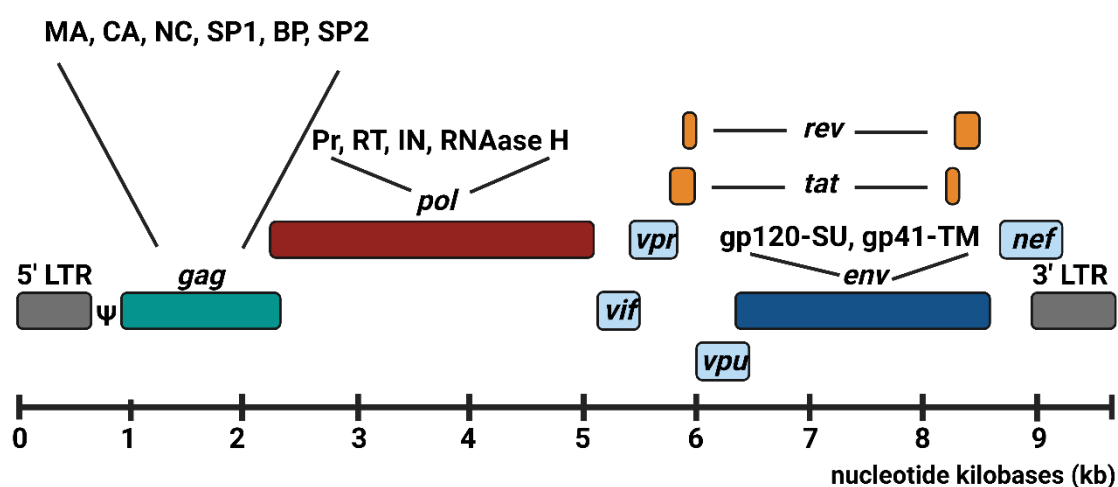
Figure 3. Schematic overview of the HIV-1 genomic organization. The dimeric gRNA is ~9 kb long and flanked by the 5' and 3' long terminal repeats (LTRs) required for transcription initiation and termination. *Gag* encodes the proteins matrix (MA), capsid (CA) and nucleocapsid (NC) that form the viral core as well as the spacer peptide 1 (SP1), budding protein (BP) and spacer peptide 2 (SP2). *Pol* codes for the viral enzymes protease (PR), reverse transcriptase (RT), integrase (IN) and RNAse H playing essential roles in the viral replication. *Env* encodes the envelope (Env) glycoprotein (gp) 160 precursor (gp160-Pr), which is cleaved into the mature gp120-surface unit (SU) and gp41-transmembrane unit (TM), respectively. *Vif*, *vpr*, *vpu*, and *nef* code for the accessory proteins, which provide for efficient replication by acting against cellular restriction factors. *Tat* and *rev* encode regulatory proteins, which are essential for viral replication as well. This figure was adapted from [34,51].

The 5' LTR harbors the promotor necessary for transcription initiation of the viral genes, while the 3' LTR includes the poly(A) sequence required for transcription termination [34]. The packaging signal Psi (ψ) is located downstream of the 5' LTR. It mediates the incorporation of viral gRNA into nascent virus particles [52]. Of the nine genes, three are the structural genes, namely *gag*, *pol* and *env*. The *gag* gene encodes the p55-group specific antigen (Gag) precursor protein, which is further processed to the matrix (MA), capsid (CA), nucleocapsid (NC), budding protein (BP) and two spacer

peptides, SP1 and SP2 (Figure 4). The cleavage of the p55-Gag precursor protein to its subunit domains is mediated by the viral protease encoded by the *pol* gene [53].
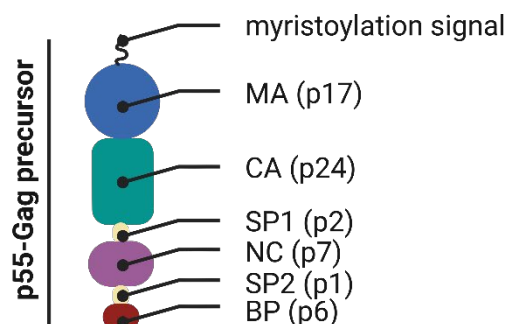
Figure 4. Schematic illustration of the p55-Gag precursor polyprotein and its subunit domains.

The structural proteins MA, CA and NC form the viral core (Figure 5). MA is an N-terminal myristoylated domain crucial for directing p55-Gag precursor proteins to the plasma membrane and assembly of the nascent particle [54]. CA contains a multimerization domain facilitating the formation of the characteristic conical capsid in a mature particle comprising both, the viral enzymes and two RNA genomes. NC is a domain fulfilling multiple functions – amongst them the structural support of Gag-Gag interactions during formation of immature particles as well as the binding and condensing of the gRNA during replication. Another subunit after processing is BP, which unlike MA, CA and NC, is not involved in the structural rearrangement of the maturing particle. Instead, it appears to be crucial to enable an efficient budding process as truncations of the BP domain or amino acid changes were demonstrated to drastically impede particle budding from the plasma membrane. The remaining spacer peptides SP1 and SP2 play a role in the assembly of CA during virus maturation and in the incorporation of Gag and Gag-Pol polyproteins into nascent particles [55–58].

The second major gene is the *pol* gene, which is expressed as Gag-Pol precursor polyprotein and further proteolytically processed into the viral enzymes protease (PR), reverse transcriptase (RT), integrase (IN) and RNase H [59]. All of them play essential roles within the retroviral life cycle. The third and final major gene, *env*, encodes the envelope (Env) glycoprotein (gp) 160 precursor (gp160-Pr), which predominantly oligomerizes into trimers. Further proteolytic processing of each monomer by furin or

furin-like proteases results in the generation of two subunits, namely gp120-SU (surface unit) and gp41-TM (transmembrane-unit), respectively (Figure 5) [60–63].
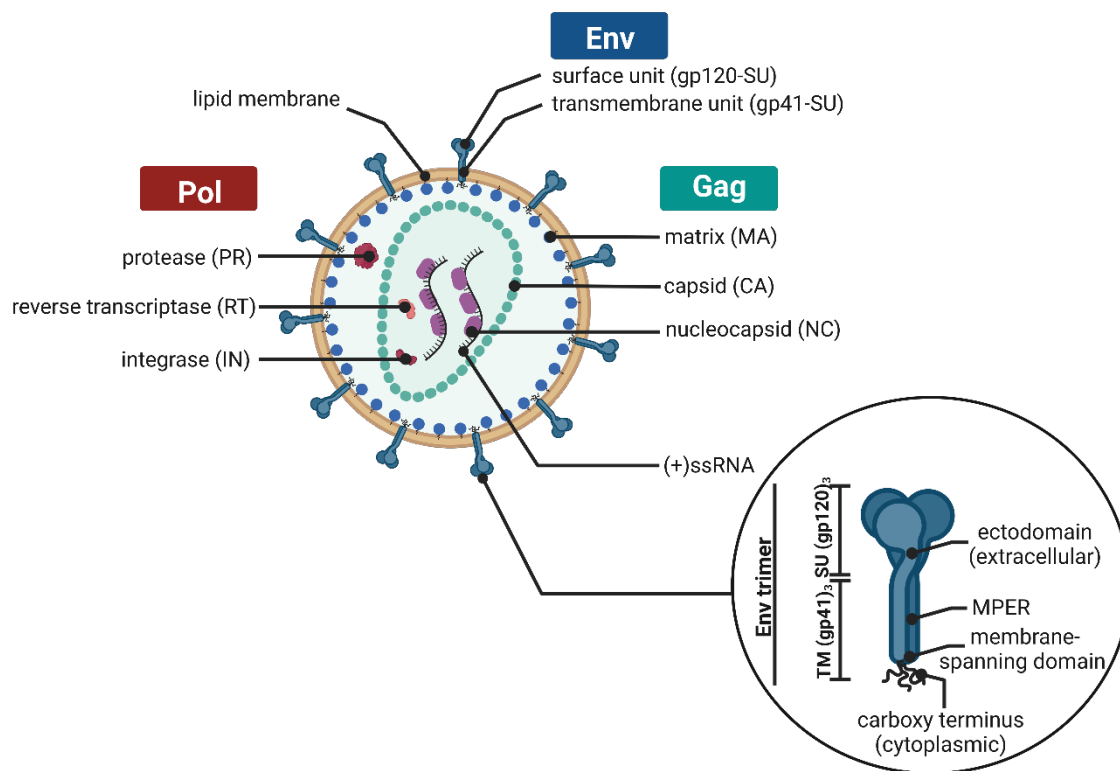
Figure 5. Simplified structure of the HIV-1 virion and one Env trimer. The membrane proximal external region (MPER) of HIV-1 gp41 is located in the extracellular space [64]. This figure was adapted from [34,65,66].

The remaining genes of HIV-1 code for the accessory proteins (Vif, Vpr, Vpu/Vpx, Nef), which play a role in acting against cellular restriction factors to provide for efficient replication, and the regulatory proteins (Tat, Rev), which are essential for viral replication as well [34].

The next subchapter provides a more detailed description of the role of aforementioned viral proteins and their specific functions in the HIV replication cycle.

6.1.4.   The HIV-1 life cycle

The retrovirus life cycle begins with the invasion of infectious virions into the host cell. HIV in particular targets human immune cells which are primarily CD4+ T cells, macrophages and dendritic cells. The virion attachment to the host cell is mediated by the binding of gp120-SU of the Env trimer to the primary CD4+ receptor as well as to the co-receptors CCR5 and CXCR4, respectively (Figure 6, step 1). This binding event induces

conformational changes in the Env trimer initiating the gp41-mediated fusion of the virion with the host cell membrane (Figure 6, step 2) [67,68]. Following successful membrane fusion, the capsid is released into the cytoplasm of the host cell further trafficking to the cell nucleus. Upon nuclear import of the capsid (Figure 6, step 3), it partially uncoats and reverse transcription from viral gRNA catalyzed by the viral reverse transcriptase is completed (Figure 6, step 4). In parallel, RNAase H catalyzes the hydrolysis of viral gRNA after a copy of deoxyribonucleic acid (cDNA) has been synthesized. The consecutive integration of synthesized cDNA into the host cell genome is mediated by the viral integrase resulting in the generation of a provirus (Figure 6, step 5). After integration of the provirus two events can take place. The virus either enters latency in non-activated or naïve infected CD4+ and memory T cells, or the production process of new viruses is initiated. During latency, the small pool of CD4+ and memory T cells harboring proviruses is described as the main virus reservoir [34,69–77].
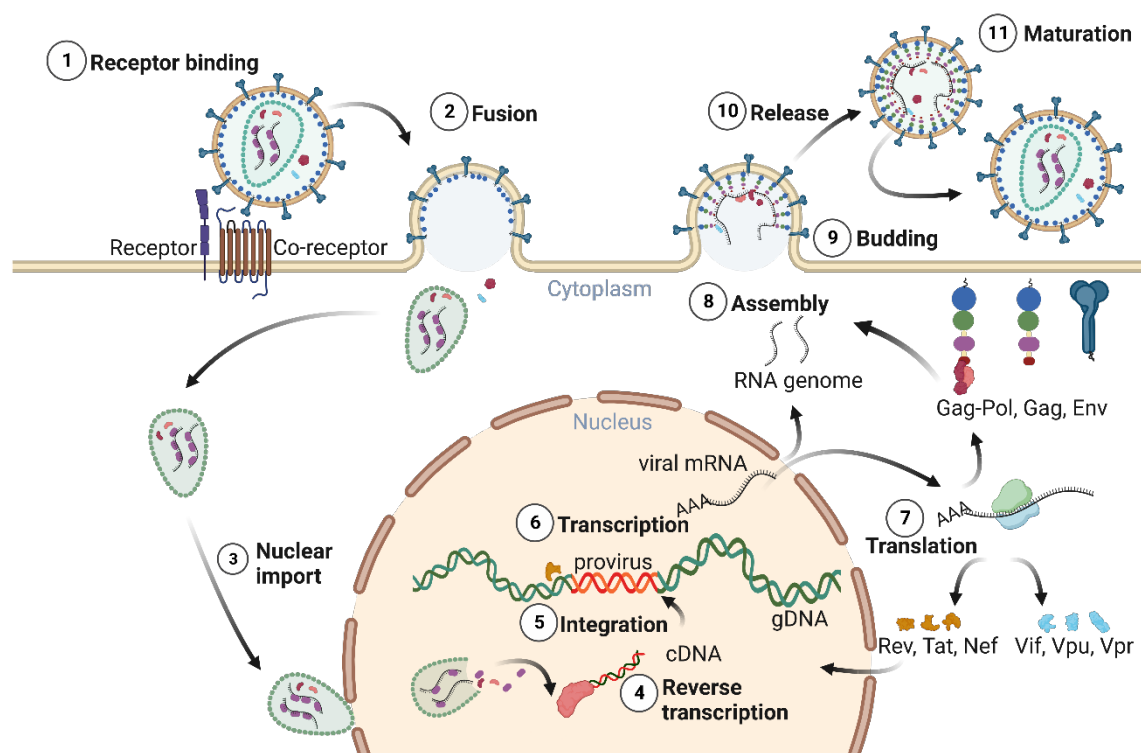
Figure 6. Schematic illustration of the HIV-1 life cycle. Major steps of the replication cycle: Virion attachment to host cell receptors (step 1), fusion with the host cell membrane (step 2), import of the viral capsid into the cell nucleus (step 3), reverse transcription from viral RNA(step 4), genome integration of reverse transcribed cDNA (step 5), transcription of the provirus genome (step 6), translation of viral proteins (step 7), assembly of the nascent HIV-1 particle (step 8), budding from the cell membrane (step 9), release of immature virions (step 10) and maturation (step 11). This figure was adapted from [34,65,78].

Upon binding to the trans-activation response (TAR) element in the viral promotor of the provirus, the accessory protein Tat (trans-activator of transcription) starts the transcription process, which is further conducted using the host cell machinery (Figure 6, step 6). The resulting viral messenger RNAs (mRNAs) undergo a complex splicing process after which they are exported for the subsequent translation in the cell cytoplasm (Figure 6, step 7) [79,80]. The hereby generated gp160 precursor polyproteins are trafficked to the rough endoplasmic reticulum for posttranslational modifications (PTM), which account for up to 50 % of the molecular mass in gp160-Pr [81]. Gp160-Pr proteins further oligomerize, predominantly into trimers $(gp160)_3$, which pass through the Golgi apparatus where further processing by furin or furin-like proteases occurs. The proteolytic processing of gp160-Pr results in the formation of heterotrimers consisting of three mature gp120 surface subunits (gp120-SU) as well as three gp41 transmembrane (gp41-TM) subunits (Figure 5). Non-covalent interactions stabilize both subunits in the heterotrimer $(gp120/gp41)_3$ to form the Env spike on the cell surface [60,63]. The correct processing into Env spikes in this step is a major prerequisite for the subsequent virion infectivity [82]. After translation of immature p55-Gag precursor proteins, two viral gRNA molecules associate to the NC domain of p55-Gag. During this assembly, the myristoylation signal present at the N-terminus of p55-Gag precursor proteins anchors the p55-Gag:gRNA complex in the host cell membrane. P55-Gag precursor proteins further orchestrate the p55-Gag:gRNA complex together with Gag-Pol precursor proteins, Env proteins and accessory proteins to the budding site (Figure 6, step 8) [54,83]. Immature HIV particles then bud from the host cell membrane and are subsequently released into the extracellular space (Figure 6, step 9 and 10). The budding presumably occurs at so-called lipid rafts, which are small lipid-enriched domains in the membrane. The membrane of HIV particles was reported to reveal a strikingly similarity to that proposed for such lipid rafts and frequently comprises sphingomyelin, dihydrosphingomyelin, plasmalogen plasmenylethanolamine, cholesterol and phosphatidylserine [84]. During maturation, p55-Gag and the Gag-Pol precursor proteins undergo extensive proteolytic cleavage catalyzed by the viral protease PR. This leads to the liberation of the mature subunits MA, CA, and NC as well as the viral enzymes PR, RT, IN and RNAase H in the newly formed HIV-1 virion (Figure 6, step 11) [55,56,65].

6.1.5. Disease transmission and pathology

The transmission of HIV-1 among humans can take several routes. Between those routes, the exposure to infectious virions through penetration of mucosal surfaces during sexual contact represents by far the most frequent, while percutaneous transmission among injection drug users plays a subordinate role [85]. Vulnerable groups with a high risk for acquiring HIV infection are therefore men having male sexual contacts (61 %), persons with heterosexual contacts (28 %), injection drug users (8 %) and male injection drug users having male sexual contacts (3 %) [86].

The infection begins with the eclipse phase, in which infection of the first cells takes place and a viral reservoir is established (Figure 7).
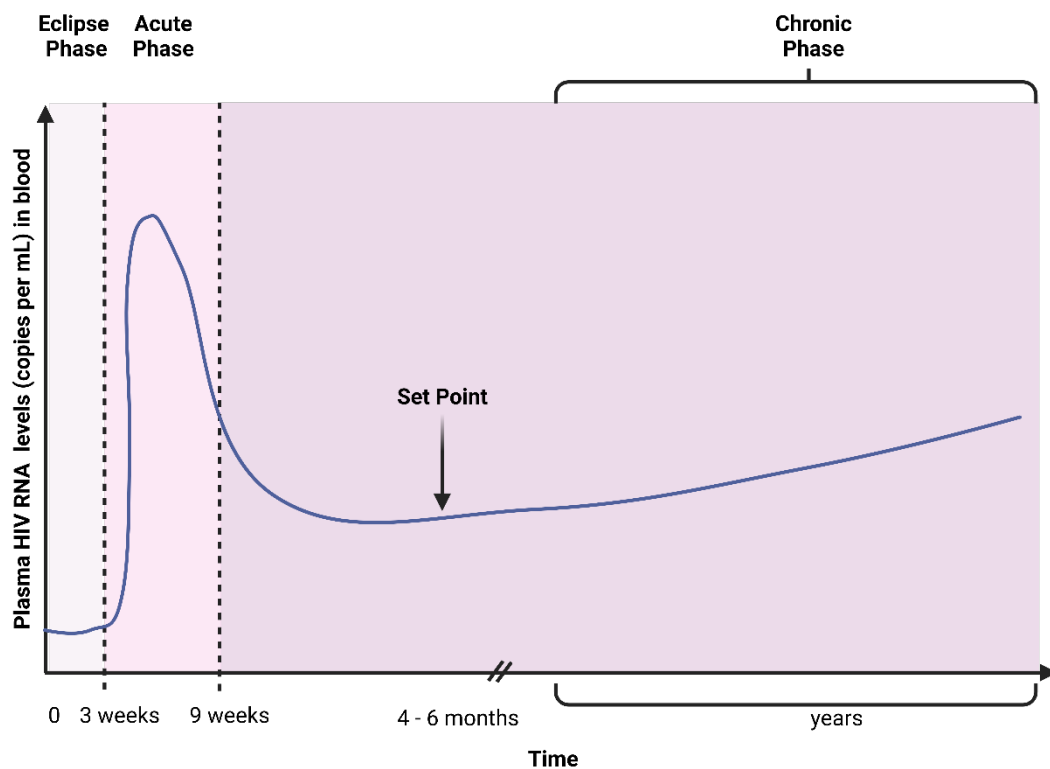
Figure 7. Illustration of the different clinical stages of HIV infection. After initial infection of the first cells in the eclipse phase, HIV spreads through the lymphoid system. The following acute phase can be characterized by flu-like symptoms or is nearly asymptomatic while the viral plasma level peaks at this time. After app. 9 weeks the viral plasma level decreases and the chronic phase together with an individual viral load (set point) is established. The chronic phase can take years until destruction of CD4+ T cells lead to immunodeficiency and chronic inflammation. This figure was adapted from [87].

The acute phase of the infection taking place approximately three to nine weeks after the primary infection, begins either with flu-like symptoms or is nearly asymptomatic, while the viral plasma level peaks at this time. Later, the viral plasma level declines until

reaching a viral set point. This is when the infection becomes chronic and an individual stable viral load (HIV RNA) can be detected in the infected person. The chronic phase can take years and is accompanied with a progressive loss of CD4+ T cells from initial 500 to 1200 cells per µL blood in healthy adults to a low count of less than 100 cells per µL blood [34,87,88]. Untreated HIV infection results in AIDS-defining diseases and a lethal outcome roughly 10 years post infection. These AIDS-related deaths are no direct consequence of the virus infection but instead mostly caused by the acquisition of opportunistic infections such as *Toxoplasma gondii* resulting in toxoplasmosis, *Pneumocystis jirovecii* leading to pneumonia and human herpesvirus 8 causing Kaposi's sarcoma [28–30,89].

6.2.   Immune responses to HIV-1 and implications for vaccine design
6.2.1.   The interplay between HIV-1 and the immune system

As a response to the lymphatic dissemination of viruses within the eclipse phase, the immune system is activated. The activation initiates a complex interplay between the cell mediated (T cell) and humoral (B cell) immune response. As part of the cell mediated response, an increased number of cytotoxic T lymphocytes (CTLs) eradicate infected cells through recognition of viral epitopes exposed on the surface of infected cells by human leukocyte antigen (HLA) class I molecules. In addition, T cell mediated immunity is supported by CD4+ T cells recognizing viral epitopes via HLA class II molecules displayed on antigen-presenting cells (APCs). These antigen-presenting cells acquire viral epitopes either via phagocytosis or by receptor-mediated endocytosis. Following activation of macrophages leads to the subsequent release of cytokines together with chemokines, which orchestrate further immune responses [90]. HIV induced CTL responses are mainly directed against Gag proteins and have been reported to correlate with decelerated disease progression [9,91]. The exceptional ability for disease control can be only found in less than 1 % of HIV infected individuals. These individuals are described as "elite controllers" [92].

In parallel to the induced T cell mediated immunity, the activation of B cells takes place, which in turn start the production of antibodies mainly directed against Env. The Env trimer can transition between three distinct prefusion conformations associated with the sensitivity of a virion to antibody neutralization [93]. Most of the Env antibodies

generated upon HIV infection target sites (epitopes) in gp120 and gp41 which are easily accessible on immature Env precursors but usually not exposed on the mature Env trimer. Those sites are considered immunodominant sites, as they elicit the vast majority of Env-specific antibodies (Figure 8).
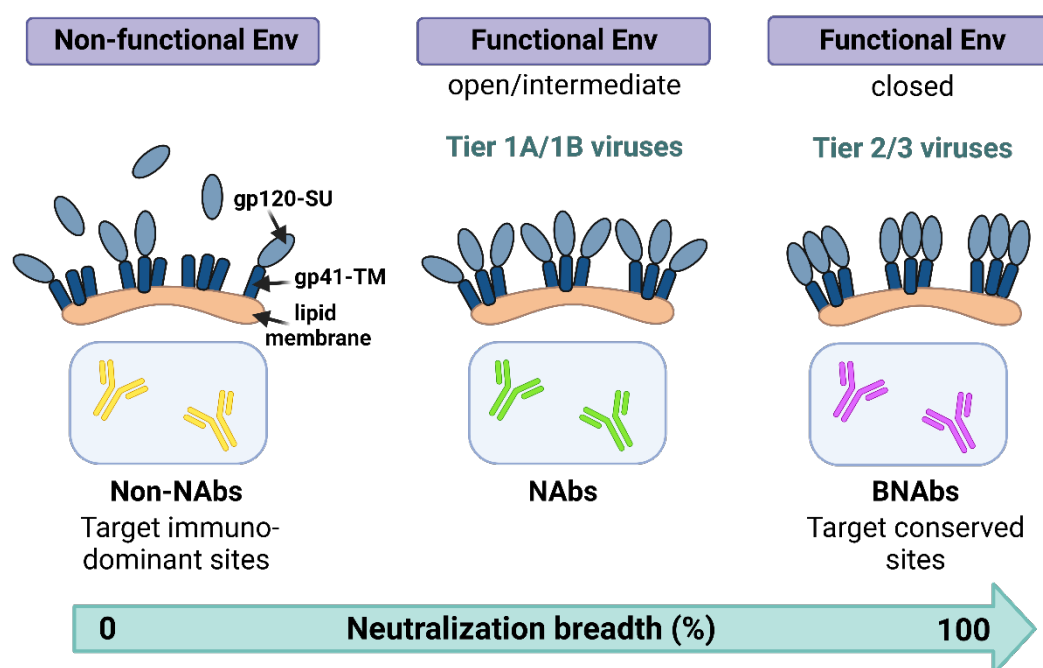
Figure 8. Correlation between the neutralization breadth of antibodies and the ability to target Env trimers. Tier 1A, tier 1B and tier 2/3 viruses have a predominantly open, intermediate and closed Env trimer conformation respectively. Viruses (tier 1A/1B) sensitive to neutralization exhibit a predominantly open/intermediate conformation while viruses more resistant to neutralization have a higher proportion of Env trimers in the closed conformation. Consequently, Env trimers in the closed conformation would likely elicit broadly neutralizing antibodies (bNAbs) with broader neutralization capacity (breadth) while Env trimers in the open/intermediate conformation would rather induce the production of neutralizing antibodies (NAbs) with lower neutralization breadth. Non-functional Env trimers would therefore elicit non-NAbs. This figure was adapted from [94].

The elicited antibodies can be present in high abundance, however do not exhibit features for binding the functional Env trimer, and thus do not mediate virus neutralization [95]. In contrast to these so-called non-neutralizing antibodies (non-NAbs), neutralizing antibodies (NAbs) target mostly cognate epitopes in the conformational open or intermediate state of functional Env trimers. However, NAbs typically reveal limited neutralization breadth. This is sufficient to neutralize tier 1A and tier 1B HI-viruses – specific strains which are most sensitive to neutralization. In comparison, broadly neutralizing antibodies (bNAbs) exhibit a remarkable neutralization breadth including difficult to neutralize tier 2 and tier 3 HI-viruses by targeting predominantly conserved

epitopes in the closed state of functional Env trimers [94]. In addition, some of the most potent bNAbs can penetrate the dense glycan shield of the Env trimer (25 potential N-linked glycosylation sites per gp120) that usually impedes antibody recognition [96]. BNAbs are rare and could thus far only be isolated from just a few sera of chronicle HIV infected individuals after 2-4 years post initial infection. The long period to develop such antibodies results from the constant selection pressure in the presence of a mutating virus. A high viral diversity and divergence in infected individuals is assumed to contribute to the emergence of bNAbs as well [97–99]. Still, while bNAbs are rarely induced in HIV infected individuals, a vaccination induced bNAb response in vaccinees, to neutralize tier-2 viruses dominating human transmissions, is commonly referred to as the ultimate goal and at least one important correlate of protection against infection and disease progression [8,98,100].

Despite the combined effort of the T cell and B cell response, the immune system is unable to fully eradicate the virus, leading to a lethal outcome in the majority of infected individuals. Therefore, possibilities for additional treatment were already investigated in the early phases of the global HIV epidemic.

6.2.2.   HIV-1 treatment and prevention

In the beginning of the HIV/AIDS epidemic, treatment was limited to the administration of the first approved antiretroviral drug zidovudine (Retrovir) in 1987, whereas substantial progress was made in the following decades [101,102]. This progress was made possible by the approval of further state-of-the-art drugs targeting and inhibiting different steps of the retroviral life cycle (Figure 9) [103,104]. Today, 25 different HIV medicines have received market approval by the US Food and Drug Administration (FDA) [102]. These drugs are administered in a stringent life-long treatment regimen and in a combination of three or four antiviral compounds in order to reduce the risk for emerging drug resistant virus variants frequently observed after monotherapy [105–107]. Today HIV-infected individuals receiving highly active antiretroviral therapy (HAART) significantly benefit from improved long-term prognosis. In addition HIV infection has become a manageable chronic disease [104]. Such antiretroviral drugs impede HIV replication, suppressing viral load in the infected patient to a steadily low level and preventing the progressive loss of CD4+ T cells. As a further result, HIV transmission

can be reduced by 93 % in a relationship between an HIV-negative and -positive partner, who initiated HAART shortly after diagnosis [108].
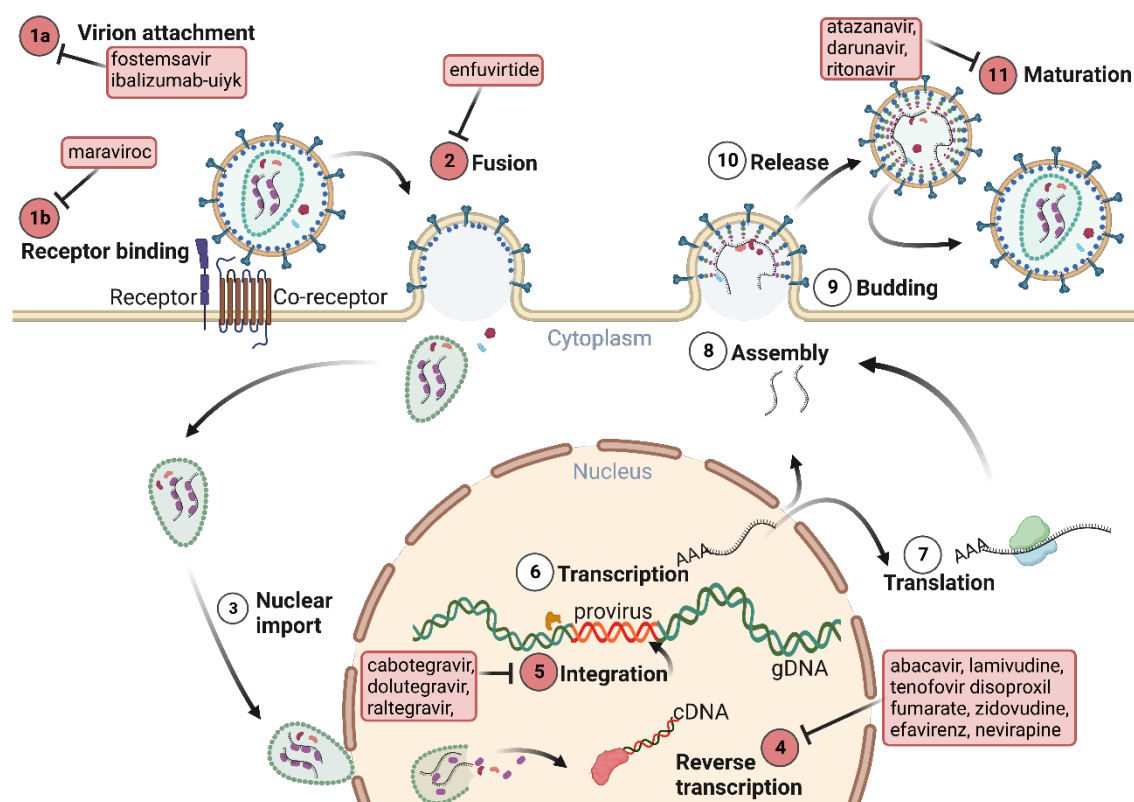
Figure 9. Steps of the HIV-1 lifecycle representing targets for antiretroviral drugs. Some examples for FDA-approved drugs are given in the red squares [102]. Attachment and post-attachment inhibitors prevent HIV-1 virions from entering the host cell (step 1a and 1b). Fusion inhibitors prevent HIV-1 virions from entry by inhibiting gp41-mediated fusion with the host cell membrane (step 2). Nucleoside reverse transcriptase inhibitors (NRTIs) and non-nucleoside reverse transcriptase inhibitors (NNRTIs) prevent the reverse transcription of cDNA from viral gRNA in the invading virion (step 4). Integration inhibitors block the viral enzyme integrase which is required for insertion of the cDNA into the host cell chromosome (step 5). Protease inhibitors prevent immature virions to become infective due to inhibition of the viral protease (step 11).

In addition, individuals living with a high risk for acquiring HIV infection have the possibility to receive preventive measures in the form of a pre-exposure prophylaxis (PrEP) [109]. In 2021, the FDA approved the antiretroviral drug "cabotegravir extended-release (ER) injectable suspension" under the trade name Apretude™, which is assumed to largely improve life quality among individuals taking PrEP. Unlike daily oral PrEP, Apretude™ is long-acting and injectable reducing the administration to six times per year [110]. In case of a possible exposure to HIV after occupational contact (e.g. blood) or non-occupational contact (e.g. needle stitch, oral or unprotected sex), post-exposure prophylaxis (PEP) is used as an emergency measure. However, PEP should be taken

within the first 72 h after the possible exposure to reduce the transmission risk effectively [111].

While the health quality of infected individuals is significantly improved and the timeframe to lethal outcome is prolonged, antiretroviral drugs still do not contribute to the full eradication of the virus and to a complete recovery of the life quality prior to infection. Infected individuals will need life-long antiretroviral treatment and continuous access to respective medication to avoid a rebound of viral load upon HAART interruption [112].

6.2.3. Hurdles in HIV-1 vaccine development

Despite the advances, a quarter of HIV infected individuals worldwide still has no access to antiretroviral therapy in 2021 [113]. An alternative and financially more sustainable solution for HIV prevention, such as a prophylactic vaccine conferring immunity, is still not available. Coping with the broad genetic diversity of HIV remains the major challenge in developing a globally effective vaccine. Immune escape variants and the ability of HIV to establish latent infection, hamper the efficient eradication of disseminated viruses and viral reservoirs by the immune system and HAART [6]. One of the major obstacles is the mutation rate of *env* – the highest among all HIV genes. As a consequence, the unparalleled variability of Env primary sequences and changes in the Env conformation masking sites for antibody binding are observed [114,115]. At the same time Env is considered as the main target to elicit neutralizing antibody responses [116,117]. These obstacles are a primary reason why the development of a protective HIV-1 vaccine still represents an enormous scientific challenge.

6.2.4. HIV-1 vaccine clinical trials

As summarized in chapter 5.2.1, the cellular and humoral arms of the adaptive immune system work in concert to reach protective immunity against pathogens. One pillar is the elicitation of a robust T cell response early after infection, which is considered necessary to prevent the establishment of latent HIV reservoirs. As the T cell response alone is unable to prevent the virion entry into the host cells, a second pillar is the activation of a B cell mediated immunity to generate broadly neutralizing antibodies directed against Env proteins from diverse HIV-1 clades. Triggering both pillars of the immune response

is therefore the overarching goal of HIV vaccine design. The current chapter focuses on some past and ongoing HIV-1 vaccine clinical trials, which either show promising results or utilize a novel vaccination platform.

The most frequently investigated vaccination platforms for HIV vaccine design are viral vectors, DNA vectors, protein subunits and lately mRNAs (Figure 10). All of them have in common, that they aim to produce HIV proteins, commonly referred to as antigens, in the vaccinee to be recognized as foreign and targeted by the immune system.
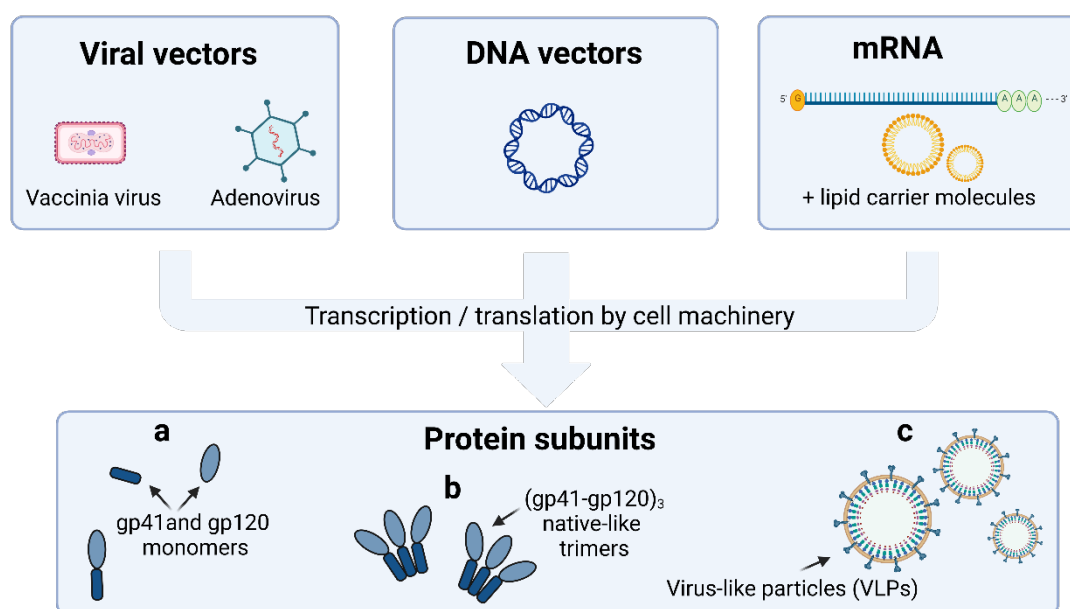
Figure 10. Overview of the most prominent HIV-1 vaccination platforms and lately upcoming mRNA based HIV-1 vaccines. Recombinant viral vectors, DNA vectors and mRNAs are typically utilized for the initial vaccination (prime) followed by a boost vaccination after some weeks or months. Protein subunit vaccines include monomeric Env proteins, native-like Env trimers and virus-like particles (VLPs) most closely resembling the parental virus morphology. Protein subunit vaccines frequently serve as boost components. The combination of two different platforms in a regimen is referred to as heterologous prime-boost vaccination [118].

Viral vector platforms utilize genetically modified replication-incompetent viruses performing single-round infections and effectively transducing the genetic information necessary for antigen production [119,120]. DNA vectors carry the genetic information on a plasmid instead [121] while lately upcoming mRNA based platforms entail the genetic information on transcripts which can be directly translated by the cell machinery

without prior transcription of DNA [122]. Protein subunit platforms directly introduce the respective HIV antigen upon administration and opposed to the prior platforms they are not used independently but are mostly used for boosting immune responses in combination with vector based vaccines. These protein subunits can be administered as independent and soluble Env derived monomers, as stabilized soluble Env trimers or as a whole assembled virus-like particle with Env proteins incorporated into the membrane, most closely resembling the original virus (Figure 10 a-c) [123–125].

Numerous HIV vaccine clinical trials employing a variety of these platforms were undertaken in the last decades. A comprehensive overview of past and ongoing trials of the last 13 years, sorted by their vaccination approach, is presented in chapter 9.1.

Of all HIV vaccine clinical trials conducted so far, RV144 (NCT00223080) carried out in Thailand between 2003 and 2009, is the sole trial showing a modest efficacy of 31.2 %. Despite the modest efficacy, this trial indicated a breakthrough and raised expectations towards a timely development of a protective HIV vaccine. Participants of this vaccine regimen received intramuscular injections of attenuated, non-replicating canarypox vectors (ALVAC-HIV vCP1521) expressing Gag, Protease and membrane-anchored Env together with an aluminum adjuvant. Booster injections were also administered and contained a soluble recombinant gp120-SU subunit vaccine of HIV subgroups B and E (AIDSVAX® B/E) [126]. The vaccine regimen was well tolerated and proved safe [127]. The analysis of the effect of vaccination revealed a specific CD4 T cell response and a neutralizing antibody response directed against the V1/V2-loop of the gp120 subunit. Both were assumed to correlate with an observed lower risk of infection [10]. The resulting efficacy of 31.2 % after 42 months of follow-up was modest, but remains the highest achieved to date. The components of ALVAC-HIV and AIDSVAX® B/E were later modified and administered in several consecutive studies but unfortunately without reproducible success in humans [128–130].

Another and more recent promising approach are so-called polyvalent HIV-1 "mosaic antigens", first designed by Fischer and colleagues in 2007 [15]. They introduced mosaic primary sequences, originating from natural sequences of HIV variants, as a novel principle for antigen design. Mosaic genes code for synthetic HIV primary sequences

composed of HIV variants of a single clade shuffled to provide maximal coverage of potential B and T cell epitopes (Figure 11).
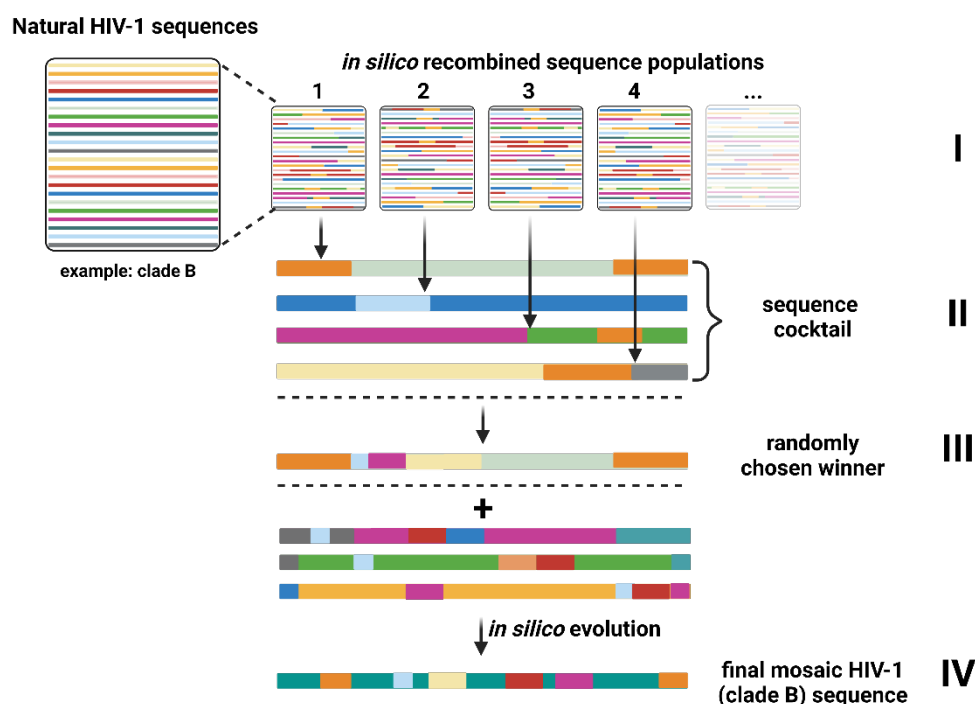
Figure 11. Schematic illustration of the mosaic HIV-1 sequence design. The natural sequences from one HIV-1 clade are assembled based on their frequency. In parallel iterative random two-point recombination events are performed leading to numerous recombined sequence populations. These sequence populations contain sequences, which are referred to as "pseudo-mosaic" sequences, as each of them consists of sections of multiple natural sequences (I). One sequence from each population is then chosen for the mosaic sequence cocktail, which is subsequently optimized (II). The cocktail sequences are analyzed regarding their extent to cover potential epitopes in the natural sequences (input). The higher the resulting coverage, the higher the calculated score for a particular sequence cocktail. Initially, the cocktail contains a randomly chosen winner sequence, which is afterwards assessed for its individual fitness score (III). Using the high-scoring sequences from various populations together with respective input sequences, a complex *in silico* evolution is performed. Parallel sequence optimization is conducted until an optimal mosaic sequence has evolved (IV). This figure was adapted from [15].

The sequence variance of resulting epitopes is required for a broad antibody mediated neutralization and a robust T cell response. This way, a potential vaccine-induced immune response against HIV-1 could be accompanied by a desired cross-reactivity against a diversity of strains. A further combination of mosaic antigens, derived from multiple different clades, could lead to a multivalent vaccine cocktail potentially effective against a variety of HIV clades. This novel approach was deemed promising as two prior pre-clinical trials by Santra *et al*. and Barouch *et al*. and two consecutive clinical trials, namely APPROACH (NCT02315703) and TRAVERSE (NCT02788045), showed

encouraging results. While the pre-clinical studies demonstrated the viability of the mosaic principle by revealing an enhanced depth and breadth of CD4+ and CD8+ T lymphocyte responses and achieved a 67 % protection against a simian HIV infection in rhesus monkeys, the clinical trials showed robust immunogenicity in humans [12,13]. Propelled by these results two highly anticipated clinical trials Imbokodo (NCT03060629) and MOSAICO (NCT03964415) were enrolled in 2017 and 2019 by Janssen Vaccines. Both regimens utilized replication-incompetent adenoviral vectors serotype 26 (Ad26) to introduce two complementary mosaic sequences per Gag-Pol and Env antigen (Figure 12).
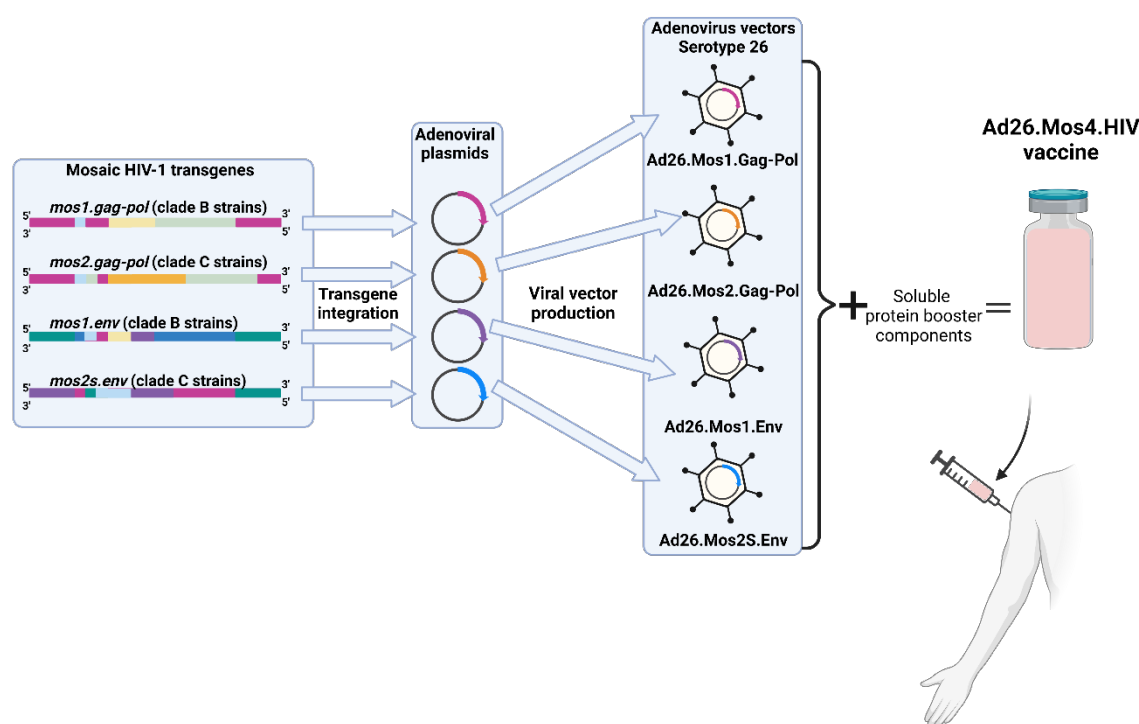
Figure 12. Overview of the Imbokodo (NCT03060629) and MOSAICO (NCT03964415) study design. The mosaic (mos) proteins Mos1.Gag-Pol, Mos2.Gag-Pol, Mos1.Env and Mos2S.Env were transferred using replication-incompetent adenoviral vectors serotype 26 (Ad26). Imbokodo entailed adjuvanted gp140 proteins of HIV-1 clade C while MOSAICO contained gp140 proteins of HIV-1 clade C together with mosaic gp140 proteins of clade C as boost components.

The mosaic (mos) proteins Mos1.Gag-Pol and Mos1.Env have the highest coverage with clade B strains of HIV-1 while Mos2.Gag-Pol and Mos2S.Env have the highest coverage with clade C strains. The pairing of antigens from two clades is supposed to confer optimal global HIV-1 sequence coverage. While Mos1.Env is a soluble Env variant, Mos2S.Env is an optimized C-terminally truncated membrane-anchored Env variant

exhibiting elevated surface expression [14,131]. Besides the four adenoviral vector components, the vaccines "Ad26.Mos4.HIV" entailed different booster components, the adjuvanted gp140 proteins of HIV-1 clade C (Imbokodo) and adjuvanted gp140 proteins of HIV-1 clade C together with mosaic gp140 proteins of clade C (MOSAICO).

While the vaccine components and vaccination regimens between both studies were comparable, the trail sites and the selection criteria of the study participants differed. Imbokodo took place in Sub-Saharan Africa, enrolling young women and MOSAICO in North America, Latin America, and Europe involving men who have sex with men and transgender individuals. Due to insufficient success demonstrated by a comparable low vaccine efficacy estimate of 25.2 % after primary analysis, Imbokodo was terminated ahead of schedule in 2022 reaching phase IIb [132]. Unfortunately and very recently, in January of 2023 the MOSAICO trial was also discontinued one year earlier than expected due to lacking efficacy in preventing HIV infections, yet the vaccine regimen proved safe [133].

Besides vector-based platforms, novel and even more sophisticated approaches are investigated as an alternative. Especially the mRNA technology by BioNTech/Pfizer and Moderna has been proven very successful in the COVID-19 pandemic and analog approaches are now tested to combat HIV/AIDS as well [134–136]. Results of pre-clinical experiments utilizing HIV mRNA vaccines were recently published by Zhang and colleagues [137]. The concept of this study followed the mRNA mediated *in vivo* generation of Env-decorated virus-like particles (VLPs) upon cellular expression in vaccinated macaques. To achieve this, simian Gag and Env delivering mRNAs were co-formulated and formation of VLPs displaying Env proteins on the surface were readily detected. The vaccinated macaques showed a 79 % risk reduction for an infection with a specific strain of the simian-human immunodeficiency virus (SHIV) – a chimeric virus composed of SIV-Gag and HIV-1 Env. In addition, experiments in mice showed an enhanced neutralizing antibody response in study groups which received the combination of *gag* and *env* mRNAs compared to those animals only receiving *gag* mRNAs. These data indicated a superior immunogenic effect of the *in vivo* generated Env-decorated VLPs upon vaccination.

VLPs can display surface antigens in a native-like conformation, which enhances immunogenicity as compared to antigens presented in soluble or poorly organized form [138–140]. In addition, VLPs can be functionalized with a variety of antigens, thus expanding the panel of possible applications [141–143]. VLP based vaccines against the Hepatitis B virus (HBV), Hepatitis E virus (HEV), Human Papilloma virus (HPV) and malaria already gained FDA approval [144]. This is why HIV-1 VLPs represent an attractive vaccination platform worth further development. The following sections will therefore provide a more detailed overview on the structure, morphology and immunogenicity of VLPs and their application as HIV-1 vaccine.

6.3. HIV-1 virus-like particles (VLPs)

Virus-like particles (VLPs) are recombinantly produced nanoscale structures of 20-200 nm that resemble the cognate parental virus in morphology [145]. The major difference between VLPs and viruses however, is their inability to replicate, warranted by the lack of viral nucleic acids. This renders VLPs as safe candidates for pharmaceutical applications. The least complex VLP structure results from the self-assembly of only one non-enveloped protein. An example for such simple and non-enveloped VLPs are those derived from the Human Papillomavirus (HPV), as their self-assembly is mediated solely by the major capsid protein 1 (L1) [146]. Other examples are enveloped VLPs derived from HIV or Influenza revealing a more complex structure characterized by the display of surface antigens [147]. To serve as promising candidate vaccines, the display of the surface antigens hemagglutinin (HA) and neuraminidase (NA) on Influenza VLPs as well as the display of Env proteins on the surface of HIV VLPs is crucial [148–150].

6.3.1. Structure and morphology

The assembly of HIV-1 VPLs depends on the expression of p55-Gag proteins, which are sufficient to form enveloped VLPs without antigen decoration [16]. Multimerization of p55-Gag proteins leads to the formation of a Gag lattice underneath the lipid bilayer of the producer cell. Subsequent budding from the cell membrane results in the release of VLPs characterized by a spherical structure. In HIV, the p55-Gag proteins represent about 50 % of the total virion mass and up to 3,617 p55-Gag monomers can be found in a single HIV VLP [17,55]. Analogue to the virus, VLPs can exist in an immature or mature form

outside the producer cells. Immature HIV VLPs are readily produced by expression of the *gag* gene in the absence of the co-expression of viral protease (PR) mediating particle maturation. Therefore, proteolytic cleavage of p55-Gag precursor proteins by PR activity can be omitted [16,51]. In the presence of PR, cleavage of the p55-Gag precursor proteins leads to the release of VLPs harboring the major subunits MA, CA and NC (Figure 13).
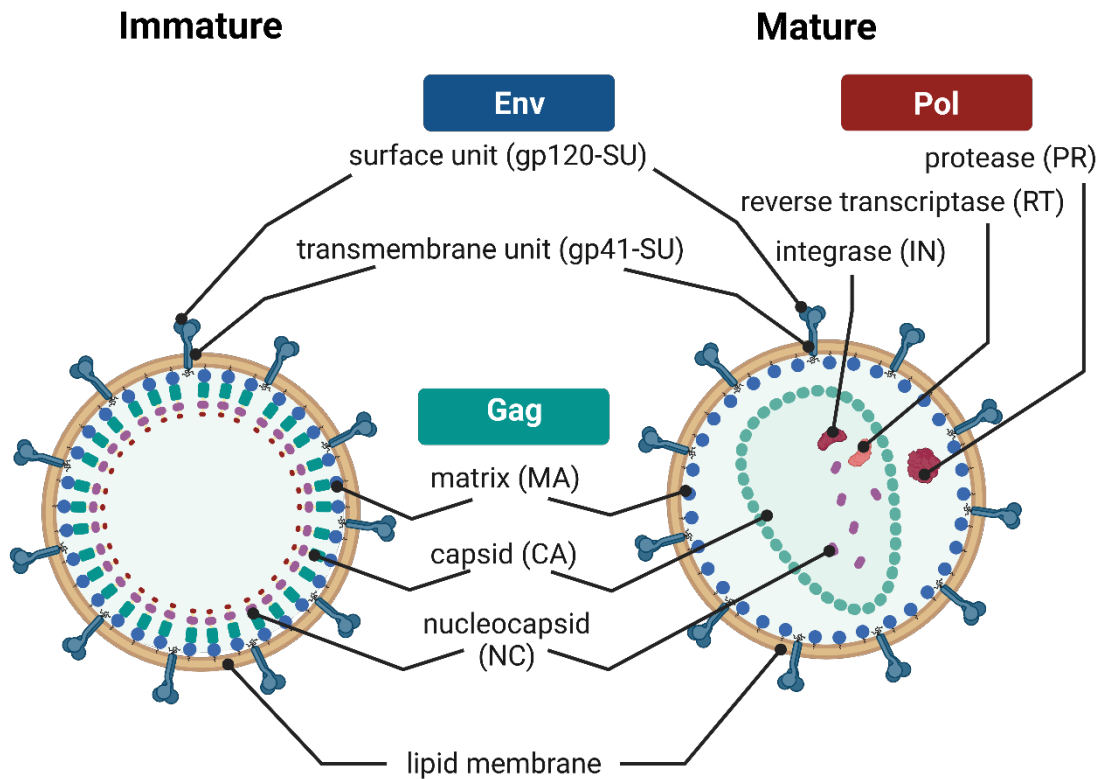
Figure 13. Schematic illustration of an immature and a mature HIV-1 VLP. The expression of Gag and Env proteins results in the formation of immature Env decorated VLPs (left). The p55-Gag precursor proteins multimerize to form the viral core. Co-expression of Pol proteins leads to generation of mature HIV-1 VLPs (right). The protease (PR) catalyzes the cleavage of the p55-Gag precursor proteins to its cognate subunits (MA, CA, and NC) causing structural rearrangement in the particle.

HIV VLPs can be produced either by sole expression of the *gag* gene or by co-expression of *env*. A significant difference between VLPs and HIV virions is the abundance of Env proteins incorporated on the surface. While VLP membranes can incorporate up to 127 Env spikes, HIV virions usually have a much lower natural spike density of around 14 Env proteins [151,152].

6.3.2.   The immunogenic properties of VLPs

The favorability of VLP based vaccines is a result of three important criteria, safety, immunogenicity and tolerability. The safety of VLPs is regarded as high, as the lack of viral genetic material renders them incapable of replication. The immunogenic properties of VLPs describe the ability to provoke efficiently an immune response and are dependent on several factors. These include the nanometer size in diameter and a highly repetitive surface organization. The small size facilitates the rapid entry of VLPs into the lymphatic system where the lower obstruction allows for the efficient uptake by antigen presenting cells (APCs), including dendritic cells (DCs) and the cross-stimulation of reactive B and T cells, respectively [18–22]. The particularly repetitive structure resulting from the presentation of antigens on the surface of VLPs at high densities enables the cross-linking of B cell receptors leading to B cell activation, and thus stimulation of the humoral immune system [18]. However, there are some factors potentially compromising the immunogenicity of enveloped VLPs displaying antigens. These are the limited VLP stability as well as the contamination with incorporated cellular proteins, lipids and nucleic acids derived from the producer cell utilized. In addition, the production of enveloped VLPs displaying structural complex glycoproteins such as HIV Env proteins requires the cautious consideration of the utilized expression system to provide sufficient complexity of post-translational modifications [51,153].

The tolerability of potential HIV VLP based vaccines in humans still needs to be assessed in separate clinical trials. The present number of clinical trials utilizing HIV VLP based vaccines remains limited to one example. In this phase I clinical trial (NCT00001053), the tolerability and immunogenicity of *in vitro* produced and purified hybrid VLPs, composed of yeast-derived protein 1 and the HIV-1 p55-Gag derived subunits MA and CA, was assessed after subcutaneous administration to 16 healthy HIV seronegative participants. These VLPs were not just well tolerated, but also immunogenic, as p24-specific antibody and T helper cell responses were observed [154,155]. The immunogenicity of HIV VLPs was demonstrated in several preclinical studies offering opportunities for their further testing in clinical trials [156–159].

6.4. Stable cell line development for recombinant protein production

As pointed out in the previous section, the right choice of the expression system represents a crucial factor for the production of HIV VLPs qualifying as candidate vaccines. Therefore, parallel progress in stable recombinant cell line development for VLP production is necessary. Considering the requirements of the product on posttranslational modifications, mammalian expression systems including Chinese Hamster Ovary (CHO) cells are primarily used for biopharmaceutical production [160,161]. The cultivation of such cells is preferably conducted in suspension rather than as adherent cells, as the growth in suspension enables the cells to reach higher densities resulting in elevated product yields [162]. The use of stable recombinant producer cell lines is the commonly preferred method to express protein of interests (POIs). In contrast to transiently transfected cells, stable cell lines usually consist of a homogenous cell population in culture permanently expressing the POI. The use of stable producer cells overcomes certain limitations of transient producer cells that suffer from a high variability of the transfection efficiency, and thus high batch-to-batch variations [163]. The common technique to produce these stable cell lines is achieved by a two-step process [164]. The first step represents the transfection of the cells using circular or linearized plasmid DNA encompassing the gene of interest (GOI) and a coupled selection marker. Stably transfected cells having integrated the plasmid into their genomes, are then screened for the expression of the selection marker, which frequently confers antibiotic resistance. The subsequent selection process is time consuming and laborious. The initial cell population is divided to several growth containers until a subpopulation has adapted to the presence of the selection pressure and exhibits the desired phenotype. An often encountered drawback in this process is the rarely occurring stable integration of the GOI into cellular gDNA demonstrated by a single-digit copy number of linearized plasmid molecules found per cell [162,164]. Further disadvantages are the integration of the linearized plasmid at random loci favoring genetic instability as well as the integration of bacterial sequences originating from the plasmid backbone leading to transcriptional silencing of the GOI [165]. Another drawback are pooled cell populations typically not producing satisfying POI yields, and hence the need to establish and time-intensively screen for clonal cell lines producing higher POI yields [164]. All of these points, limit this method to establish stable producer cells in terms of time-efficiency and cost-effectiveness.

Therefore, the growing demand for new and affordable approaches to develop stable transgenic cell lines needs to be addressed.

6.4.1. Transposon-systems as genetic tools to generate stable cell lines

Transposon-based vector systems for the establishment of stable recombinant cell lines are a favorable alternative and have become an attractive tool both in research and in industry in the past years [162,166]. Transposons are mobile genetic elements and ubiquitous in the kingdoms of life. They are recognized as fossil DNA transfer vehicles able to integrate nucleic acid sequences into the genome of their host cells – a process referred to as transposition. Three particular transposon derived vector systems show promise for use in genome engineering. *Sleeping Beauty*, reconstructed from different salmonid fish genomes, *PiggyBac*, isolated from the cabbage looper moth genome and *Tol2*, from the medaka fish genome [164,167–169]. Today, modified and optimized versions of the original transposases exhibiting improved efficiency are commonly utilized [170–174].

Transposition of genes for the purpose of genome engineering is commonly exploited employing two-component DNA transposase-derived vector systems (Figure 14). The first component, the transposase expression vector (transposase construct), includes a promotor suitable for the expression of the transposase gene in the desired producer cell and a 3´-located poly(A) tail. The minimal composition of the second component (transposon vector), encompasses an expression cassette containing a promotor for expression of the GOI and again a 3´-located poly(A) tail. In addition, the expression cassette is flanked by transposon-specific inverted terminal repeats (ITRs) necessary for its excision and later integration into the cell genome through transposase activity [162,164]. A major advantage of utilizing transposon derived vector systems is the specific integration of the expression cassette into the cell genome while bacterial sequences originating from the transposon vector backbone are not integrated. This minimizes the risk of decreasing transgene expression levels as bacterial sequences are known to attract promotor silencing [164,165].

A panel of transposon systems were assessed in a comparative study to reveal the frequencies of genomic integration in human cells [175]. This experiment included an

optimized variant of *Sleeping Beauty* (*SB100x*), a variant of *PiggyBac* codon optimized for the expression in mouse cells (*mPB*) and Tol2. *SB100x* revealed the highest frequencies of genomic integration in human cells (up to 40 copies per cell clone) while *Tol2* and *mPB* displayed low single-digit numbers up to 3 and 4 copies per cell clone, respectively. Both, *PiggyBac* and *Sleeping Beauty* are capable of transferring large genes of interests in the case of *PiggyBac* up to 200 kb, which is much larger than the cargo capacity for any viral vector system [164]. While the gene integration profile of *Sleeping Beauty* is close to random, the integration profiles of *PiggyBac* and *Tol2* are close to transcriptional units of the cellular genome, and thus foster high transgene expression levels [164,175,176]. Contrary to *Sleeping Beauty*, *PiggyBac* mediated transposition involves traceless excision and seamless integration. The transgene insertion thus rarely leaves footprints in the genome which is considered an important quality for gene therapeutic applications [177]. In addition, *PiggyBac* is highly active in cells of a variety of organisms like yeasts, plants, insects and mammals, including humans [170,171,176,178–180].
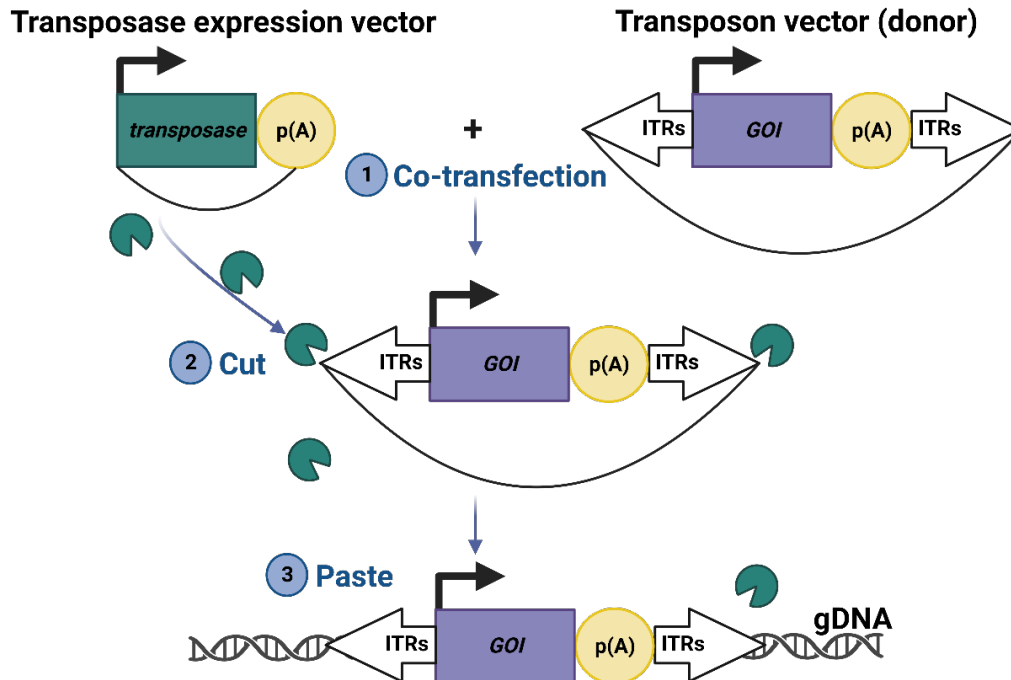
Figure 14. Schematic illustration of the two-component transposon vector system used in this study. Both, transposase construct and transposon vector are utilized for co-transfection of mammalian cells (step 1). Upon transient expression, the transposase starts to catalyze the excision of the expression cassette encompassing the gene of interest (GOI) from the transposon vector backbone (step 2). The transposase mediates integration of the excised genetic element into the cell genome (step 3). Different nucleotide motifs are favored as targets for integration by different transposases (*PiggyBac*: TTAA and *Sleeping Beauty*: TA). This figure was adapted from [164].

The aforementioned aspects represent some of the properties favoring transposon mediated gene transfer over the common method to establish transgenic cell lines by stable transfection. In addition, stable transgenic cell lines generated using transposon systems can achieve high POI yields despite being bulk populations [162,166]. In the following chapter transposon mediated gene transfer in human cells is employed to establish HIV VLP producer cell lines.

7. Part I Components of a mosaic HIV-1 vaccine mediate VLP formation and the display of Env trimers exposing neutralization-sensitive epitopes

7.1. Introduction

The number of 38.4 million people still living with HIV in 2021 depicts the ongoing global burden of this disease [181]. Undoubtedly, there is an urgent need for a prophylactic vaccine to reduce continuing HIV infections worldwide. Despite decades of research, no HIV candidate vaccine has yet mediated sufficient protection in humans to pass mandatory market approval requirements (Chapter 9.1). HIV vaccine development is severely hampered by several aspects, namely the presence of a large sequence variety and the masking of Env epitopes by extensive conformational adaptability and glycan shielding [182]. There are at least two correlates of protection against HIV infection and disease progression. These are the elicitation of a robust T cell response [11,183] and the generation of broadly neutralizing antibodies (bNAbs) [98].

Polyvalent mosaic HIV vaccines were recently tested in the highly anticipated MOSAICO trial (NCT03964415) [131,133]. During pre-clinical studies, it was not examined, whether components of the Ad26.Mos4.HIV vaccine, more specifically the synthetic mosaic Gag variants, facilitate VLP formation [16]. It therefore remained unclear, whether mosaic Gag VLPs can form in vaccinees (Figure 15). As VLPs strongly stimulate cellular and humoral immune responses, *in vivo* formed VLPs would probably contribute to the efficacy of the Ad26.Mos4.HIV vaccine [137,184–186].

Consequently, the first study aim was the examination whether the mosaic HIV-1 Gag proteins are able to form VLPs upon expression in human cells. The second aim was to assess the functional expression of Mos2S.Env proteins and their incorporation into mosaic Gag-formed HIV-1 VLPs. The Env incorporation provided and in a third step, the exposure of neutralization-sensitive epitopes in Mos2S.Env proteins required for bNAb binding, should be investigated using a VLP capture assay [187].
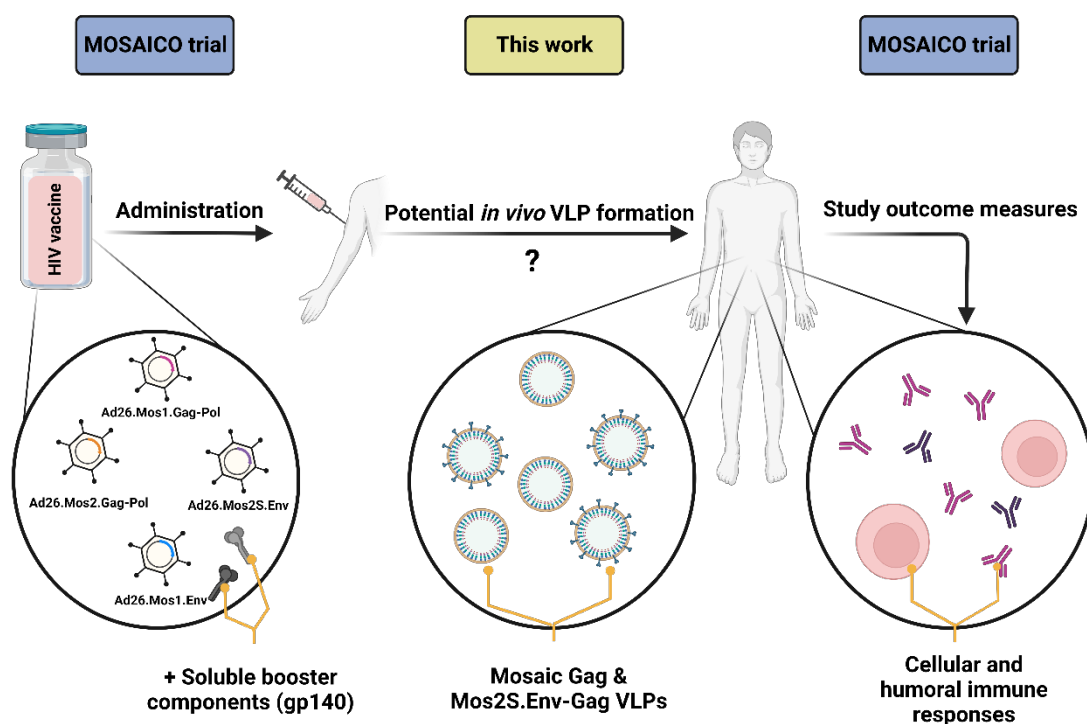
Figure 15. Schematic illustration of the working hypothesis for part one of this thesis. Left part of the figure: Components administered to MOSAICO trial participants. Middle part of the figure: Potential *in vivo* VLP formation in the vaccinees mediated by the vaccine components. Right part of the figure: Study outcome measures that are assessed after trial completion (NCT03964415).

7.2. Results
7.2.1. Establishment of stable cell lines expressing mosaic HIV-1 p55-Gag and Env proteins

In a first proof-of-concept approach, *mos1.gag* and *mos2.gag* were transiently expressed in the absence or presence of *mos2s.env* in human cells. Therefore, cell-free supernatants of 293 T cells transfected with the corresponding expression vectors (Figure 16) were harvested three days post transfection and subjected to quantification of p24 proteins using ELISA. The measured concentration of Gag proteins in these cell-free supernatants reached 110 ng/mL proving the successful expression of the respective mosaic Gag proteins in human cells and indicating the formation of VLPs.

Encouraged by these findings, stable 293-F VLP producer cell lines were established to produce larger VLP quantities enabling the in-depth characterization of these particles. Therefore, DNA transposon mediated gene transfer of *mos1.gag* and *mos2.gag* in the absence or presence of *mos2s.env* was employed. Transposition was facilitated by the highly-active *hyPBase* – an optimized variant of the *PiggyBac* transposase [170]. *HyPBase* served as the transposase expression vector while a transposon vector served as

donor for the transgene expression cassette containing the gene encoding the mosaic HIV antigen (Figure 16). The expression of each mosaic *gag* gene was geno-phenotype-coupled to the parallel expression of the puromycin resistance gene in the two vectors PB-Mos1.Gag-IpW and PB-Mos2.Gag-IpW, respectively. The third transposon vector PB-Mos2S.Env-IhW contained an expression cassette encompassing *mos2S.env* and the hygromycin resistance gene.
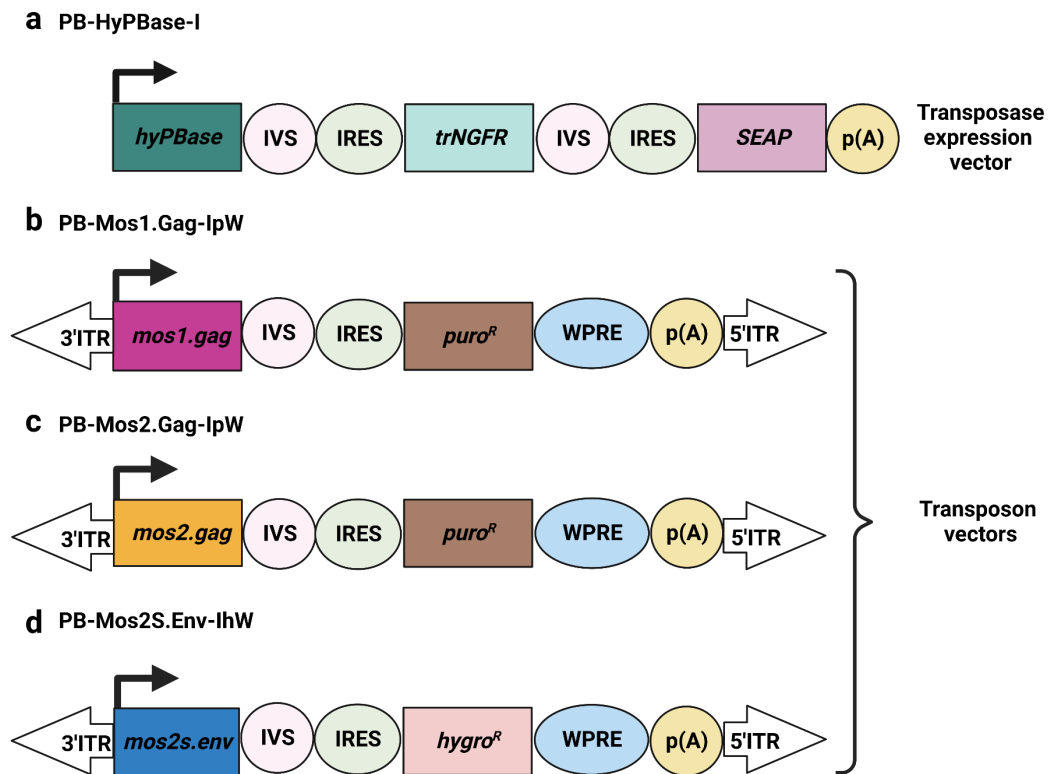
Figure 16. Schematic overview of the genetic elements in the expression cassettes of the transposase expression vector and of the mosaic HIV-1 antigen-expressing transposon vectors. The transgene expression is driven by the CMV promotor/enhancer element (PCMV) in all constructs. The polyadenylation signal p(A) of the bovine growth hormone (bgH) and a synthetic intron (IVS) to elevate expression levels are present as well. In the transposase construct the expression of *hyPBase* is coupled to the expression of the reporter genes truncated human nerve growth factor receptor (trNGFR) and secreted alkaline phosphatase (SEAP) by an internal ribosomal entry site (IRES) (a). The genes *mos1.gag*, *mos2.gag* and *mos2s.env* are flanked by the inverted terminal repeats (3' ITR and 5' ITR) derived from the *piggyBac* transposase. The expression of mosaic gag genes is coupled to the expression of the puromycin (*puroR*) resistance gene while the expression of mos2s.env is coupled to the expression of the hygromycin (*hygroR*) resistance gene. The woodchuck hepatitis posttranscriptional regulatory element (WPRE) is located downstream from each resistance gene (b-d). This figure was reproduced from [188].

The subsequent selection process was initiated four days post transfection using respective antibiotics. The concentration of puromycin and hygromycin was constantly elevated for three weeks resulting in the generation of the stable transgenic cell lines 293-F/Mos1.Gag, 293-F/Mos2.Gag, 293-F/Mos1.Gag/Mos2S.Env and

293-F/Mos2.Gag/Mos2S.Env. The selection pressure was constantly applied to maintain high-yield production of VLPs. The high antibiotic concentrations applied (10 to 15 µg/mL puromycin and 200 µg/mL hygromycin, respectively) indicated also high expression levels. The expression of mosaic Gag proteins by the stable cell lines was therefore further assessed. Cell-free supernatants (CFSN) were harvested in triplicates and subjected to ultracentrifugation to isolate putative VLPs formed by mosaic Gag variants. The analysis of the isolated pellets using a p24-specific ELISA revealed that both mosaic Gag variants were stably expressed in 293-F cells in the absence or presence of Mos2S.Env co-expression. The Gag expression levels varied among the cell lines and ranged between 17.0 (± 2.3) ng p24 per mL CFSN for Mos2.Gag and 240.0 (± 31.7) ng p24 per mL for Mos1.Gag co-expressed with Mos2S.Env (Table 1).

Table 1 Detection of Gag proteins in cell-free supernatants (CFSN) of 293-F cells stably expressing the mosaic Gag proteins in the absence or presence of Mos2S.Env. The cell-free supernatants were subjected to ultracentrifugation and resulting pellets were analyzed using a p24-specific ELISA (n=3, mean ± SD).

293-F cells	ng pelleted Gag proteins per mL CFSN	
stably expressing	mean (n=3)	± SD
Mos1.Gag	82.3	10.3
Mos1.Gag + Mos2S.Env	240.0	31.7
Mos2.Gag	46.6	16.3
Mos2.Gag + Mos2S.Env	17.0	2.3

7.2.2.   Mosaic HIV-1 p55-Gag proteins assemble into VLPs

In order to visualize the potentially formed VLPs in the pellet fraction of ultracentrifuged CFSN samples and to study their morphology, these were prepared for analysis using negative-stain transmission electron microscopy (TEM). The TEM-analysis revealed both mosaic Gag variants capable for VLP formation (Figure 17). The visualized VLPs displayed a spherical morphology and an average size of ~120 nm in accordance with previous reports describing immature particles [16,189]. The characteristic structure of immature particles was observed as well entailing a lipid bilayer derived from the producer cell and the concentric organization of the Gag lattice underneath [190,191].
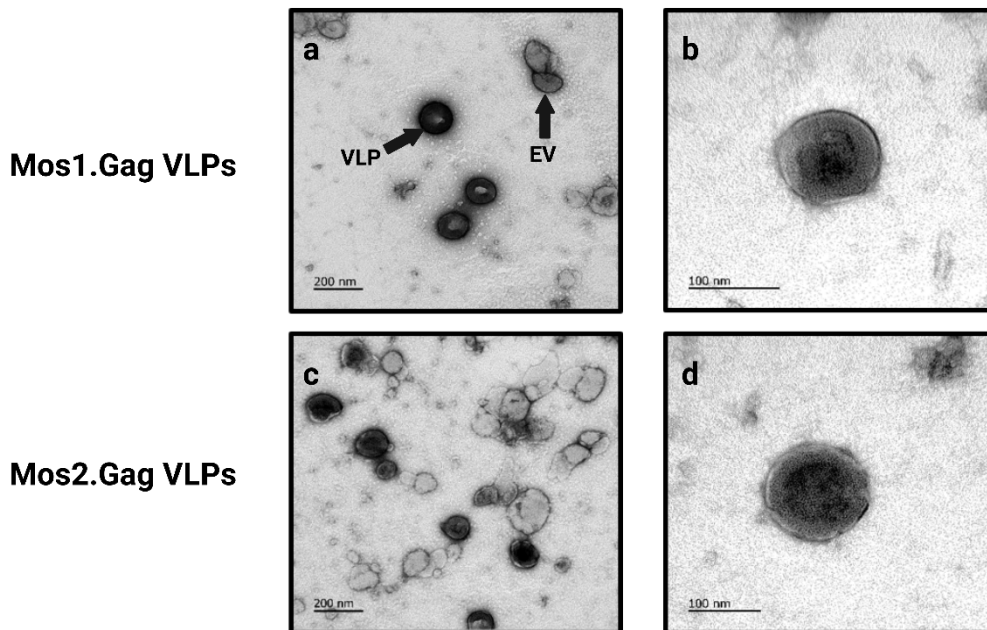
Figure 17. Negative-stain TEM images of the detected mosaic Gag mediated VLP formation. VLP samples were obtained from ultracentrifugation of cell-free supernatants harvested from stable *gag* transgenic 293-F cell lines. The arrows indicate an extracellular vesicle (EV) and a VLP. The scale bars represent 100 nm and 200 nm, respectively. This figure was reproduced from [188].

Besides the visualization of VLPs, the presence of mosaic Gag proteins in these VLPs was detected using a Western blot-analysis employing polyclonal antibodies directed against p55-Gag proteins. Resuspended VLP pellets of the four cell lines and a sample taken from naïve 293-F cells serving as negative control were subjected to SDS-PAGE. In the following Western-blot, Mos1.Gag and Mos2.Gag proteins were detected in samples of all four cell lines irrespective of the co-expression of Mos2S.Env, while degradation products of Gag precursor proteins were not observed (Figure 18). This result in combination with the prior findings from the electron microscopic-analysis confirmed the successful formation of VLPs mediated by the expression of mosaic Gag variants in human suspension cells.
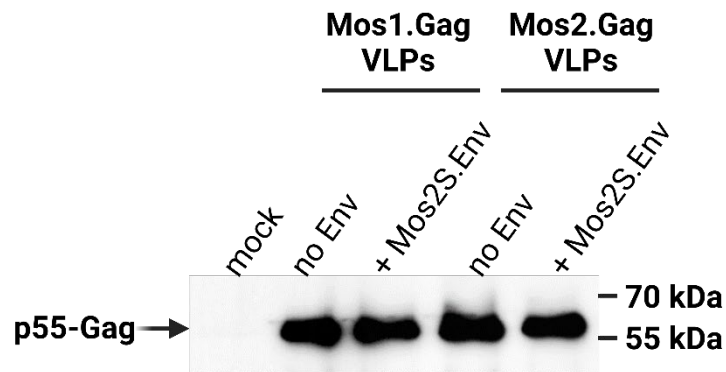
Figure 18. Detection of Gag proteins in VLP samples using Western blot-analysis. The VLPs were isolated from all four producer cell lines. A sample obtained from naïve 293-F cells served as negative control (mock). The mosaic p55-Gag precursor proteins in the VLP pellets were detected using polyclonal primary rabbit antibodies directed against HIV-1 Gag proteins followed by incubation with secondary horseradish peroxidase (HRP)-conjugated antibodies against rabbit. The arrow indicates the precursor proteins p55-Gag. The positions of the molecular weight markers are shown on the right. This figure was reproduced from [188].

7.2.3. Mos2S.Env proteins are incorporated into mosaic HIV-1 VLPs

After confirming the successful formation of VLPs mediated by mosaic Gag proteins, the potential incorporation of Mos2S.Env proteins into the respective VLPs was examined. Therefore, Western blot-analysis of the aforementioned VLP pellets was performed using polyclonal antibodies directed against the soluble surface unit (SU) of gp120 proteins (Figure 19). Again a sample taken from naïve 293-F cells served as negative control as well as samples derived from cells only expressing mosaic Gag variants. Mos2S.Env proteins were exclusively detected in samples from transgenic cell lines containing both, a variant of mosaic *gag* and *mos2s.env*, thus indicating the incorporation of Mos2S.Env proteins in both mosaic Gag formed VLP variants. Despite no observation of degradation products of Env proteins, little amounts of unprocessed precursor gp160-Pr proteins were detected. These were identified at a molecular weight of around 140 kDa instead of 160 kDa, as Mos2S.Env exhibits a truncation at the C-terminus of the gp41 transmembrane unit resulting in a shortened cytoplasmic domain compared to the full length counterpart gp160-Pr [14,131]. The barely detectable amounts of truncated (tr) gp160-Pr proteins indicated that the vast majority of the incorporated Env proteins underwent correct previous enzymatic processing.
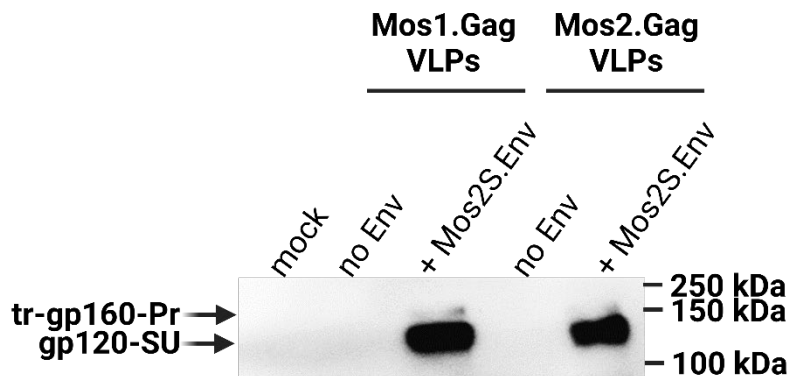
Figure 19. Detection of Env proteins in VLP samples using Western blot-analysis. The VLPs were isolated from all four producer cell lines. Samples obtained from naïve 293-F cells (mock) as well as VLP pellets from recombinant 293-F cell lines only expressing mosaic Gag variants served as negative controls. The Mos2S.Env proteins in the VLP pellets were detected using polyclonal primary goat antibodies directed against the surface unit of gp120 followed by incubation with secondary horseradish peroxidase (HRP)-conjugated antibodies against goat. The arrows indicate the unprocessed truncated precursor glycoproteins (tr-gp160-Pr) and the processed gp120-SU. The positions of the molecular weight markers are shown on the right. This figure was reproduced from [188].

To evaluate the relative abundance of Mos2S.Env proteins in mosaic Gag formed VLPs, VLP pellets were subjected to quantification of both, gp120 proteins and p24 proteins using respective ELISA. Comparable high amounts of Mos2S.Env proteins incorporated into Mos1.Gag and Mos2.Gag formed VLPs were observed. The gp120 amount for Mos1Gag VLPs was 96 ng per µg p24 and for Mos2Gag VLPs 176 ng per µg p24.

7.2.4. Displayed Mos2S.Env proteins expose neutralization-sensitive epitopes

While the presence of Mos2S.Env proteins on mosaic Gag formed VLPs was successfully demonstrated employing Env-specific ELISA, these results do however not allow any conclusions on the quality of displayed Env antigens. Native-like Env trimers on the surface of the produced VLPs are crucial, as they expose neutralization-sensitive epitopes more effectively compared to non-functional Env proteins and are required to elicit NAbs in vaccinees [150,192,193]. To assess the exposure of such neutralization-sensitive epitopes, qualitative immunoprecipitation experiments using four different bNAbs, targeting three different epitopes within the gp120-SU of Env proteins, were conducted. In addition, the monoclonal antibody (MAb) 5F3 targeting the transmembrane unit gp41-TM was utilized to prove the incorporation of this subunit into the lipid membrane of the VLPs. Samples derived from naïve 293-F cells (mock) and VLP samples not presenting any Env proteins (bald Mos1.Gag and Mos2.Gag VLPs) served as additional negative

controls, while human IgG antibodies were utilized as isotype controls. To conduct the VLP capture assay the antibodies 2G12, 447-52D, PG9, PG16 and 5F3 were coupled to protein G-coated magnetic beads. VLP samples were then standardized to 100 ng Gag proteins and added to antibody-coated beads. Enrichment of the VLPs bound to the antibody-coated beads was conducted in a magnetic field. VLPs were eluted and subjected to subsequent Western blot-analysis, using polyclonal antibodies directed against p55-Gag proteins (Figure 20).
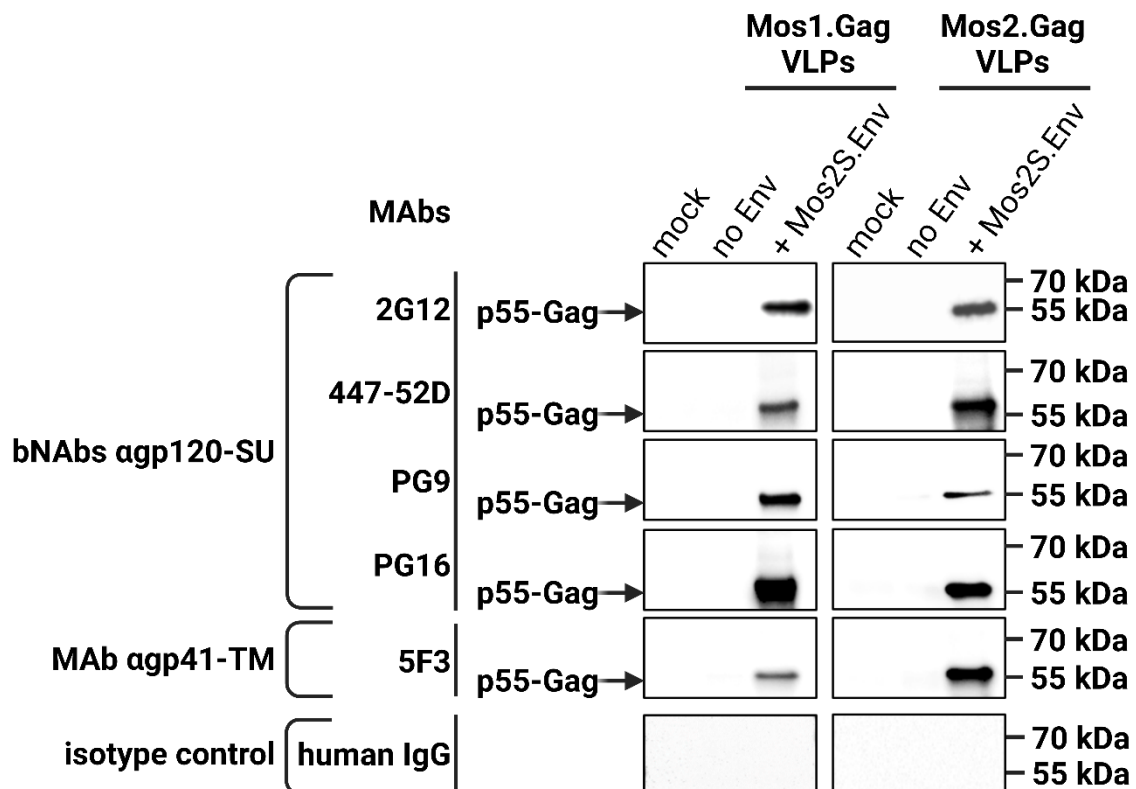
Figure 20. Detection of Gag proteins in immunoprecipitated VLP samples using Western blot-analysis. Samples of naïve cells (mock), VLP samples of *gag* transgenic 293-F cells and VLP samples immunoprecipitated using human IgG isotype control antibodies served as negative controls. The VLP input amounts for the VLP capture assay were standardized to 100 ng Gag proteins for all samples. The bNAbs 2G12, 447- 52D, PG9, PG16 as well as the gp41-TM-specific MAb 5F3 and the isotype control antibodies (human IgG), which were coated to magnetic beads for VLP capture are shown on the left. The positions of the molecular weight markers are shown on the right. The arrows on the left indicate the positions of detected p55-Gag proteins. This figure was reproduced from [188].

Gag directed antibodies were chosen, as these proteins are present in much higher abundance than Env proteins in HIV-derived VLPs enhancing the sensitivity of the assay. This approach thus allows for the sensitive and indirect detection of epitopes in Env proteins displayed even at low density on VLPs [187]. The resulting Western blot-images

showed that p55-Gag proteins were detected in all Env-positive VLP samples, while none of the negative controls revealed detectable amounts of Gag precursor proteins.

According to the aforementioned data, the results from the immunoprecipitation experiments reveal the efficient incorporation of Mos2S.Env proteins into VLPs formed by both mosaic Gag variants, as the target epitope in the ectodomain of gp41-TM was displayed and recognized by MAb 5F3 [194]. In addition, the exposure of three different bNAb target epitopes and their structural integrity, namely, in the V1/V2-loop (bNAbs PG9 and PG16) [195–197] in the V3-loop (bNAb 447-52D) [198] and of highly conserved clusters of oligomannose residues on the outer domain of gp120-SU (bNAb 2G12) [194,199,200], was demonstrated. An illustrative overview of these target epitopes on the Env trimer is provided in Figure 21.

I. gp120: outer domain (2G12)

II. gp120: V3-loop (227-45D)

III. gp120: quaternary V1/V2-loop (PG9 and PG16)

IV. gp41: TM ectodomain (5F3)
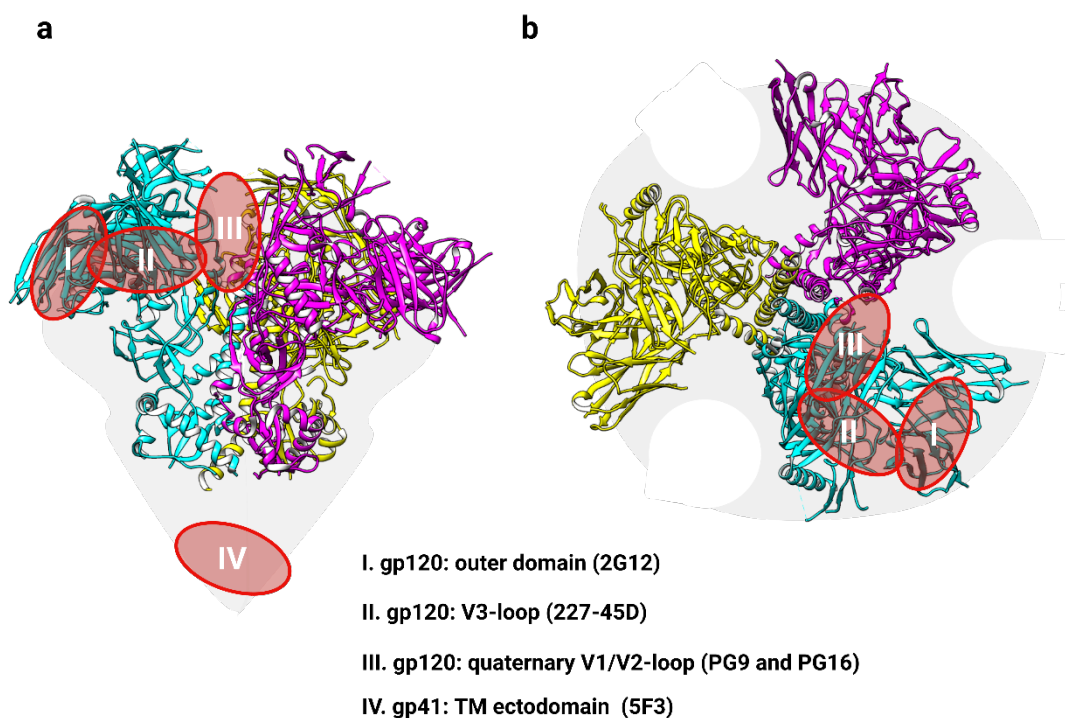
Figure 21. Schematic illustration of the Env trimer including the epitopes targeted by the utilized MAbs. The side view (left, a) and the top view (right, b) are presented. The grey areas represent the glycan shield. BNAb 2G12 targets the outer domain, bNAb 447-52D targets the third variable (V3) domain, bNAbs PG9 and PG16 are preferably quaternary structure dependent and target the first and second variable (V1/V2) domain of gp120. Mab 5F3 targets the ectodomain in the transmembrane (TM) region of gp41.The illustrative model is based on the cryo-EM structure of the HIV-1 Env trimer BG505 SOSIP.664 (protein data bank accession number: 7TFO) [201] and was generated using the software Chimera 1.13.1 [202].

7.3. Discussion

This work was a proof-of-concept study, in which mosaic HIV Gag protein variants, derived from vaccine components of the recently discontinued MOSAICO trial (NCT03964415), were tested for their ability to mediate VLP formation. The present results were recently published in the journal *Virology* [188]. This work revealed the functional formation of VLPs formed by mosaic Gag proteins upon expression in human cells as it was previously observed by Chapman and colleagues [203]. The present findings also demonstrated that mosaic Env proteins are efficiently incorporated into VLPs formed by both Gag variants. This was assessed by the relative abundance of gp120 monomers per µg Gag proteins in VLP pellets, which was 7-fold (Mos2S.Env on Mos1.Gag VLPs) to 14-fold (Mos2S.Env on Mos2.Gag VLPs) higher than recently observed for Env variants displayed on SIV-Gag VLPs [137]. The increased membrane incorporation of Env proteins was previously shown in animal studies to enhance immunogenicity [159,204]. Further Western blot-analysis of Mos2S.Env proteins in isolated VLP pellets demonstrated that the vast majority of gp160 precursor proteins was processed to their cognate subunits gp120-SU and gp-41-TM, respectively. This proteolytic processing is crucial for vaccine design, as HIV-1 neutralization largely depends on the recognition of mature Env trimers by bNAbs [205–208]. The exposure of bNAb epitopes on Mos2S.Env-proteins deemed probable, as these Env proteins exhibited large amounts of fully-processed heterodimers [150,192,193,208]. To assess the presence of these neutralization-sensitive epitopes, a VLP capture assay was performed [187]. The bNAbs PG9, PG16, 447-52D and 2G12 target different epitopes in the surface unit gp120-SU of the Env proteins (Figure 21). The utilization of bNAbs was instrumental in demonstrating the exposure of these neutralization-sensitive epitopes on Mos2S.Env proteins displayed on VLPs. Compared to 447-52D targeting the V3-loop and 2G12 targeting the gp120 outer domain, the bNAbs PG9 and PG16 are exceptional, as they preferably bind quaternary structure dependent epitopes and do not bind monomeric Env proteins [98,150,197]. Therefore it can be assumed that Mos2S.Env proteins displayed on the surface of mosaic Gag VLPs are predominantly present in their trimeric Env form. This trait emphasizes the quality of a potential vaccine component as Env trimers, rather than non-functional monomeric Env units, are supposed to induce neutralizing antibody responses [95,195]. To further validate the potential presence of Mos2S.Env trimers on

mosaic Gag formed VLPs biochemical characterization of the produced Env-decorated VLPs employing native PAGE- or cryoelectron microscopic-analysis could be utilized [99,157,209–211].

Based on the present findings, the potential *in vivo* formation of mosaic Gag VLPs upon vaccination of MOSAICO trial participants with the adenovirus vectored vaccine "Ad26.Mos4.HIV" seems very likely. There are additional factors substantiating this assumption. The first factor is the vaccine composition entailing, amongst others, adenovirus derived vectors enabling the cellular expression of Mos1.Gag-Pol and Mos2.Gag-Pol proteins. The second factor is the vaccine regimen that included the administration of large amounts of vector particles which should have multiply transduced plenty of the cells in the needle track and diffusion area [212–217]. As equal quantities of all four adenovirus vectors were utilized, cells were likely generated expressing a variety of Gag and Env variants upon vaccine administration. The *in vivo* assembly of such VLPs is presumably accompanied by previous maturation cleavage of p55-Gag precursor proteins, mediated by the viral protease encoded within *pol* in the mosaic *gag-pol* constructs. Therefore, mature rather than immature VLPs are likely being formed *in vivo*, revealing superior immunogenicity as compared to immature particles and previously demonstrated in animal studies [159,218].

In order to shed light on the immunogenicity of Mos2S.Env-decorated mosaic Gag VLPs, their independent investigation in preclinical studies would be required. The value of *in vivo* formed Gag VLPs has been widely studied conducting immunization experiments in animal models [137,184–186]. Frequently observed parameters were the elicitation of Env- and Gag-specific CD4+ T cells as well as an enhanced Env-specific B cell response producing neutralizing antibodies. Accordingly, Mos2S.Env-decorated mosaic Gag VLPs could contribute to robust immune responses in vaccinees and most importantly elicit broadly neutralizing antibodies. Despite the discontinuation of the MOSAICO trial, the present findings warrant further testing of *in vitro* produced and purified Mos2S.Env-decorated mosaic Gag VLPs in pre-clinical animal models. The outcome may further legitimate the application of mosaic VLPs in prime-boost regimens of clinical trials [219,220].

The production of such mosaic HIV-1 VLP based vaccines would require larger scales than those utilized in this work, in addition to higher product yields. The rapid establishment of high MAb-producing cell lines from a stable producer cell pool has been recently highlighted by the use of a commercialized *PiggyBac*-derived transposase [166]. The results support the herein chosen approach to employ *hyPBase* mediated transposition for the rapid establishment of high VLP-producing cell lines. However, the established VLP-producing cell lines could reveal genomic instabilities resulting from spontaneous unintended genome integration of the linearized transposase vector upon transfection of the cells. This could further lead to sustained expression of *hyPBase*, and thus mobilization of transposase-derived Gag and Env encoding expression cassettes. To prevent a future VLP manufacturing cell line from such genetic instability the use of mRNA encoding the transposase should be considered. Here, the transposase is not expressed from a plasmid vector, but instead from co-transfected mRNA unable to integrate into the genome [166,221–223]. Besides stable highly efficiently VLP-producing cell lines, a further important aspect in pharmaceutical biotechnology is process scalability. The upscaling of the established Mos1.Gag VLP-producing cell line to grow in 2 L bioreactors using a fed-batch system was already successfully performed by external collaborators in this project [224–226]. The presented downstream process optimization resulted in a final product purity of >80 % indicating the potential of the developed process for HIV-1 VLP-based vaccine manufacturing.

The immature mosaic HIV-1 VLPs produced in this study may represent an alternative or add-on component to anticipated *in vivo* formed mature VLPs in MOSAICO trial participants. Due to the mosaic design of these antigens, the VLPs should cover the major spectrum of globally circulating HIV strains. The enormous sequence variation of HIV poses one of the challenges, why despite decades of research and numerous clinical trials, no HIV vaccine has yet reached mandatory market approval requirements against infection and disease progression. Two approaches to prophylactic HIV vaccine design are generally considered. The first one is the induction of a vaccine-mediated sterilizing immunity preventing acquisition of infection while the second is a vaccine-induced immunity allowing infection. The latter approach can be subdivided into three different paths, which are I) the reduction of the initial peak viremia and viral load set point, II) the suppression of viremia to an undetectable level and III) the stimulation of viral clearance

before disease [227]. Most of the recent vaccine trials focus on conferring a sterilizing immunity, which is considered the ideal solution owing to the unique biology of HIV facilitating the generation of proviruses and establishment of latent virus reservoirs upon infection. However, the number of unsuccessful vaccine efficacy trials increasingly indicates that this goal is hardly achievable. Thus, the investigation of HIV vaccines suppressing viremia after infection to reduce disease progression, limiting the burden for antiretroviral therapy and preventing transmission would be a reasonable alternative. However, there are some challenges related to the final efficacy measurements of vaccines that do not prevent HIV acquisition [227,228]. The typical vaccine efficacy measurement which determines the ratio of prevented HIV infections within a study group is not applicable. Instead, one of the important assessments is the verification of a low viral load after HIV infection, which is correlated to an asymptomatic progression and decreased contagiousness [229–231]. As the viral load can vary among individuals and in the course of infection, the testing and licensing of such vaccines entails significant challenges. In addition, prolonged follow-up investigations would be necessary adding expenses [227].

The development of a prophylactic HIV vaccine therefore remains a tremendous task. Addressing the unique biology of HIV, several factors need to be considered to fulfill this task e.g. the vaccination approach, the vaccination platform, the design of the clinical trial requiring large study groups and long follow-up investigations as well as the complexity to define immune correlates of protection.

8.   Part II Production of bi-fluorescent HIV VLPs for potential applications in downstream process optimization

8.1.   Introduction

While first part of this thesis focused on the vaccine-induced *in vivo* HIV VLP formation, this second examines aspects of the production and purification of HIV VLP candidate vaccines. As observed in the manufacturing of other biologics, the HIV VLP downstream process is challenged by the presence of contaminants mostly originating from the producer cells. The initial removal of large contaminants such as cells, cell debris and protein aggregates at laboratory scale is commonly achieved employing low-speed centrifugation [51]. However, the lacking scalability of this method requires an alternative for large scale manufacturing. Depth filtration through membranes is hence the most prominent solution, as it enables the cost-effective clarification of cell culture broths at industrial scales (Figure 22). Although ultrafiltration has a low resolution, it is sufficient to retain VLPs in the retentate fraction while larger biopolymers such as protein aggregates and nucleic acids are removed with the permeate [232]. Frequently, depth filtration is followed by additional nuclease treatment of the retentate employing benzonase to degrade residual host cell-derived nucleic acids. A major challenge in the downstream process of virus-derived particles is the contamination of the culture broth with extracellular vesicles (EVs). These are commonly observed in the production of enveloped viruses and HIV VLPs as they are co-released by the producer cells [23–25]. EVs are a heterogeneous particle class and can be divided into exosomes (Ø 5-150 nm) and microvesicles (Ø 50-500 nm), and thus overlap with the size of HIV VLPs (Ø ~120 nm) [23,144,188]. Besides the similarity in size, HIV VLPs and EVs share comparable particle densities of 1.15-1.18 g/L (HIV VLPs) [233] and of around 1.14-1.20 g/L (EVs) [234], respectively. Though density gradient centrifugation allows the separation of HIV VLPs from considerable larger and smaller EVs with different densities in general, a separation of VLPs from EVs displaying same or similar densities is almost impossible to achieve [188,235]. Due to the lacking scalability and the incomplete removal of these contaminants, ultracentrifugation is thus largely limited to the utilization at lab scale. For pharmaceutical applications, higher product purities are required to meet the quality and safety specifications for the administration to humans. Vaccine-related

issues regarding the tolerability may arise from the presence of host cell proteins (HCPs), which are commonly incorporated on the surface of both EVs and VLPs [153,236]. The excessive presence of HCPs in the product could cause undesired effects in the vaccinees, as immune responses can be distracted from HIV Gag and Env proteins towards immunogenically non-relevant proteins. To increase the relative level of immune-relevant viral proteins in the final product, high purification grades of the HIV VLP preparations are thus required. Purification of HIV VLPs at large-scale is frequently achieved by chromatography and filtration based methods [24,25,51,224,237]. Both techniques can be easily scaled up and facilitate working under the guidelines of good manufacturing practice (GMP). Tangential flow filtration (TFF) is commonly utilized prior to chromatography to concentrate virus-derived particles, to remove small impurities and to perform buffer exchange. However, the design of the TFF process needs careful consideration, as pressure variations, high shear forces, and foaming can impair the final product quality [238]. The lipid envelope of HIV VLPs makes them sensitive to physicochemical conditions including pH variations and varying osmotic pressures. In addition, shear forces can cause a process called "shedding" on Env-decorated HIV-1 VLPs [51]. During shedding, the weak non-covalent interaction between the surface unit gp120-SU and the transmembrane unit gp41-TM in the Env heterotrimer facilitates the dissociation of both units. Remaining dysfunctional gp41-TM stumps on the VLP surface, as well as soluble gp120-SU monomers, expose non-neutralizing and immune-decoy epitopes deteriorating the quality of the immune response [192]. The optimization of HIV VLP TFF processes is thus valuable for future industrial production [237,239]. The filtration of HIV VLP containing suspensions is followed by anion exchange chromatography (AEX) or alternatively heparin affinity chromatography [24,25]. Based on the electrochemical properties of VLPs and using elution buffers with different ionic strength, the separation from EVs can be achieved. Collaborators of this project aimed at improving the purification of HIV VLPs after performing depth filtration and UF/DF in the process. The intermediate product purity of app. 20 % that was reached after UF/DF was increased to over 80 % after AEX [224]. Despite these promising results, further process optimization is required to gain higher product purities of >99 %. The purification is commonly followed by a polishing step in which remaining impurities are removed by size-exclusion chromatography (SEC). Further concentration of the product as well as an

optional buffer exchange are performed by TFF/DF [238]. The mandatory sterilization of the produced VLPs can be achieved by passage through filters with a pore size of 0.22 µM. However, this method is accompanied by considerable product losses. Valkama *et al*., 2020 observed 30-50 % loss in the sterilization of lentiviral vectors [240]. Additional sterilization is dispensable when the production process is performed aseptically [238]. The final step of the process is the formulation of the HIV VLP based vaccine in which lyophilization is conducted for log-term storage [225].
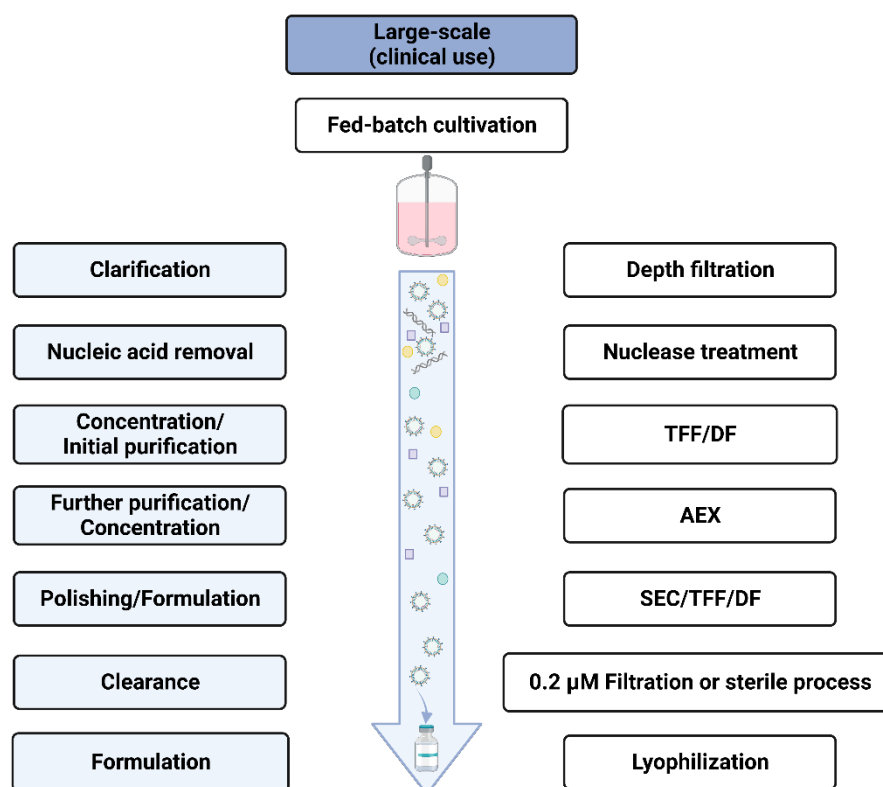
Figure 22. Process flow diagram showing the production of HIV VLPs and subsequent downstream processing. Production of VLPs is performed in fed-batch cultivation. Cells and cell-debris are removed and VLPs are captured from the culture supernatant during clarification. Nuclease is added to degrade cellular nucleic acids. Tangential flow filtration (TFF) and diafiltration (DF) are used for concentration. Anion exchange chromatography (AEX) is utilized for further purification and concentration. Polishing is performed by size-exclusion chromatography (SEC) and TFF or DF to remove remaining impurities. Product sterility is ensured by a final filtration step or by downstream processing under sterile conditions. Lyophilization is performed for the formulation of the VLPs. This figure was adapted from [51,225].

Another important aspect of the downstream processing is the final product quantification. While lentiviral ELISA kits are commonly utilized for the quantification of HIV derived particles at laboratory scale, it remains disadvantageous due to its low cost-effectiveness. In addition, this method does not allow the differentiation between intact HIV VLPs and protein monomers, unless the analyzed samples are subjected to prior ultracentrifugation. At industrial scale, quantification of virus derived particles is

often performed using state-of-the art techniques like nanoparticle tracking-analysis (NTA), flow virometry or chromatography coupled to multiangle light scattering (MALS) detectors [238,241,242]. These techniques allow for particle detection in parallel to quantification. Research groups around Cervera have further developed the quantification of HIV VLPs to a straightforward fluorescence based approach [235,241]. The green fluorescent protein (GFP) was fused to the core protein Gag and facilitated the proper detection and quantification of HIV VLPs. Fluorescence-tagged HIV VLPs not just allow the proper quantification in a heterologous suspension, but also facilitate the discrimination from non-fluorescent EVs.

In this work, the concept of GFP-tagged HIV VLPs was expanded by introducing a second fluorescence reporter dTomato fused to the transmembrane domain (TM) of the platelet derived growth factor receptor-beta (PDGFR β). PDGFR β TM mediates the incorporation of dTomato in the cell membrane and membrane-anchored reporter proteins should be present in the lipid bilayer of nascent VLPs and EVs as well, provided they locate at the site of particle budding. This way GFP-tagged HIV VLPs should reveal a double fluorescence while co-released EVs should only reveal single fluorescence (Figure 23). This concept has not yet been investigated and is supposed to enable the rapid discrimination of HIV-1 VLPs from EVs and the parallel quantification of both in heterologous suspensions. This novel tool is thus anticipated to prove helpful for determining the purity of VLPs in fractions obtained after different manufacturing steps during downstream processing. The ratio of VLPs and EVs is a valuable parameter to assess for the product purity. This work provides first insights into the design of the respective genetic constructs encoding the fluorescent fusion proteins and aims to prove their functionality upon expression in human cells.
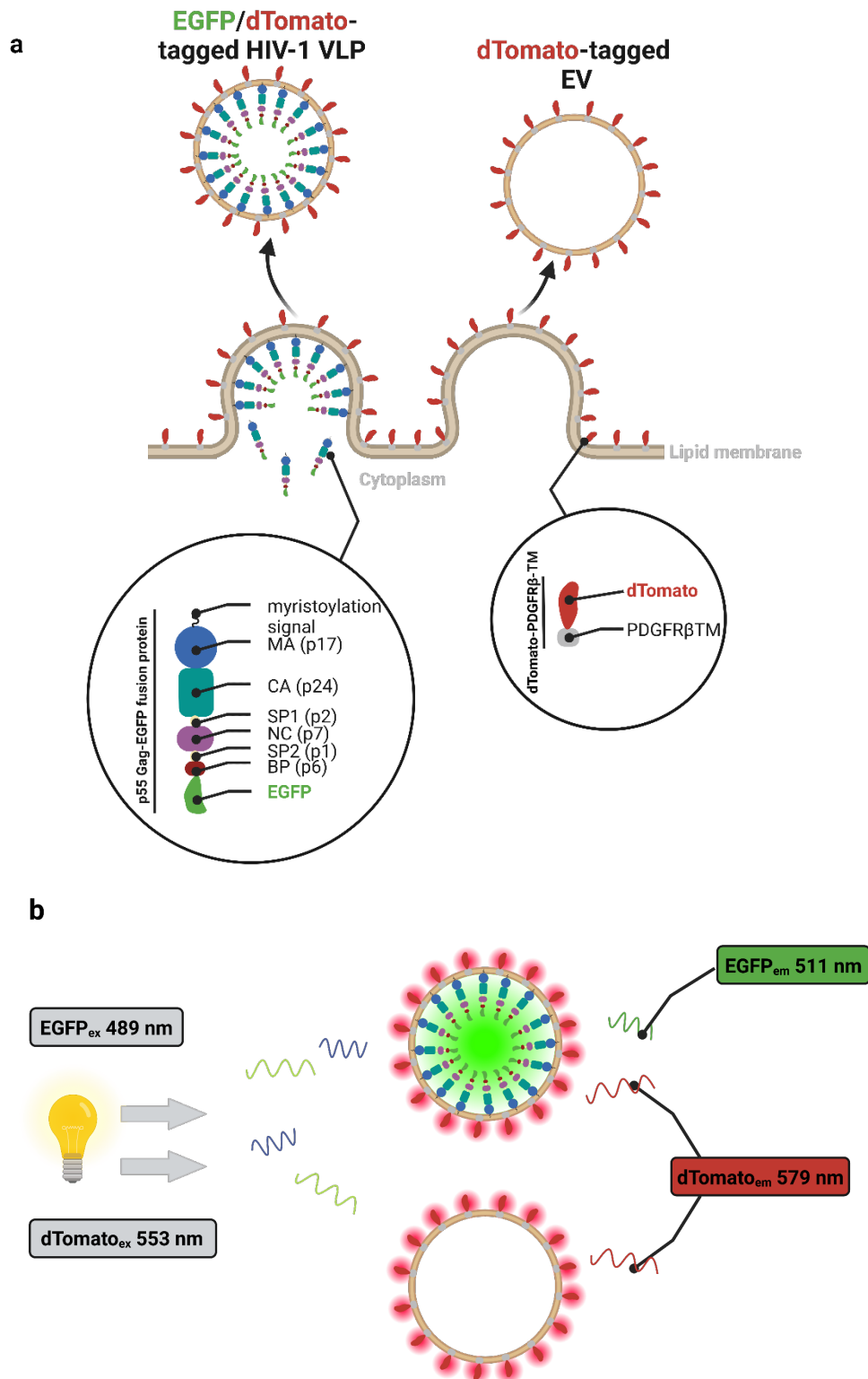
Figure 23. Schematic illustration of the bi-fluorescent HIV-1 VLP principle. The p55-Gag precursor protein of HIV-1 is C-terminally fused to the enhanced green fluorescent protein (EGFP). Immature Gag-EGFP VLPs bud from the producer cell membrane, which already contains incorporated dTomato proteins fused to the transmembrane (TM) domain of the platelet-derived growth factor receptor β (PDGFR β; a). The proof of concept is achieved by exciting HIV VLPs and co-released EVs. The particles should reveal double-fluorescence (HIV VLPs) and single-fluorescence (EVs), respectively (b).

8.2.   Results
8.2.1.   Functional expression of EGFP-tagged p55-Gag and dTomato membrane-anchored fusion proteins

To generate transposon vectors enabling the expression of the fluorescent fusion proteins, two expression constructs were generated (Figure 24). The first transposon vector PB-Mos1.Gag/EGFP-lpW contained the fusion gene *mos1.gag-egfp* coupled to the puromycin resistance gene. In addition, a *Sleeping Beauty*-based transposase vector SB-dTomato/PDGFR-β-TM-lnW was generated encompassing the fusion gene *dTomato-pdgfr β tm* coupled to the neomycin resistance gene.
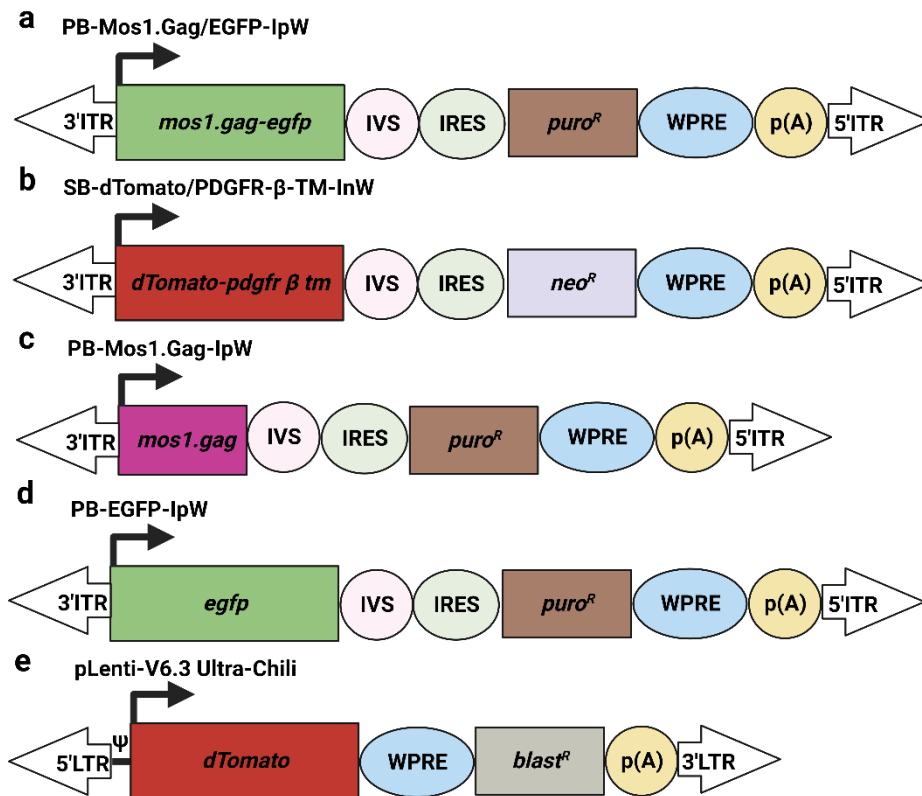
Figure 24. Schematic overview of the genetic elements in the expression cassettes of the fluorescent fusion protein expressing transposon vectors and control vectors. The structural organization of the expression cassettes is essentially the same as previously described for transposon vectors (Figure 16). The expression cassette entailing the fusion gene *egfp-mos1.gag* is flanked by the inverted terminal repeats (3' ITR and 5' ITR) derived from the *PiggyBac* transposase. The expression of *egfp-mos1.gag* is coupled to the expression of the puromycin (*puroR*) resistance gene (a). The expression cassette entailing the fusion gene *dTomato-pdgfr β tm* coupled to neomycin (*neoR*) expression is flanked by the inverted terminal repeats (3' ITR and 5' ITR) derived from the *Sleeping Beauty* transposase (b). PB-Mos1.Gag-lpW was previously described (Figure 16) and served as additional negative control in transient transfection experiments (c). The *PiggyBac* derived vector PB-EGFP-lpW served as positive control for EGFP expression in transient transfection experiments (d). The lentiviral vector pLenti-V6.3 Ultra-Chili was utilized as positive control for dTomato expression in transient transfection experiments. The transgene expression was coupled to the expression of the blasticidin (*blastR*) resistance gene. The expression cassette of this vector was flanked by long terminal repeats and included the packaging signal ψ (e).

In order to assess the functionality of the generated transposon vectors SB-dTomato/PDGFR-β-TM-lnW and PB-Mos1.Gag/EGFP-lpW, transient transfection experiments using 293T cells were performed. The cellular expression of the fluorescence reporters from each construct was visualized using fluorescence microscopy (Figure 25, I+II).
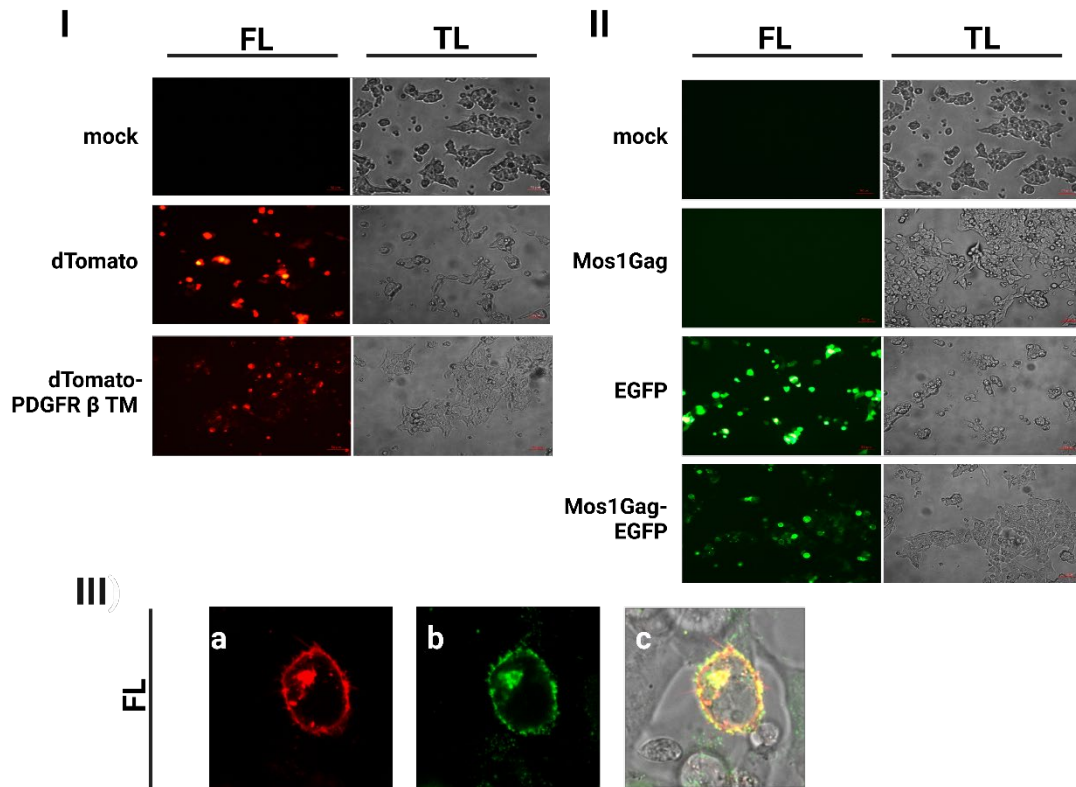
Figure 25. Fluorescence-microscopic images of transiently transfected 293T cells expressing the fusion proteins dTomato-PDGFR β TM (I) and the EGFP-Gag (II), respectively. Fluorescence (FL) and translucent (TL) images were taken three days post transfection with the respective vectors. Naïve 293T cells (mock) served as negative control. Cells transfected with vectors expressing the fluorescent proteins dTomato and EGFP, respectively served as positive control. The scale bar represents 50 μm. The figures were reproduced from [243]. Confocal images of a 293T cell transiently expressing the fusion proteins dTomato-PDGFR β TM and EGFP-Gag three days post transfection (III). The lipid membrane was visible in red along with a specific red point inside the cell (a). Gag-EGFP (green) was accumulated in close proximity to the lipid membrane and at a specific point inside the cell as well (b). Co-localization of Gag-EGFP and dTomato-PDGFR β TM (lipid membrane) was observed in yellow in the merged image (c).

Naïve cells (mock) as well as cells transfected with the vector PB-Mos1.Gag-IpW enabling the expression of untagged Mos1.Gag proteins served as negative controls. While the negative controls revealed no detectable fluorescence signals upon excitation, cells producing either the dTomato-PDGFR β TM or Mos1.Gag-EGFP fusion protein emitted red and green fluorescent signals, respectively. The observed red fluorescence for cells producing the dTomato-PDGFR β TM fusion protein was comparable to the one exhibited by cells of the positive control, which were previously transfected with a vector

facilitating the sole expression of dTomato. Analog observations were made for green fluorescent cells transfected with the vector encoding Mos1.Gag-EGFP and cells of the corresponding positive control exclusively expressing EGFP. In summary, detection of red or green fluorescence in 293T cells transfected with the vectors SB-dTomato/PDGFR-β-TM-lnW and PB-Mos1.Gag/EGFP-lpW demonstrated the successful expression of the two as fusion proteins (dTomato or EGFP).

In a following experiment the parallel localization of both reporter proteins in a single cell was assessed employing fluorescence confocal microscopy (Figure 25, III). Therefore, 293T cells were transiently co-transfected with the previously described vectors. Three days post transfection, cells were analyzed using confocal microscopy. The lipid membrane of the observed cells emitted red fluorescence proving that the transmembrane domain of the platelet derived growth factor receptor β facilitated the anchoring of dTomato proteins in the cell membrane. In addition, green fluorescence was observed in proximity to the lipid membrane where budding of HIV-1 VLPs takes place. While these observations were anticipated, the detection of a point-shaped accumulation of fusion proteins within the cell was unexpected. Analogue observations for Gag-EGFP proteins were made in previous reports and could be explained with the Gag-induced recruitment of the endosomal sorting complex required for transport (ESCRT) that catalyzes membrane fission during particle budding [56,244].

After confirming the functional expression of both fluorescence reporters, a p24-specific ELISA was performed to assess whether the fusion of EGFP impedes Mos1.Gag production. In addition, adverse effects of the parallel co-expression of the dTomato-PDGFR β TM fusion protein on Mos1.Gag expression were analyzed. For this, Mos1.Gag obtained from cell-free supernatant of transiently transfected cells served as positive control while cell-free supernatant from non-transfected cells served as negative control. The Gag concentrations were 3,114 (± 639) ng/mL for Mos1Gag, 2,730 (± 339) ng/mL for Mos1.Gag-EGFP and 2,852 (± 520) ng/mL for Mos1.Gag co-expressed with dTomato-PDGFR β TM. The results demonstrated that the expression of Mos1.Gag was neither significantly affected by the fusion to EGFP nor influenced by the parallel absence or presence of dTomato-PDGFR β TM (Table 2).

Table 2. Detection of Gag proteins in cell-free supernatants (CFSN) of 293T cells transiently expressing the
EGFP-tagged mosaic Gag proteins. Analysis was performed using a p24-specific ELISA (n=4, mean ± SD).

293T cells	ng Gag per mL CFSN	
transiently expressing	mean (n=4)	± SD
Mos1.Gag	3,114	639
Mos1.Gag-EGFP	2,730	339
dTomato-PDGFR β TM + Mos1.Gag-EGFP	2,852	520

8.2.2. Establishment of stable cell lines expressing fluorescently tagged fusion proteins

The previous results obtained from fluorescence microscopic- as well as from p24-
specific ELISA-analysis confirmed the functionality of both generated expression
constructs in the vectors PB-Mos1.Gag/EGFP-lpW and SB-dTomato/PDGFR-β-TM-
lnW, respectively. These were hence utilized for the following establishment of
transgenic human cell lines. This time a combination of *SB100x* and *hyPBase* mediated
transposition was employed for establishing the desired three cell lines (Figure 26).

The first cell line 293-F/PB-Mos1.Gag/EGFP-lpW was established by co-transfection of
the transposase vector encoding *hyPBase* and the vector encoding the Mos1.Gag-EGFP
fusion protein followed by a selection process using puromycin. In order to generate the
second cell line, 293-F cells were transfected with the transposase vector coding for
SB100x and the vector encompassing the dTomato/PDGFR-β-TM-lnW expression
cassette. The following selection with neomycin resulted in the establishment of the cell
line expressing 293-F/dTomato/PDGFR-β-TM-lnW. This cell line was attempted to serve
as a reference cell line for the later detection of dTomato-tagged extracellular vesicles in
cell-free supernatants and as starting material for the establishment of the third cell line
293-F/dTomato/PDGFR-β-TM-lnW/PB-Mos1.Gag/EGFP-lpW. Therefore, the cell line
293-F/dTomato/PDGFR-β-TM-lnW was again transfected utilizing the transposase
vector encoding *hyPBase* and the vector encompassing the fusion gene *mos1.gag-egfp*.
The combination of two transposon systems circumvents the excision of the first
transgene cassette containing *dTomato-pdgfr β tm* which was previously integrated
through *SB100x* activity, as *hyPBase* utilizes different ITRs for recognition. The

establishment of the third cell line was completed when cells showed resistance to puromycin (10 µg/mL) in addition to G418 (200 µg/mL).
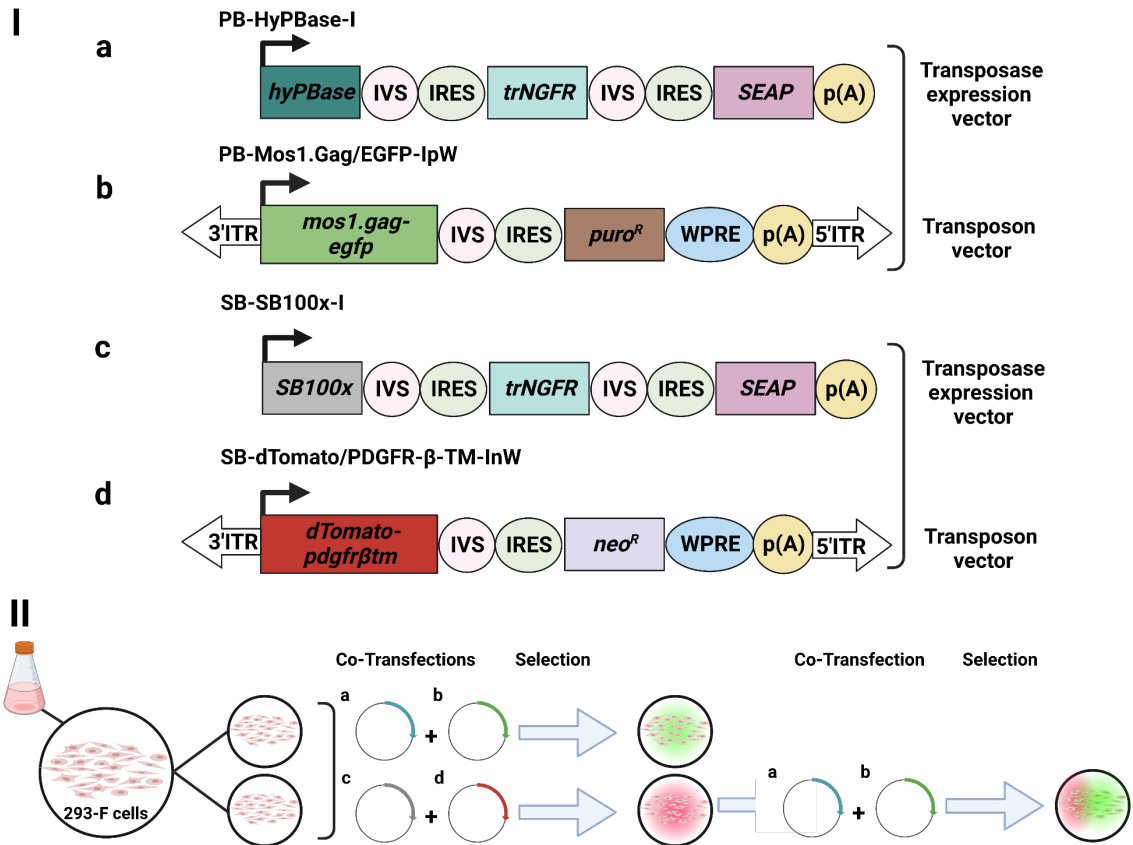
Figure 26. Schematic overview of the utilized transposon vectors and transposase expression vectors to generate stable 293-F cell lines expressing fluorescence-fusion proteins (I). The structural organization of the expression cassettes was previously described (Figure 16, Figure 24). The *PiggyBac* derived transposon vectors were utilized for the establishment of the stable EGFP-Gag producer cell line (green; II). To establish the dTomato-PDGFR β TM-expressing cell line (red), *Sleeping Beauty* derived transposon vectors were used for transfection. After completion of the selection process, this cell line was again transfected utilizing the *PiggyBac* derived transposon vectors to facilitate expression of EGFP-Gag proteins (red and green).

Upon passaging of the three cell lines, it became apparent that resulting cell pellets exhibited visible red and green fluorescence compared to cell pellets from naïve cells, thus corroborating the prior findings that both reporter proteins were successfully expressed (Figure 27 a). Subsequently, the cell lines expressing Mos1.Gag-EGFP fusion proteins were assessed concerning their ability to mediate VLP formation. Therefore, the cell-free supernatants of all cell lines and those from naïve cells were subjected to ultracentrifugation. The cell line which solely expressed the fusion protein dTomato-PDGFR β TM produced a light red shimmer at the bottom of the centrifuge tube, supposedly resulting from the presence of dTomato-tagged EVs. The parallel ultracentrifugation of cell-free supernatants of Mos1.Gag-EGFP expressing cell lines

resulted in brightly colorful pellets, which gave a first indication of unhampered VLP formation mediated by the fusion proteins (Figure 27 b).
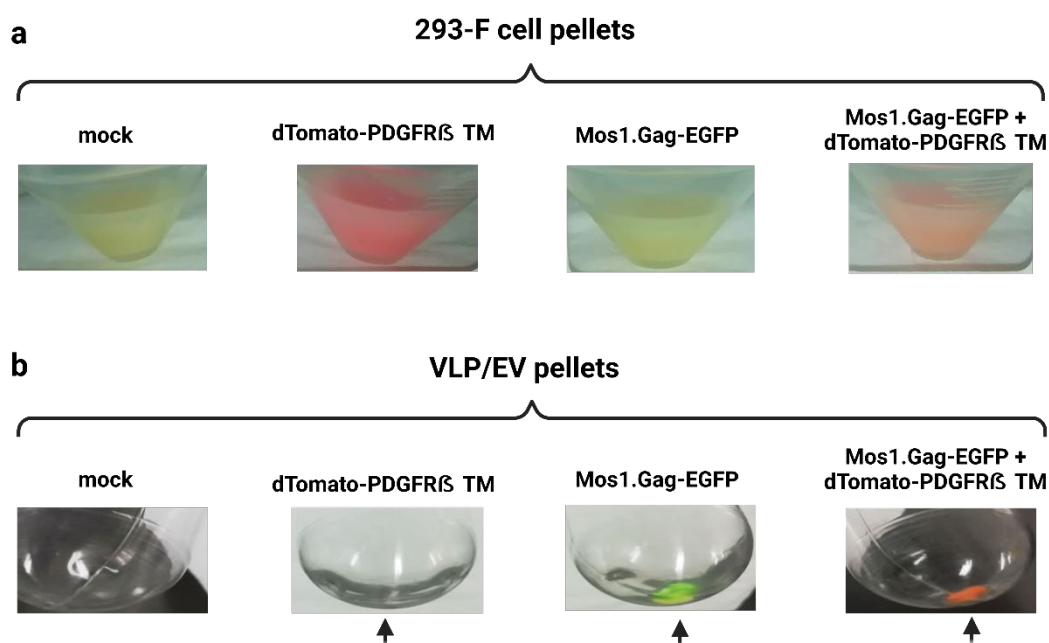
Figure 27. Detection of visible red and green fluorescence in cell pellets (a) and VLP pellets (b) from stable VLP producer cell lines and the reference cell line only expressing the fusion protein dTomato-PDGFR β TM. A sample obtained from naïve 293-F cells served as negative control (mock). The arrows at the bottom of the tubes indicate the pellets visible upon ultracentrifugation of cell-free supernatants.

8.2.3. VLP formation mediated by Gag-EGFP and incorporation of dTomato-PDGFR β TM fusion proteins

To examine, whether VLPs and EVs were concentrated upon ultracentrifugation, isolated pellets were subjected to TEM-analysis (Figure 28). Analogue to the previous observation made for Mos1.Gag proteins, Mos1.Gag-EGFP fusion proteins were demonstrated to assemble into HIV VLPs upon stable expression in 293-F cells. Moreover, the resulting EGFP-tagged HIV VLPs were comparable in size and morphology to Mos1.Gag-formed formed particles in the absence of EGFP (Figure 17) [16,188]. The demonstrated ability of Gag-EGFP fusion proteins to form fluorescent HIV VLPs is in accordance with the findings made by Gutiérrez-Granados and colleagues [241].
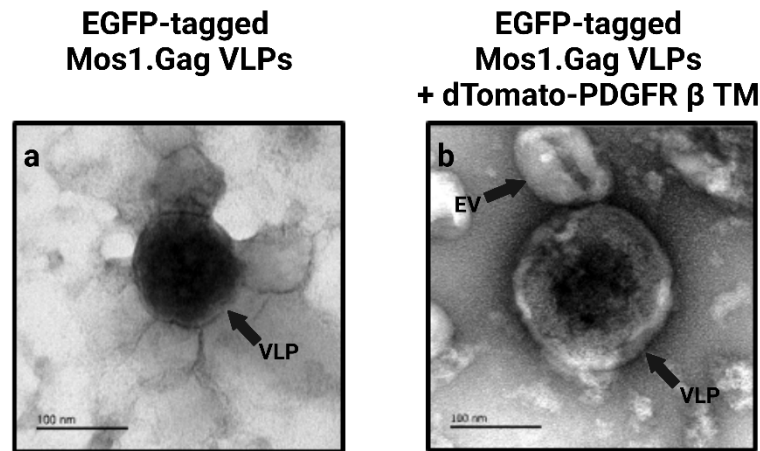
Figure 28. Negative-stain TEM images of the detected Gag-EGFP mediated VLP formation. VLP samples were obtained from ultracentrifugation of cell-free supernatants harvested from 293-F cell lines stably expressing Gag-EGFP in the absence (a) or presence of dTomato-PDGFR β TM co-expression (b). The arrows indicate an extracellular vesicle (EV) and VLPs. The scale bars represent 100 nm.

After successful visualization of VLPs using TEM-analysis, the presence of EGFP-tagged Mos1.Gag proteins in these VLPs, as well as the incorporation of dTomato-PDGFR β TM fusion proteins in the lipid bilayer of EVs and VLPs, was assessed using Western blot-analyses. Therefore, the resuspended VLP pellets of the three cell lines, a negative control representing a sample taken from naïve 293-F cells and a positive control containing a VLP pellet from *mos1.gag* transgenic cells, were subjected to SDS-PAGE. Upon blotting, membranes were incubated with polyclonal antibodies (pAbs) directed against p55-Gag, EGFP and dTomato, respectively (Figure 29).

The negative control revealed no detectable proteins in any of the three Western blots, indicating that unspecific binding of the three utilized polyclonal antibodies did not occur. In the Western blot-analysis performed with polyclonal antibodies directed against dTomato proteins, these proteins were exclusively detected both, in EV and VLP samples of cell lines expressing dTomato-PDGFR β TM in the absence or presence of Gag-EGFP. Despite the observation of presumed degradation products of these fusion proteins, full-length dTomato-PDGFR β TM proteins were readily detected at the expected size of 40.8 kDa in both samples. As the amount of dTomato-PDGFR β TM proteins in Gag-absent samples was low when using the standard procedure for SDS-PAGE sample preparation, 10x higher sample concentrations were subjected to Western blot-analysis employing dTomato-specific antibodies (Figure 29 a). In a next Western blot-analysis

p55-Gag precursor proteins were readily detected at the expected size of 55.9 kDa in the positive control utilizing polyclonal antibodies directed against Gag proteins (Figure 29 b).
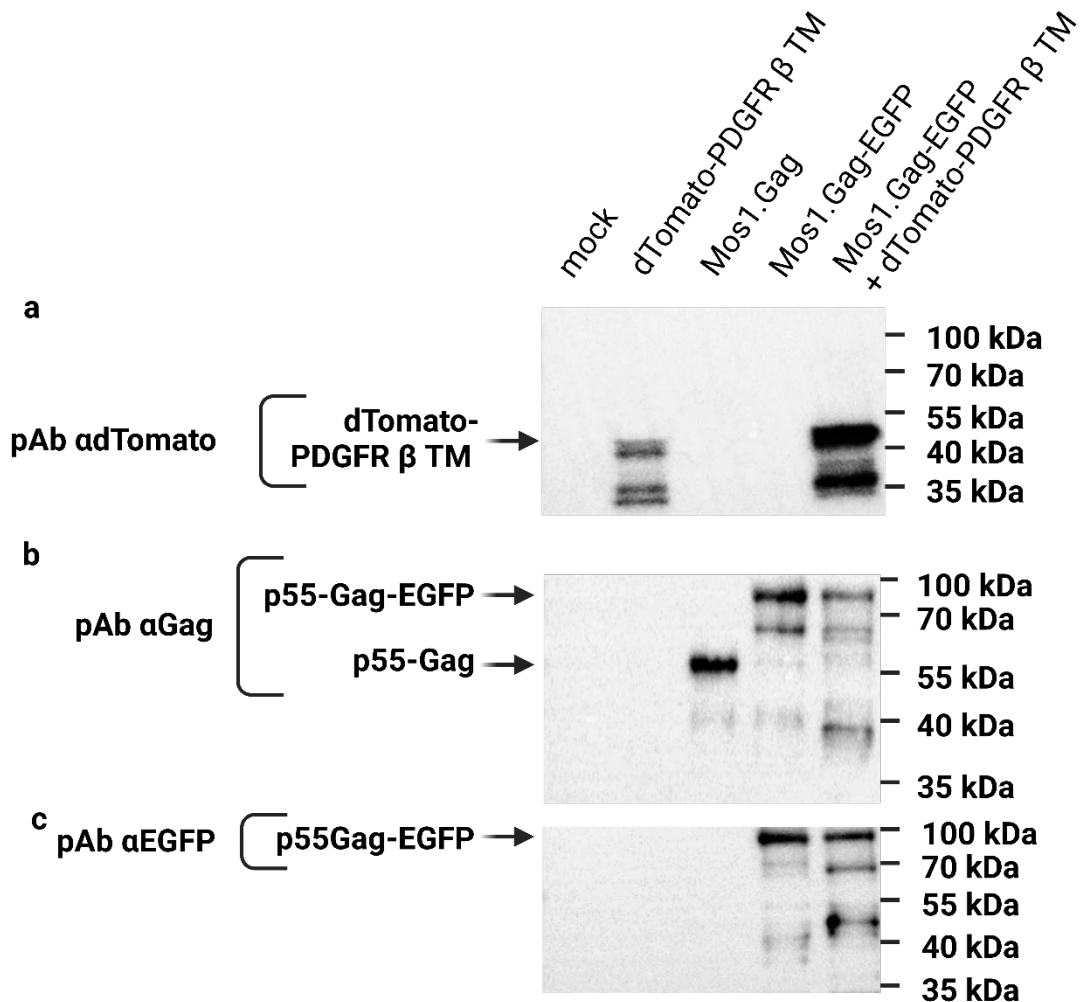
Figure 29. Detection of Gag, EGFP and dTomato in VLP samples using Western blot-analyses. Samples of naïve cells (mock) served as negative controls. The dTomato proteins were detected using polyclonal primary goat antibodies directed against dTomato followed by incubation with secondary horseradish peroxidase (HRP)-conjugated antibodies against goat (a). The mosaic p55-Gag precursor proteins in the VLP pellets were detected using polyclonal primary rabbit antibodies directed against HIV-1 Gag proteins followed by incubation with secondary horseradish peroxidase (HRP)-conjugated antibodies against rabbit (b). EGFP was detected in VLP samples using polyclonal HRP-conjugated rabbit antibodies directed against GFP (c). The positions of the molecular weight markers are shown on the right. The arrows on the left indicate the positions of detected Gag, EGFP and dTomato alone or as fusion proteins.

Full-length fusion proteins were also detected in the two samples containing the Mos1.Gag-EGFP fusion proteins (85.4 kDa) along with presumed degradation products. In order to prove the presence of EGFP in these fusion proteins, polyclonal antibodies directed against EGFP were utilized in another Western-blot analysis. Mos1.Gag-EGFP

fusion proteins with a molecular weight of about 85 kDa, and thus similar to the previously detected Gag-EGFP fusion proteins using pAbs against Gag were readily detected. Again, some presumed degradation product were observed (Figure 29 c). In order to quantify the fluorescent VLP production of both Mos1.Gag-EGFP producing cell lines, VLP samples were subjected to a p24-specific ELISA performed in triplicates. Both cell lines revealed high concentrations of 5.7 ($\pm$ 1.0) x 10^9 VLPs/mL cell-free supernatant for 293-F/PB-Mos1.Gag/EGFP-lpW and 6.4 ($\pm$ 1.1) x 10^9 VLPs/mL cell-free supernatant for 293-F/dTomato/PDGFR-β-TM-lnW/PB-Mos1.Gag/EGFP-lpW. These results advanced the previously reported concentration of 2.7 x 10^9 VLPs/mL in cell-free supernatants for GFP-tagged HIV-1 VLPs transiently produced in 293-F cells [244].

8.3.   Discussion

VLPs are increasingly utilized in vaccine development [245]. The co-release of EVs with similar physicochemical properties represents a bottleneck for following downstream processes. Despite the development of superior chromatographic and filtration techniques for HIV-1 VLP manufacturing, there is still a large demand for further improvement. The research groups around Cervera and co-workers were the first to produce HIV VLPs tagged with EGFP to enable quick detection and quantification using NTA and spectrofluorometric instruments [235,241,246]. In this work, the generation of EGFP-tagged HIV VLPs was reproduced and served as the basis for developing a new concept, which should allow for the efficient high-throughput discrimination of VLPs from EVs in heterologous suspensions using fluorescence detectors. This concept employs a second dTomato reporter protein anchored in the lipid membrane facilitated by fusion to the transmembrane domain of PDGFR β. This approach was already shown to enable the display of various proteins on the surface of retroviral VLPs and proved successful in this study as well [247–249]. The reported findings demonstrated the first successful presentation of dTomato fluorescence proteins on the surface of HIV VLPs formed by Mos1.Gag-EGFP. The detection of the fluorescence fusion proteins using Western blot-analysis confirmed the previously observed color patterns exhibited by respective VLPs and EVs pelleted upon ultracentrifugation. The low concentration of dTomato in the absence of Gag expression, and thus in VLP-free EV-containing samples hereby corresponded with the dimly red color of the obtained EV pellet. On the other hand, the

large amount of dTomato proteins detected in VLP pellets using Western blot-analysis indicated the efficient incorporation of dTomato fusion proteins into both, EVs and VLPs. In addition, VLP formation was not hindered by fusion of EGFP to Mos1.Gag, clearly observable by the bright green color exhibited by the VLP pellet. The observed red to orange fluorescence of the pellet containing both fusion reporter proteins was expectable as well, as the EGFP-tagged VLPs were demonstrated to be surrounded by a lipid bilayer displaying dTomato proteins [247–249].

These findings served as a proof-of-principle and offer the opportunity to further drive this concept towards a technically mature method for the straightforward quantification of HIV-1 VLPs in parallel to their discrimination from EVs. Follow-up investigations are necessary to substantiate the present data. The confocal-microscopic analysis of VLP budding events from the stable recombinant cells could provide visual proof of the bi-fluorescent VLPs and mono-fluorescent EVs, respectively [250]. The use of nanoparticle tracking-analysis would be an ideal method to further validate the proven concept, as it allows the combined detection of the particle number, their size distribution and their fluorescence in heterologous suspensions [241]. The efficient in-process tracking of EGFP-tagged HIV-1 VLPs was already demonstrated helpful in the optimization of the purification process when using size-exclusion chromatography (SEC) coupled to multi-angle light scattering (MALS) in combination with fluorescence monitoring [242]. Thus, MALS mediated detection would ideally be available in combination with fluorescence devices in the future purification process of the produced bi-fluorescent HIV-1 VLPs and mono-fluorescent EVs. Together, they should enable particle detection, discrimination and quantification. However, the herein presented concept can work without such instruments, as fluorescence plate readers commonly available in research facilities, should already suffice for the performance of high-throughput assays. As the established producer cell lines already revealed high productivities in a standard shaking-culture, they are promising tools for upscaling experiments in bioreactor systems. Higher product yields would enable chromatographic methods for purification representing the first step towards the optimization of existing HIV-1 VLP downstream processes. The established bi-fluorescent cell lines could serve as a valuable tool for HIV-1 VLP downstream process optimization to achieve very high product purity of >99 %, thus abiding highest standards set for the desired administration of the produced VLPs to humans.

9.   Conclusion

In summary and as shown in this thesis, the expression of HIV mosaic Gag sequences recently utilized in the vaccine clinical trial MOSAICO (NCT03964415) induced functional VLP formation in human cells. The demonstrated detection of neutralization-sensitive epitopes in Mos2S.Env proteins on the surface of these VLPs is crucial for the quality as a potential vaccine component. The administration of such Mos2S.Env-decorated mosaic Gag VLPs could contribute to robust immune responses in vaccinees - most importantly by eliciting broadly neutralizing antibodies.

In the second part of this thesis, a concept for the improved isolation and purification of such HIV VLPs was validated. As demonstrated with initial experiments, HIV VLPs can be separately detected and distinguished from contaminating extracellular vesicles when both particle types harbor fluorescent proteins. As the established expression cell line expressed red fluorescence proteins anchored in the cell membrane, both, HIV VLPs and extracellular vesicles displayed respective fluorescence signals. The additional marking of HIV VLPs through fusion of Gag to EGFP resulted in particles displaying double fluorescence. The established cell lines might thus serve as valuable tools to develop rapid screening methods during the purification of enveloped VLPs and for the optimization of existing downstream processes.

10. Material and Methods

10.1. Materials
10.1.1. Technical devices

Table 3. List of technical devices utilized in this work.

Device	Item name	Company, country
Centrifuge	ROTINA 420R	Hettich, Germany
Centrifuge	MIKRO 200 R	Hettich, Germany
Confocal microscope	LSM 980 with Airyscan 2	Carl Zeiss, Germany
Electron microscope	200 kV JEOL JEM-2100PLUS	JEOL, Germany
Fluorescence microscope	Axio Vert.A1	Carl Zeiss, Germany
Freezer (-80 °C)	HERAfreeze HFC-series 8740	Thermo Fisher Scientific, USA
Imaging system	ChemiDoc XRS+ System	Bio-Rad, USA
Incubator (adherent 293 cells)	Heracell™ incubator	Thermo Fisher Scientific
Incubator (bacteria)	Heratherm™	Thermo Fisher Scientific, USA
Incubator (suspension 293 cells)	Minitron	Infors HT, Switzerland
Microplate reader	Multiskan™ FC	Thermo Fisher Scientific, USA
Orbital shaker (bacteria)	MaxQ™ 4000	Thermo Fisher Scientific, USA
Power supply	PowerPac™ Basic Power Supply	Bio-Rad, USA
Rotator	REAX2	Heidolph Instruments, Germany
Safety cabinet (293 cells)	HERAsafe KSP18	Thermo Fisher Scientific, USA
Safety cabinet (bacteria)	HERAsafe KS12	Thermo Fisher Scientific, USA
Spectrophotometer	UV5Nano	Mettler Toledo, USA
Thermal mixer	T100 Thermal Cycler	Bio-Rad, USA
Thermal mixer	Cooling Thermal Shake Touch	VWR, USA
Thermal mixer	Cel Media TS basic	Cellmedia GmbH und Co. KG, Germany
Transluscent microscope	VWR VisiScope IT404 Inverted Phasecontrast Microscope	VWR, USA
Ultracentrifuge	Optima XE centrifuge	Beckman Coulter, USA
Vortexer	neoVortex®	neoLab Migge GmbH, Germany
Water bath	Julabo TW12 EcoTemp	Julabo GmbH, Germany

10.1.2. Chemicals

All chemicals were obtained from Carl Roth (Germany), Sigma Aldrich (USA) and Thermo Fisher Scientific (USA).

10.1.3. Software

The search for literature, protein sequences and nucleotide sequences was performed using the databases provided by the national center for biotechnology information (NCBI) [251]. Nucleotide and protein sequences were analyzed using the basic local alignment search tool (BLAST) [252]. Protein sequences were further analyzed using the expert protein analysis system (Expasy) [253,254]. The molecular model of the HIV Env trimer was prepared using Chimera [202]. Molecular cloning was performed *in silico* using the SnapGene software [255]. The melting temperature of oligonucleotides was calculated using the online tool "Oligo Calculator version 3.27" [256]. The image data obtained from confocal microscopy were analyzed using the software imageJ [257]. Data obtained from ELISA were analyzed using Microsoft Excel (2016) [258]. The thesis was written in Microsoft Word (2016) [259]. References were included in this document using citavi [260]. The figures in this thesis were created with BioRender.com.

10.2. Methods in Molecularbiology
10.2.1. Molecular cloning of the expression constructs
10.2.1.1. Molecular cloning of the mosaic Gag and Env expression constructs

For the cloning of *mos1.gag*, *mos2.gag* and *mos2s.env* into respective donor vectors, transposon vectors were generated based on the genetic design of previously described *Sleeping Beauty* derived vectors of our group [261]. The DNA sequences for the *hyPBase* ITRs originated from the plasmid PB-CAG-DDdCas 9VP192-T2A-GFP-IRES-Neo, which was a gift from Timo Otonkoski (Addgene plasmid #102885; http://n2t.net/addgene:102885; RRID:Addgene_102885) [262]. The DNA sequences for the ITRs were synthesized (GenScript, USA) and inserted into pUC57 resulting in pUC57-hyPBaseITRs. The transgene expression cassettes of the *Sleeping Beauty* derived donor vectors SB-egfp-IpW and SB-egfp-IhW, respectively, were inserted into pUC57-hyPBaseITRs using FseI restriction sites leading to the generation of the vectors PB-egfp-IpW and PB-egfp-IhW, respectively. The DNA sequences for the mosaic genes were taken from the patent US 10,369,214 (Chapter 9.3) [14]. These DNA sequences were synthesized using codon optimization for expression in human and Chinese hamster ovary (CHO) cells and inserted in the vector pUC57 (GenScript, USA). The amplification of mosaic genes was conducted using the primer pairs 1 and 2 from Table 9. Prior to the insertion of *mos1.gag* and *mos2.gag* amplicons in the vector PB-lpW by Gibson

assembly, the vector was linearized utilizing the restriction enzymes BamHI and BstXI [263]. The Gibson assembly generated the vectors PB-Mos1.Gag-IpW and PB-Mos2.Gag-IpW, respectively. The third insert *mos2s.env* and the vector PB-IhW were amplified using the primer pairs 3 and 4 from Table 9 and following assembly of the amplicons to obtain the vector PB-Mos2S.Env-IhW was performed using Gibson assembly [263].

10.2.1.2. Molecular cloning of the *hyPBase* expression construct

The DNA sequence encoding the *hyPBase* [170] was taken from the pCAG-hyPBase vector (Gene bank accession number: OL519599.1). The sequence was synthesized using codon optimization for expression in human and CHO cells and was inserted into pUC57 (GenScript, USA). The amplification of *hyPBase* from this plasmid was facilitated using the primer pair 5 from Table 9. The resulting amplicon was flanked by restriction site motifs for the restriction enzyme NotI. These were utilized to exchange the *Sleeping Beauty SB100x* transposase gene in CMV-SB100x [261] by that of *hyPBase* to generate PB-hyPBase-I.

10.2.1.3. Molecular cloning of the Mos1.Gag-EGFP expression construct

The gene *mos1.gag* was amplified from the vector pUC57-mos1gag using the primer pair 6 Table 9. The gene *egfp* was amplified from the vector PB-egfp-IpW using the primer pair 7 from Table 9. Both amplicons were afterwards assembled using overlap-extension (OE)-PCR. The vector PB-egfp-IpW was linearized using the restriction enzymes BamHI and BstXI. The fusion gene *mos1.gag-egfp* was subsequently inserted in the linearized vector by Gibson assembly [263] resulting in the generation of the vector PB-Mos1.Gag/EGFP-lpW.

10.2.1.4. Molecular cloning of the dTomato-PDGFR β TM expression construct

To prepare the cloning of the fusion gene *dTomato-pdgfr β tm* into the donor vector, several intermediate products had to be generated. First of all, the puromycin resistance gene in the vector SB-egfp-IpW was exchanged with the neomycin resistance gene from the vector SB-neo. Both vectors were already available in our working group. The vector SB-egfp-IpW was linearized utilizing the restriction enzymes PsyI und CsI. The

neomycin resistance gene was amplified from SB-neo using the primer pair 8 from Table 9. The amplicon was inserted into SB-egfp-IpW using Gibson assembly [263] to obtain the vector SB-egfp-InW (intermediate product 1). The expression cassette including the genes *enhanced cyan fluorescent protein* (*ecfp)* and *platelet derived growth factor receptor β transmembrane* (*pdgfr β tm)* was amplified from pDisplay-AP-CFP-TM, which was a gift from Alice Ting (Addgene plasmid #20861; http://n2t.net/addgene:20861; RRID:Addgene_20861) using the primer pair 9 from Table 9 [264]. The vector SB-egfp-InW was linearized using the restriction enzymes AgeI and Bsp14071I and the *ecfp-pdgfr β tm* amplicon was subsequently inserted using Gibson assembly [263]. The resulting vector was SB-ecfp-pdgfr-β-TM-lnW (intermediate product 2). In order to provide a recognition site for the restriction enzyme Bsp14071I in this vector, a *QuikChange*[TM] PCR was performed utilizing the primer pair 10 from Table 9 [265]. The resulting vector was SB-ecfp-pdgfr-β-TM-lnW-QC (intermediate product 3). The gene *dtomato* was amplified from the vector pLenti-V6.3 Ultra-Chili, which was a gift from Ewa Snaar-Jagalska (Addgene plasmid #106173; http://n2t.net/addgene:106173; RRID:Addgene_106173) using the primer pair 11 from Table 9. The *dTomato* amplicon was hydrolyzed using the restriction enzymes SgsI and Bsp14071I. The same restriction enzymes were utilized to linearize the vector SB-ecfp-pdgfr-β-TM-lnW-QC. The linearized vector and the *dTomato* insert were ligated. The resulting final product was SB-dTomato/PDGFR-β-TM-lnW.

10.2.2. Molecular cloning methods
10.2.2.1. Restriction digests and ligations

Restriction digests, dephosphorylations and ligations of plasmid DNA and of DNA fragments were performed utilizing enzymes from the companies NEB, USA and Thermo Fisher Scientific, USA. The protocols were followed according to the manufacturer's instructions. The incubation of the reaction samples was performed in the thermal mixer Cooling Thermal Shake Touch (VWR, USA). Examples of the reaction mixtures are given in Table 4 and Table 5.

Table 4. Exemplary reaction mix for restriction digests using fast digest enzymes from Thermo Fisher Scientific (USA). The total reaction volume was 20 µL. The standard procedure involved the incubation of the sample mixture at 37 °C for maximal 10 min.

Component	Volume (µL)
Plasmid DNA or DNA fragment	variable (up to 1 µg)
10x FastDigest® Green buffer	2
FastDigest® enyzme	1
DEPC-H_2O	to 20

Table 5. Exemplary reaction mix for ligations using T4-ligase from NEB (USA). The total reaction volume was 20 µL. The standard procedure involved the incubation of the sample mixture at room temperature for app. 2 h or overnight at 4 °C.

Component	Volume (µL)
Plasmid DNA or DNA fragment	variable
T4-DNA ligase reaction buffer	2
T4-ligase	1
DEPC-H_2O	to 20

10.2.2.2. Polymerase chain reaction (PCR)

The amplification of nucleotide sequences from DNA fragments or plasmids were conducted using PCR. A PCR mix consisted of the following components: plasmid DNA or DNA fragments, deoxynucleoside triphosphates (dNTPs; NEB, USA), diethyl pyrocarbonate (DEPC)-treated H_2O (Carl Roth, Germany), primers (Eurofins Scientific SE, Luxembourg), polymerase, buffer and optional GC enhancer (Table 6). The PCRs were performed using either the Q5® High-Fidelity DNA Polymerase, the Phusion® High-Fidelity DNA Polymerase or the Q5® Hot Start High-Fidelity DNA Polymerase in combination with the appropriate buffer (NEB, USA). The negative control contained additional DEPC-H_2O instead of DNA. The reaction vials containing the PCR mix were then transferred to the thermal cycler T100 (Bio-Rad, USA) and the temperature protocol was started (Table 7). The annealing temperatures (T_A) were calculated based on the DNA sequences of the primers using the program Oligo Calculator version 3.27 [256]. The elongation time was calculated based on the length in kilobases (kb) of the desired product assuming that the Q5® High-Fidelity DNA Polymerase would require 20-30 sec/kb for elongation as stated by the manufacturer. In order to join two DNA fragments and amplify the resulting product overlap-extension (OE)-PCR was performed. The reaction mixture was essentially the same as stated in Table 6. The protocol consisted of two steps. In the first step the fragments in the PCR reaction mix were joined in a short PCR program,

which was performed for 10 cycles and an annealing temperature that was 4 °C higher than the calculated T_A for the primers. In the next step, this PCR mix served as template in a freshly prepared PCR mix, which otherwise contained the same components. Amplification of the template was conducted in the thermal cycler using the annealing temperature for the primer pair and a total PCR cycle number of 20.

Table 6. Exemplary reaction mix for a standard PCR using the Q5® High-Fidelity DNA Polymerase (NEB, USA) in a reaction volume of 25 µL.

Component	Final cocentration
Plasmid DNA or DNA fragment	~50 ng
dNTPs (10 mM)	200 µM
Forward primer (10 µM)	0.5 µM
Reverse primer (10 µM)	0.5 µM
Q5® High-Fidelity DNA Polymerase	0.5 U
5x Q5 Reaction Buffer	1x
5x Q5 Reaction GC enhancer	1x
DEPC-H_2O	to 25 µL

Table 7. Standard temperature program utilized in the thermal cycler for conducting PCRs.

Step	Temperature (°C)	Time	Cycle number
Inital denaturation	95	3 min	1
Denaturation	95	30 sec	
Annealing	variable	variable	25-34
Extension	72	1 min	
Final extension	72	5-15 min	1
Hold	4		∞

10.2.2.3. Site-directed mutagenesis using *QuikChange*™ PCR

Site-directed mutagenesis in a plasmid was performed using a method based on the *QuikChange*™ PCR previously developed by Stratagene (USA) [265]. This method was used to provide a recognition site for the enzyme Bsp14071I in the vector SB-ecfp-pdgfr-β-TM-lnW (Chapter 8.2.1.4). The PCR mix was prepared analogue to the example given in Table 6. As additional control served a PCR mix, which was prepared without Q5® High-Fidelity DNA Polymerase (NEB, USA) in order to prove the amplification of the template in the samples. This control was necessary, as both the template and the product size were the same. The amplification of the DNA template was performed in the thermal cycler. The temperature program entailed an annealing temperature of 52 °C, an elongation time of 3 min per cycle and 25 cycles in total. After completing the program,

the PCR mix was prepared for agarose gel electrophoresis and resulting visualized DNA products were isolated from the gel (Chapter 8.2.2.5). The maximal sample volume of 17 µL was utilized for ligation (Chapter 8.2.2.1). In order to degrade methylated template DNA, 1 µL of the restriction enzyme DpnI (NEB, USA) was added to the ligation mix. Incubation was performed for 2 h at room temperature before 5 µL of this mix were utilized for the transformation of competent *E. coli* cells (Chapter 8.2.3.1).

10.2.2.4. Gibson assembly

The Gibson assembly was performed to join DNA fragments in a single isothermal reaction [263]. The Gibson assembly master mix was prepared according to Table 8 and stored in aliquots of 10 µL at -20 °C. The DNA fragments, which were planned for the assembly, were added in a total volume of 10 µL to one aliquot of the Gibson assembly master mix. The following incubation was performed at 50 °C for 1 h using the T100 Thermal Cycler (Bio-Rad, USA). Transformation of competent *E. coli* cells was carried out subsequently using 5 µL of the Gibson assembly mix (Chapter 8.2.2.4).

Table 8. Components of the Gibson assembly master mix. The enzymes were obtained from the companies NEB, USA and Thermo Fisher Scientific, USA.

Components	Volume (µL)
sterile dest. H_2O	309
ISO buffer*	60
T5-Exonuclease	24 (8 U)
Phusion polymerase	18 (18 U)
Taq-Ligase	39 (390 U)

* Components of the ISO buffer: ~780 mM/pH 7.5 Tris-Cl, ~69 mM $MgCl_2$, ~1.4 mM dNTP mix (NEB, USA), ~69 mM DTT, 0.03 % PEG-8000, ~6.9 mM NAD^+

10.2.2.5. Agarose gel electrophoresis and isolation of DNA fragments from gels

Agarose gel electrophoresis was conducted to separate the DNA fragments according to their size. Agarose gels with a concentration of 1 % were prepared and stained with 0.1 % SYBR™ Safe (Thermo Fisher Scientific, USA). The DNA samples were mixed with DNA Gel Loading Dye (6x) (Thermo Fisher Scientific, USA) and loaded on the gel. The DNA standard GeneRulerTM 1 kb Plus (Thermo Fisher Scientific, USA) was utilized for size determination of the DNA fragments. The gel run was performed using the PerfectBlue gel system (VWR, USA) in 1x TAE buffer (Carl Roth, Germany). The gels were run for app. 1 h at 120 V using the PowerPac™ Basic Power Supply (Bio-Rad,

USA). The DNA was visualized using the ChemiDoc XRS+ System and the corresponding software Image Lab™ version 5.2.1 (Bio-Rad, USA). DNA fragments were isolated from agarose gels using the Monarch® DNA Gel Extraction Kit (NEB, USA) according to the manufacturer's instructions. The melting of gel slices was performed in the thermal mixer Cooling Thermal Shake Touch (VWR, USA). Following centrifugation steps were carried out using the centrifuge MIKRO 200 R (Hettich, Germany).

10.2.2.6. Oligonucleotides

The herein utilized oligonucleotides were obtained from the company Eurofins Scientific SE, Luxembourg (Table 9). The oligonucleotides (primer) were adjusted to a concentration of 10 µM before using them for DNA amplification.

Table 9. Oligonucleotides utilized for the molecular cloning of the expression constructs.

Primer pair no.	Primer name	DNA sequence (5'→3')
1	mos1gag-fw	ttctgcagtcgacggtaccgcgggcccggtaccgatatcgcggccgcaccatg
	mos1gag-rv	ctcgcagacagcgaattaattccagcacaaagcttccagcacactggcccgggcta
2	mos2gag-fw	ttctgcagtcgacggtaccgcgggcccggtaccgatatcgcggccgcaccatg
	mos2gag-rv	ctcgcagacagcgaattaattccagcacaaagcttccagcacactggcccgggcta
3	mos2s.env-fw	ctagagaacccactgcttactggcttatcggctcggtaccgatatcgc
	mos2s.env-rv	ttccagcacactggttacttgtacagctcgaagcttccagcacactggc
4	pb-lhw-fw	tagtagcccgggccagtgtgctggaagcttcgagctgtacaagtaaccagtgtgctggaa
	pb-lhw-rv	catggtgcggccgcgatatcggtaccgagccgataagccagtaagcagtgggttctctag
5	hypbase-fw	atattatagcggccgcaccatggggagtagcctggacgacgagc
	hypbase-rv	atattatagcggccgctcatcagaaacaggactggcacatgtcgatattatg
6	OE-mos1gag-fw	attctgcagtcgacggtaccgcgggcccggaccatgggggcaagagcaag
	OE-mos1gag-rv	ccgggcccgcggtaccgtcgactgcagaattctgagctcgtcgacccgccctgggaggatgggtcgtttcc
7	OE-egfp-fw	aattctgcagtcgacggtaccgcgggcccgggatccaccggccggtcgccaccatggtgagcaagggcga
	OE-egfp-rv	tggccctcgcagacagcgaattaattccagttacttgtacagctcgtccatgc
8	neomycin-fw	agcccacggtgcgcctcgccacccgcgacgatgggatcggccattgaacaagatgg
	neomycin-rv	aggcaccgggcttgcgggtcatgcaccaggagatcagaagaactcgtcaagaaggc
9	ecfp-pdgfr β tm-fw	cagtcgacggtaccgcgggcccgggatccaaccatggagacagacacactcc
	ecfp-pdgfr β tm-rv	cagttatctatgcggccgctttacttgtacctaacgtggcttcttctgcc
10	QC-ecfp-pdgfr β tm-fw	(PHOSP)agctcgtccatgccgagag
	QC-ecfp-pdgfr β tm-rv	(PHOSP)gtacaagcggccgcggctg
11	dtomato-fw	atattaggcgcgccgatggtgagcaagggcgagga
	dtomato-rv	ccacgtcacctgcttgtttgag

10.2.2.7. Determination of the DNA concentration

The concentration of DNA in samples was measured using the spectrophotometer UV5Nano (Mettler Toledo, USA). The procedure entailed the proper mixing of samples, which was conducted using the neoVortex® (neoLab Migge GmbH, Germany).

10.2.2.8. DNA sequencing

In order to prove the correct insertion of the expression cassettes into plasmids, DNA sequencing was conducted by the company Microsynth, Switzerland. The DNA samples were prepared according to the instructions by the service provider.

10.2.3. Cultivation of *Escherichia coli* (*E. coli*)
10.2.3.1. Preparation of competent bacterial cells and their transformation

NEB Stable Competent *E.coli* cells (NEB, USA) were transformed with the generated plasmids in order to select for plasmid clones and to increase the plasmid number. Competent cells were prepared using the rubidium chloride method [266]. 100 mL Luria broth (LB) medium [267] were inoculated with the cells and incubated at 37 °C and 300 rpm in the MaxQ™ 4000 orbital shaker (Thermo Fisher Scientific, USA). As soon as the OD_{600} had reached app. 0.5, the cells were pelleted at 4000 rpm at 4°C for 10 min using the centrifuge ROTINA 420R (Hettich, Germany). The resulting cell pellet was resuspended using 33 mL solution I (100 mM RbCl, 50 mM $MnCl_2$, 30 mM/pH 5.8 potassium acetate, 10 mM $CaCl_2$, 15 % glycerol [w/v]). The resuspended cells were incubated on ice for 1 h and the centrifugation step was repeated. The resulting cell pellet was resuspended in 8 mL solution II (10 mM MOPS, 10 mM RbCl, 75 mM $CaCl_2$, 15 % glycerol [w/v]). The cells were incubated on ice for 15 min and shock-frozen in liquid nitrogen in 50 µL aliquots, which were stored in the HERAfreeze (Thermo Fisher Scientific, USA) at -80 °C. The transformation of competent cells was performed as follows. The competent cells were chilled on ice and the respective plasmid was added in a maximal volume of 5 µL. After 30 min incubation on ice, the cells were heat shocked at 42 °C for 30 sec. The cells were subsequently chilled on ice for 5 min. The mixture was spread on LB-agar plates containing 100 µg/mL ampicillin. The selection was performed with the antibiotic ampicillin, as all utilized plasmids contained the *bla* gene encoding the β-lactamase conferring ampicillin resistance. The following incubation of

the plates was performed in the incubator Heratherm™ (Thermo Fisher Scientific, USA) at 37 °C overnight or at room temperature for three days.

All steps involving the cultivation of *E.coli* cells were perfomed under sterile conditions by working in the bio-safety cabinet HERAsafe KS12 (Thermo Fisher Scientific, USA).

10.2.3.2. Cultivation of cell clones and isolation of plasmid DNA

In order to isolate plasmid DNA from the respective *E. coli* cell clone, 5 mL LB medium containing 100 µg/mL ampicillin were inoculated with one colony from the LB agar plate followed by overnight-incubation at 37 °C using 300 rpm in the orbital shaker MaxQ™ 4000 (Thermo Fisher Scientific, USA). The isolation of plasmid DNA from 4 mL *E.coli* culture was performed using the GeneJET Plasmid-Miniprep-Kit (Thermo Fisher Scientific, USA) according to the manufacturer's instructions. The procedure entailed the proper mixing of samples, which was conducted using the neoVortex® (neoLab Migge GmbH, Germany) and the centrifugation of samples, which was performed with the centrifuge MIKRO 200 R (Hettich, Germany). In order to isolate large amounts of plasmid DNA from cell cultures, a volume of 100 mL LB medium containing 100 µg/mL ampicillin was inoculated 1:100 using an overnight culture of an *E. coli* cell clone. Following incubation was performed at 37 °C using 300 rpm in the orbital shaker MaxQ™ 4000 (Thermo Fisher Scientific, USA) until the next day. The subsequent isolation of plasmid DNA was conducted using the NucleoBond Xtra Midi kit (Macherey-Nagel, Germany). The procedure entailed the proper mixing of samples, which was conducted using the neoVortex® (neoLab Migge GmbH, Germany) and the centrifugation of samples, which was performed with the centrifuge ROTINA 420R (Hettich, Germany).

10.3. Methods in cell biology
10.3.1. Eukaryotic cells and media

Adherent human embryonic kidney HEK293T cells (ATCC: CRL-3216) were grown in high glucose (4.5 g/L) Dulbecco's modified Eagle's medium (DMEM) supplemented with l-glutamine and 10 % fetal bovine serum (FBS; Gibco, Germany). Cells were cultivated at 37 °C in a humidified atmosphere containing 5 % CO_2 in a Heracell™ incubator (Thermo Fisher Scientific). For cultivation, flasks with a growth area of 75 cm² and vent

caps were utilized or 6-well plates with a growth area of 9.6 cm^2 (both Carl Roth, Germany). For passaging, cells were detached using 1 mM ethylenediamine-tetraaceticacid (EDTA) in 1x phosphate-buffered saline (PBS; Thermo Fisher Scientific, USA).

Human suspension 239-F cells (#R79007, RRID: CVCL_D603, Thermo Fisher Scientific, USA) were grown in serum-free 293-F-FreeStyle-Expression-Medium (Thermo Fisher Scientific, USA). The cultivation was mostly carried out in volumes between 50 and 200 mL medium using 125 mL to 500 mL disposable shaker flasks with vent caps (Nalgene Nunc International, USA). The incubation was performed at 37 °C, 8 % CO$_2$ and 135 rpm using a Minitron shaker incubator with an orbit of 5 cm (Infors HT, Switzerland).

All steps involving the cultivation of human cells, were carried out under sterile conditions by working in the bio-safety cabinet HERAsafe KSP18 (Thermo Fisher Scientific, USA).

10.3.2. Freezing and thawing of cells

Cell stocks of stable 293-F cell lines were prepared for long-term storage. Therefore, pellets containing 1×10^6 to 2×10^6 cells were prepared from a cell culture using a centrifugation step at 100 x g for 3 min at room temperature and the centrifuge ROTINA 420R (Hettich, Germany). The pellet was chilled on ice for 5 min and afterwards resuspended in 1 mL 293-F-FreeStyle-Expression-Medium (Thermo Fisher Scientific, USA) containing 10 % dimethyl sulfoxide (DMSO) [v/v]. Alternatively, the pellet was resuspended in 1 mL ibidi Freezing Medium Classic (ibidi GmbH, Germany). The suspension was transferred into a cryogenic vial. Initial freezing of the cell stock was performed using a Mr. Frosty™ Freezing Container (Thermo Fisher Scientific), which was placed at -80 °C in the HERAfreeze (Thermo Fisher Scientific, USA). After one day the cell stock was transferred into liquid nitrogen.

Thawing of the cell stocks was conducted at 37°C using a water bath (Julabo TW12 EcoTemp; Julabo GmbH, Germany). The cell suspension was afterwards transferred to 17 mL 293-F-FreeStyle-Expression-Medium (Thermo Fisher Scientific, USA), which was pre-warmed in a 125 mL disposable shaker flask with vent cap (Nalgene Nunc

International, USA). Adherent cell suspensions were resuspended in 17 mL supplemented DMEM medium (Gibco, Germany) and the suspension was transferred into flasks with a growth area of 75 cm² and vent caps (Carl Roth, Germany). Culturing of the cells was performed as stated above.

10.3.3. Transfection methods

Transient transfection of adherent 293T cells with DNA vectors was performed according to the instructions provided with the transfection reagent TransIT-X2® (Mirus Bio LLC, USA). The procedure entailed the proper mixing of samples, which was conducted using the neoVortex® (neoLab Migge GmbH, Germany). Transfections were carried out in 6-well plates with a growth area of 9.6 cm^2 (Carl Roth, Germany) and using a seeding density of 6 x 10^5 293T cells per well. The DNA mix was prepared using the reduced-serum medium Opti-MEM™ (Gibco, Germany). For the case that two donor vectors were co-transfected the ratio between both vectors was 1:1. In order to check for successful transfection, the plasmid PB-egfp-IpW encoding EGFP was co-transfected as a control. This control was entailed only for experiments involving the donor vectors PB-mos1.gag-IpW, PB-mos2.gag-IpW and PB-mos2s.env-IhW and represented a fifth of the total DNA amount (2.5 µg) that was utilized for the transfection. Transient transfection experiments in which the generated fluorescence fusion gene constructs were tested, were carried out in 6-well plates with a growth area of 9.6 cm^2 (Carl Roth, Germany) and a seeding density of 3 x 10^5 293T cells per well. Cells were co-transfected with the fluorescence fusion gene donor vectors and respective transposase expression vectors in a ratio of 4:1. Cells transfected with the vector pLenti-V6.3 Ultra-Chili and a pUC plasmid for fill-up (transfection ratio 4:1) served as a positive control for dTomato expression. Three days post transfection, the cells were analyzed using fluorescence microscopy (Axio Vert.A1; Carl Zeiss, Germany) and if applicable, harvested cell-free supernatants were subjected to p24-specific ELISA (Cell Biolabs, USA).

In order to generate stable 293-F cell lines, transfection of the cells was performed in adaption to Berg *et al*., 2020 [162]. Cells were harvested from a culture displaying high viability of >90 %. In total, 30 x 10^6 cells were pelleted by a centrifugation step at 100 x g for 3 min at room temperature using the centrifuge ROTINA 420R (Hettich, Germany). The cell pellet was resuspended in 6 mL 293-F-FreeStyle-Expression-Medium (Thermo

Fisher Scientific, USA). In the meantime the transfection mixtures were prepared. The first mixture contained DNA vectors with a total amount of 50 µg and 1.35 mL 293-F-FreeStyle-Expression-Medium (Thermo Fisher Scientific, USA). The entailed DNA amount consisted of a 1:4 plasmid ratio for *hyPBase* mediated transposition. One part represented the DNA vector encoding *hyPBase* and four parts represented the respective donor vector(s). For the case that two donor vectors were co-transfected the ratio between both vectors was 1:1. For *Sleeping Beauty* mediated transposition a 1:10 plasmid ratio was utilized. One part represented the DNA vector encoding *SB100x* and nine parts represented the respective donor vector(s). For the case that two donor vectors were co-transfected the ratio between both vectors was 1:1, as well. The second transfection mixture contained 1.35 mL 293-F-FreeStyle-Expression-Medium (Thermo Fisher Scientific, USA) together with 150 µL of 40 kDa polyethylenimine (PEI; Polysciences, USA) in a concentration of 1 g/L. Both, the DNA and the PEI mix were each properly vortexed (neoVortex®; neoLab Migge GmbH, Germany), mixed and incubated for 15 min at room temperature before adding them to the cells. Afterwards, the cells were cultivated for 3 h at standard procedure in the presence of 9 mL 293-F-FreeStyle-Expression-Medium (Thermo Fisher Scientific, USA). The cultivation was continued until the next day when the medium was exchanged with new medium. Afterwards, the cultivation was continued and the selection process, to maintain stable transfected cells, was started.

10.3.4. Establishment of stable 293-F cell lines

Four days post transfection, the selection process was initiated with moderate concentrations of either puromycin, hygromycin or G418 [162]. The pressure was constantly elevated over a period of app. 21 days. Afterwards, selection pressures entailing high concentrations were maintained during cultivation (Table 10).

Table 10. Overview of the applied selection pressures for the cultivation of stable recombinant 293-F cell lines.

Cell line	Selection pressure
293-F/Mos1.Gag	15 µg/mL puromycin
293-F/Mos2.Gag	15 µg/mL puromycin
293-F/Mos1.Gag/Mos2S.Env	10 µg/mL puromycin, 200 µg/mL hygromycin
293-F/Mos2.Gag/Mos2S.Env	10 µg/mL puromycin, 200 µg/mL hygromycin
293-F/PB-Mos1.Gag/EGFP-lpW	15 µg/mL puromycin
293-F/dTomato/PDGFR-β-TM-lnW	200 µg/mL G418
293-F/dTomato/PDGFR-β-TM-lnW/ PB-Mos1.Gag/EGFP-lpW	10 µg/mL puromycin, 200 µg/mL G418

10.3.5. Cell counting and microscopy

Cell densities were assessed by cell staining with 0.1 % erythrosine b solution [w/v] and subsequent manual cell counting using the VWR VisiScope IT404 Inverted Phasecontrast Microscope (VWR, USA) and a Neubauer counting chamber. Fluorescence microscopy was performed using the microscope Axio Vert.A1 (Carl Zeiss, Germany) together with the ZEISS ZEN (blue edition) Microscopy Software (Carl Zeiss, Germany). Confocal microscopy of transiently transfected 293T cells was supported by Dr. Christian Jüngst and performed at the CECAD Cologne Imaging Facility using the instrument LSM 980 with Airyscan 2 (Carl Zeiss, Germany). The image data were analyzed using the software imageJ [257].

10.3.6. Harvest of cell-free supernatants from transiently transfected 293T cells

Supernatants were harvested from transiently transfected 293T cells three days post transfection by centrifugation of the culture medium at 300 x g for 3 min at room temperature using a Rotina 420R centrifuge (Hettich, Germany). To remove contaminating cells, the supernatants were filtered through polyvinylidene difluoride (PVDF) membranes with a pore size of 0.45 µm diameter (Carl Roth, Germany). The resulting cell-free supernatants were stored at -20 °C until further experiments were conducted.

10.3.7. Harvest of supernatants from cell cultures and isolation of VLP pellets

Stable VLP producer cell lines were cultivated in 293-F-FreeStyle-Expression-Medium (Thermo Fisher Scientific, USA) together with respective selection pressures at a start density of 0.6×10^6 cells/mL. Four days later, the supernatants were harvested from

cultures revealing a viability of >80 %. Contaminating cells were removed employing low-speed centrifugation of 50 mL cell suspension at 100 x g for 3 min at room temperature using a Rotina 420R centrifuge (Hettich, Germany). Remaining cells and cell debris were subsequently removed by passage through polyvinylidene difluoride (PVDF) membranes with a pore size of 0.45 µm diameter (Carl Roth, Germany). The resulting cell-free supernatants were directly subjected to ultracentrifugation, stored at 4 °C for up to ten days or frozen at -20 °C for long-term storage. VLP pellets were obtained by concentrating cell-free supernatants in ultra clear centrifuge tubes (Beckman Coulter, USA) employing ultracentrifugation at 112,700 x g for 90 min at 4 °C using a SW28 swing-out rotor and an Optima XE centrifuge (Beckman Coulter, USA). The supernatant was discarded and resulting VLP pellets were resuspended in PBS (Thermo Fisher Scientific, USA) containing 15 % trehalose [w/v] (Carl Roth, Germany). The resuspended VLP pellets were stored at -80 °C using the HERAfreeze HFC-series 8740 (Thermo Fisher Scientific, USA) [268].

10.4.   Methods in protein biochemistry
10.4.1. Sodium dodecyl sulfate-polyacrylamide gel electrophoresis (SDS-PAGE)

To separate proteins according to their molecular weight, denaturing SDS-PAGE was performed. The VLP samples, which were obtained after ultracentrifugation from cell-free supernatants were resuspended in 1x PBS and standardized to their productivities. The resuspended VLPs were then mixed with 4x ROTI®Load (Carl Roth, Germany) followed by heat treatment at 95 °C in the thermal mixer Cel Media TS basic (Cellmedia GmbH und Co. KG, Germany) for 10 min. The sample master mix for the isolated Mos1.Gag and Mos2.Gag VLPs in the absence or presence of Mos2S.Env proteins contained following components 50 µL VLP suspension (eq. 1.75×10^4 cells/mL), 25 µL 1x PBS, 19 µL ROTI®Load. The sample master mix for the fluorescent VLPs (EGFP-Gag) was prepared as follows; 10 µL VLP suspension (eq. 1×10^5 cells/mL), 65 µL 1x PBS, 25 µL ROTI®Load. The PageRuler prestained protein ladder (Thermo Fisher Scientific, USA) and the Precision Plus Protein Dual Color Standards (Bio-Rad, USA) served as protein standards. SDS-PAGE gels were loaded with 10 µL of the protein standard and 10 to 30 µL of each sample. The electrophoresis was conducted with 10 % and 4-15 % pre-cast Mini-PROTEAN® TGX™ protein gels (Bio-Rad, USA). In addition, self-casted gels with gradients of 4-12 % and 4-8 %, respectively were utilized

(Table 11). The gels were inserted in the vertical tank of the Mini-PROTEAN Tetra Cell gel electrophoresis system (Bio-Rad, USA) together with 1x SDS-PAGE buffer (ROTIPHORESE®; Carl Roth, Germany) and were connected with the PowerPac™ Basic Power Supply (Bio-Rad, USA). The gel run was initiated using a voltage (V) of 80 for 20 min followed by a separation step between 130 V and 150 V for app. 50 min.

Table 11. Composition of the self-casted 4-12 % SDS-PAGE gels (volumes per gel).

Components	12 % separating gel	4 % stacking gel
dH$_2$O	3.4 mL	1.5 mL
1.5 M Tris-Cl, pH 8,8	2.5 mL	-
0.5 M Tris-Cl, pH 6.8	-	625 µL
10 % SDS	100 µL	25 µL
30 % Acrylamide/Bis solution	4 mL	335 µL
TEMED	5 µL	2.5 µL
10 % APS	50 µL	12.5 µL

10.4.2. Western blot-analysis

Proteins were blotted from the SDS-PAGE gels onto PVDF-membranes (Carl Roth, Germany). Therefore, gel blotting papers (Whatman plc, UK) were soaked in blotting buffer (25 mM Tris, 190 mM glycin, 5 % methanol [v/v]). Meanwhile the PVDF membrane was activated in methanol and rinsed with dH$_2$O. The sandwich consisting of gel blotting papers, PVDF membrane and the SDS-PAGE gel was assembled and blotting was performed at 25 V for 60 min using the Trans-Blot® Turbo™ system (BioRad Laboratories, USA). Blocking of the PVDF membrane was performed using TBST buffer (20 mM/pH 7.2 Tris-Cl, 150 mM sodium chloride, 0.05 % Tween20 [v/v]) including 2 % milk powder for 60 min at room temperature or overnight at 4 °C. The primary antibody, diluted in TBST buffer containing 2 % milk powder, was added to the PVDF membrane (Table 12). Incubation was performed for at least 2 h at room temperature while shaking or at 4 °C overnight. Afterwards, three washing steps á 5-10 min in TBST buffer followed to remove unbound primary antibody. The second antibody, diluted in TBST buffer containing 2 % milk powder, was added to the PVDF membrane and following incubation was performed for 2 h at room temperature (Table 12). The washing steps were repeated and the PVDF membrane was incubated for app. 2 min with the SuperSignal™ West Pico PLUS Chemiluminescent Substrate (Thermo Fisher Scientific, USA). The chemiluminescent signal visualization was enabled using the imager ChemiDoc XRS (BioRad Laboratories, USA) together with the corresponding software Image Lab™

version 5.2.1 (Bio-Rad, USA). The detected proteins in the samples were compared regarding their molecular weight with the detected protein pattern of the standard. The molecular weights for the proteins in the samples were previously calculated using the tool provided on the Expasy platform [253,254].

Table 12. List of polyclonal antibodies, which were utilized in Western blot-analyses. Antibodies were diluted in TBST buffer containing 2 % milk powder. HRP: Horseradish peroxidase.

Antibody	Dilution	Item number, company, country
Chicken α rabbit IgG H + L coupled to HRP	1:5,000	A15987, Thermo Fisher Scientific, USA
Donkey α goat IgG coupled to HRP	1:5,000 and 1:1,000	ab97110, Abcam, UK
Goat α dTomato	1:1,000	Origene, TA150129, OriGene Technologies, Inc., USA
Goat α HIV-1 gp120-SU	1:1,000	ab21179, Abcam, UK
Rabbit α GFP coupled to HRP	1:1,000	A10260, Invitrogen, USA
Rabbit α HIV-1 p55+p24+p17	1:2,000	ab63917, Abcam, UK

10.4.3. Enzyme-linked immunosorbent assay (ELISA)

VLP pellet samples and VLP-containing cell-free supernatants were analyzed using the HIV-1 p24 capsid ELISA kit (Cell Biolabs, USA) to determine the p55-Gag concentration. Deviated from the manufacturer's instruction the range of the p24 standard curve was changed from eight values between 0 to 100 ng/mL to eight values between 0 to 25 ng/mL. The VLP concentration in pelleted samples was calculated based on the findings by Lavado-García *et al*., 2021 that one VLP produced in 293 cells contains 3,617 Gag monomers [17]. Samples containing VLPs displaying Mos2S.Env proteins were additionally analyzed using a HIV-1 gp120 Clade C ELISA kit (Immune Technology, USA). The values for the standard curve were chosen between 0 to 125 ng/mL and further instructions were followed according to the manufacturer. After completing an ELISA, the plate was analyzed using the microplate reader Multiskan™ FC (Thermo Fisher Scientific, USA).

10.4.4. VLP capture assay

The VLP capture assay was performed as previously described by Rosengarten & Schatz in 2022 [187]. Prior to the capture assay, the VLP input amount was standardized to 100 ng Gag proteins per sample by using a p24-specific ELISA. The monoclonal antibodies (MAbs) PG9, PG16, 2G12 and 447-52D and 5F3 were obtained from Polymun

Scientific, Austria. The human IgG antibody (02-7102) that served as isotype control was purchased from Invitrogen, USA. In short, 10 µg of each antibody were coupled to protein G-coated magnetic beads (Dynabeads® Protein G; Invitrogen, USA). Subsequent incubation was performed for 3 h under rotation (Heidolph Instruments, Germany). The VLP pellet samples containing 100 ng Gag proteins were added to the antibody-coated beads and incubated for 2 h under rotation (Heidolph Instruments, Germany). Elution of the VLPs was then performed by addition of 60 µL 1x PBS (Thermo Fisher Scientific, USA) and 20 µL 4x ROTI®Load (Carl Roth, Germany). Following heat treatment at 95 °C in the thermal mixer Cel Media TS basic (Cellmedia GmbH und Co. KG, Germany) for 10 min lead to sample denaturation. The denatured protein samples were separated from the beads using a magnetic separation rack (NEB, USA). Subsequently, 10 µL of each sample were subjected to SDS-PAGE and Western blot-analysis was conducted in the following.

10.4.5. Preparation of VLP pellets for the electron microscopic-analysis

VLPs were visualized by transmission electron microscopy using the negative staining method. The concentrated VLP samples were resuspended in 10 to 50 µL in PBS (Thermo Fisher Scientific, USA) containing 15 % trehalose [w/v] (Carl Roth, Germany) [268]. These samples were stored at -80 °C using the HERAfreeze HFC-series 8740 (Thermo Fisher Scientific, USA) until following sample preparation was conducted by Beatrix Martiny from the CECAD Cologne Imaging Facility. Therefore, 10 to 50 µL 2 % paraformaldehyde were added to the VLP samples. From this solution 5 µL were transferred to copper grids. Incubation on the grids was performed for 20 min at room temperature and followed by seven washing steps of each 2 min using PBS. The VLP samples were fixed on the grids using 1 % glutaraldehyde [v/v] in PBS. Afterwards, washing steps with dH_2O for each 2 min were performed. The sample staining was conducted by incubation with 1 % uranyl acetate solution [w/v] for 4 min at room temperature in the dark followed by air-drying the grids. The visualization of the samples was supported by Beatrix Martiny utilizing a 200 kV JEOL JEM-2100PLUS transmission electron microscope (JEOL, Germany).

11.   Appendix

11.1. List of HIV vaccine clinical trials

Table 13. HIV vaccine clinical trials of the past 13 years that enrolled ≥100 study participants. The trials are sorted according to the utilized vaccine technology. The data were collected from https://clinicaltrials.gov and the official study identifiers (study IDs) are stated below.

Vaccine technology	Priming	Boosting	Vaccine trial/ Study ID	Study phase	Duration	Location	Group size	Vaccine regimen	Outcome	Literature
Virus vector	Adenovirus (Ad.26 and Ad.35)		IAVI B003/ IPCAVD-004/ NCT01215149	I	2010-2012	East Africa, South Africa, USA	218	Vector priming and boosting with two HIV-1 vaccines (Ad26.EnvA and Ad35.Env), both administered IM at a dose of 5 x 10^{10} vp in homologous and heterologous regimens at two schedules (0 and 3 months or 0 and 6 months)	No vaccine-associated serious adverse events	[269]
Virus vector	Canarypox virus (vCP1521)	soluble protein subunit	RV 305/ NCT01435135	II	2012-2021	Thailand	162	Late boost regimens (RV 144 trial) including adjuvanted AIDSVAX B/E (2v gp120) alone, ALVAC-HIV (vCP1521) alone or ALVAC-HIV/AIDSVAX B/E combination at weeks 0, 24, IM administration of ALVAC-HIV at a dose of 1 x 10^6 CCID50 and AIDSVAX B/E (300 µg dose/antigen for a total of 600 µg/dose)	Well tolerated; No vaccine efficacy	[126,128,270]
Virus vector	Canarypox virus (vCP1521)	soluble protein subunit	RV 306/ NCT01931358	II	2013-2021	Thailand	360	The RV144 regimen plus IM administration of ALVAC-HIV (vCP1521) at a dose of 1 x 10^6 CCID50 at months 0 and 4, different combinations of ALVAC-HIV/AIDSVAX B/E (300 µg dose/antigen for a total of 600 µg/dose) at different time points	Safe and well tolerated; No vaccine efficacy	[126,129,271]
Virus vector	Canarypox virus (vCP1521)	soluble protein subunit	HVTN 097/ NCT02109354	I	2013-2015	South Africa	202	ALVAC-HIV (vCP1521) administered IM at a dose of 1 x 10^6 CCID50 at months 1 and 2, than two IM booster injections of adjuvanted AIDSVAX B/E (2v gp120) (300 µg dose/antigen for a total of 600 µg/dose) at months 4 and 7, different combinations of a Hepatitis B and a Tetanus toxoid vaccine	Significantly higher cellular and humoral immune responses than in RV144; No vaccine efficacy	[272,273]
Virus vector	Canarypox virus (vCP2438)	soluble protein subunit	HVTN 100/ NCT02404311	I, II	2015-2018	South Africa	252	IM administration of ALVAC-HIV (vCP2438) using 1 x 10^6 CCID50, administration of 2v gp120-MF59 adjuvant each protein at a total dose of 100 µg at month 3, 6, 12 or at month 30	Boosting at month 12 can improve the durability of the vaccine-induced immune responses; No vaccine efficacy	[272,274–276]

Vaccine technology	Priming	Boosting	Vaccine trial/ Study ID	Study phase	Duration	Location	Group size	Vaccine regimen	Outcome	Literature
Virus vector	Adenovirus (Ad.26)	Ad.26 or Vaccinia virus together with soluble protein subunits	APPROACH/ CR106152/ HIV-V-A004/ IPCAVD009/ NCT02315703	I, II	2014-2022	South Africa, Uganda, Rwanda, Thailand, USA	393	Priming (IM) with 5 x 10^{10} vp Ad26.Mos.HIV (Ad26.Mos.1.Env,Ad26.Mos1.Gag-Pol, Ad26.Mos2.Gag-Pol) at week 0 and 12; Boosting (IM) twice with Ad26.Mos.HIV at weeks 24 and 48 in combination with adjuvanted clade C gp140 at either low or high dose (50 µg or 250 µg of total protein); Boosting with MVA-Mosaic vaccine (MVA.Mos.1.Env, MVA.Mos1.Gag-Pol, MVA.Mos2.Gag-Pol) using 1 x 10^8 pfu at week 24 and 48 in combination with adjuvanted clade C gp140 at either low or high dose (50 µg or 250 µg of total protein); MVA-Mosaic vaccine (1 x 10^8 pfu) or adjuvanted clade C gp140 (250 µg of total protein) at week 24 and 48	Safe and tolerable; The Ad26/Ad26 plus clade C gp140 vaccine induced 67 % protection against (SHIV)-SF162P3 infection when challenging rhesus mon-keys intrarectally six times	[277]
Virus vector	Canarypox virus (vCP2438)	soluble protein subunit	HVTN 702/ NCT02968849	II, III	2016-2021	South Africa	5407	IM administration of ALVAC-HIV (vCP2438) using 1 x 10^6 CCID50 at months 0, 1 followed by IM injection of ALVAC-HIV (vCP2438) and 2v gp120-MF59 adjuvant each protein at a dose of 100 µg at months 3, 6 and 12.	No vaccine efficacy	[130,276,278]
Virus vector	Adenovirus (Ad.26)	Adeno-virus (Ad.26) in combi-nation with soluble protein subunits	TRAVERSE/ CR108152/ NCT02788045	I, II	2016-2022	Rwanda, USA	201	Priming (IM) with 3v Ad26.Mos.HIV* (Ad26.Mos.1.Env, Ad26.Mos1.Gag-Pol, Ad26.Mos2.Gag-Pol) at week 0, 12 followed by boosting (IM) with Ad26.Mos.HIV vaccine and adjuvanted clade C gp140 (250 µg of total protein) at week 24, 48; Priming (IM) with 4v Ad26.Mos4.HIV* (Ad26.Mos.1.Env, Ad26.Mos.2S.Env, Ad26.Mos1.Gag-Pol, Ad26.Mos2.Gag-Pol) at week 0, 12 followed by boosting (IM) with Ad26.Mos4.HIV vaccine and adjuvanted clade C gp140 (250 µg of total protein) at week 24, 48 *Ad26.Mos.HIV and Ad26.Mos4.HIV each administered at a dose of 5 x 10^{10} vp	The 4v vaccine regimen was safe, well tolerated and found to elicit higher immune responses than the 3v vaccine regimen	[131]

Vaccine technology	Priming	Boosting	Vaccine trial/ Study ID	Study phase	Duration	Location	Group size	Vaccine regimen	Outcome	Literature
Virus vector	Adenovirus (Ad.26)	Adeno-virus (Ad.26) in combi-nation with soluble protein subunits	Imbokodo/ HVTN 705/ VAC89220HPX 2008	II	2017-2022	Malawi, Mozam-bique, South Africa, Zambia, Zimbab-we	2637	Ad26.Mos4.HIV* (Ad26.Mos.1.Env, Ad26.Mos.2S.Env, Ad26.Mos1.Gag-Pol, Ad26.Mos2.Gag-Pol) at month 0, 3 followed by boosting (IM) with Ad26.Mos4.HIV vaccine in the absence or presence of adjuvanted clade C gp140 (250 μg of total protein) at month 6, 12 *Ad26.Mos.HIV and Ad26.Mos4.HIV administered at a dose of 5 x 10^{10} vp	The vaccine regimen did not cause harm and was well tolerated, vaccine efficacy point estimate of 25.2 %	[132,277]
Virus vector	Adenovirus (Ad.26)	Adeno-virus (Ad.26) in combi-nation with soluble protein subunits	CR108207/ VAC89220HPX 2003/ NCT02935686	I, II	2017-est. 2023	Kenya, Rwanda, USA	155	Priming (IM) with Ad26.Mos4.HIV* (Ad26.Mos.1.Env, Ad26.Mos.2S.Env, Ad26.Mos1.Gag-Pol, Ad26.Mos2.Gag-Pol) at week 0, 12 followed by boosting (IM) with Ad26.Mos4.HIV vaccine and either adjuvanted clade C gp140 (250 μg of total protein) or adjuvanted 2v gp140 (125 μg clade C gp140, 125 μg mosaic gp140) at week 24, 48 Late boost regimen after completion of the primary vaccination series administering adjuvanted 2v gp140 (80 μg clade C gp140, 75 μg mosaic gp140) within 4 weeks prior to week 192 and app. 3 years after the primary vaccination series *Ad26.Mos4.HIV administered at a dose of 5 x 10^{10} vp		
Virus vector	Canarypox virus (vCP2438)	Canary-pox virus in combi-nation with soluble protein subunits	HVTN 107/ NCT03284710	I, II	2017-2019	Moazam-bique, South Africa, Zimbabwe	132	IM administration of ALVAC-HIV (vCP2438)* at months 0, 1, 3, 6, and 12 Boosting (IM) with - 2v gp120/MF59-adjuvanted (TV1.C gp120, 1086.C gp120) each at a dose of 100 μg at month 0,1,6,12 or 3,6,12 - 2v gp120/Alum-adjuvanted (TV1.C gp120, 1086.C gp120) each at a dose of 100 μg at month 3,6,12 - 2v gp120 (TV1.C gp120, 1086.C gp120) each at a dose of 100 μg at month 3,6,12 *1 x 10^6 CCID50		

Vaccine technology	Priming	Boosting	Vaccine trial/ Study ID	Study phase	Duration	Location	Group size	Vaccine regimen	Outcome	Literature
Virus vector	Canarypox virus (vCP2438)	Canary-pox virus in combination with soluble protein subunits	HVTN 120/ NCT03122223	I, II	2018-2020	Tanzania, USA, Zimbab-we	160	IM administration of ALVAC-HIV (vCP2438)* at months 0, 1, 3, 6 Boosting (IM) with - 2v gp120/MF59-adjuvanted (TV1.C gp120, 1086.C gp120) each at a dose of 100 µg at month 3, 6 - 2v gp120/AS01B-adjuvanted (TV1.C gp120, 1086.C gp120) each at a dose of 20 µg or 100 µg at month 3, 6 *1 x 10^6 CCID50		
Virus vector	Adenovirus (Ad.4)	soluble protein subunit	190069/ 19-I-0069/ NCT03878121	I	2019-est. 2024	USA	300	INT administration either of Ad4-Env150KN or Ad4-Env145NFL at day 0 and month 2 at a dose of 1 x 10^8 vp followed by boosting (IM) with VRC-HIVRGP096-00-VP (trimer 4571) at a total dose of 500 µg at month 6		
Virus vector	Adenovirus (Ad.26)	Adeno-virus (Ad.26) in combi-nation with soluble protein subunits	Mosaico/ CR108604/ 2018-003666-13/VAC89220H PX3002/ HVTN 706/ NCT03964415	III	2019-2023	Argent-ina, Brazil, Mexico, Peru, Italy, Poland, Puerto Rico Spain, USA	3900	Priming (IM) with Ad26.Mos4.HIV* (Ad26.Mos.1.Env, Ad26.Mos.2S.Env, Ad26.Mos1.Gag-Pol, Ad26.Mos2.Gag-Pol) at month 0, 3 followed by boosting (IM) with Ad26.Mos4.HIV vaccine and adjuvanted 2v clade C and mosaic gp140 at month 6, 12	Terminated ahead of schedule due to lacking protection. The vaccine regimen proved safe.	[133]
DNA vector	DNA	Vaccinia virus	HVTN 106/ NCT02296541	I	2014-2020	Switzer-land, USA	105	IM administration of one out of three DNA vaccines (DNA Nat-B env, DNA CON-S env, DNA Mosaic env) at a dose of 4 mg at months 0, 1, 2; IM administration of a MVA-CMDR vector (1 x 10^8 pfu) at months 4 and 8		[279]
DNA vector	DNA	Vaccinia virus	rTV/ ChiCTR190002 1422	II	2019-2021	China	160	DNA and rTV vectors constructs harboring HIV-1 CN54 *gag*, *pol* and *env* genes; Priming (IM) with 2 mg or 4 mg DNA vaccine followed by rTV boost twice after DNA prime in different week intervals (24, 36, 48)	Well tolerated and safe	[280]
DNA vector	DNA	soluble protein subunit	RV 460/ NCT04826094	I	2021-est. 2023	Kenya	126	Priming (IM) with 2 mg of an Env-C Plasmid DNA vaccine at weeks 0,4,12 alone or combined with different adjuvants and boosting with or without adjuvanted HIV Env gp145 C.6980 protein at a dose of 100 µg at weeks 20, 32, 56		

Vaccine technology	Priming	Boosting	Vaccine trial/ Study ID	Study phase	Duration	Location	Group size	Vaccine regimen	Outcome	Literature
mRNA			HVTN 302/ NCT05217641	I	2022-est. 2023	USA	108	IM administration of BG505 MD39.3 mRNA, BG505 MD39.3 gp151 mRNA or BG505 MD39.3 gp151 CD4KO mRNA at low dose (100 µg) or high dose (250 µg) at months 0, 2 and 6		
Protein subunit			HVTN 115/ NCT03220724	I	2017-est. 2023	USA	117	IM administration of CH505TF gp120, CH505w53 gp120, and CH505w78 gp120 in different combinations and adjuvanted with GLA-SE containing all three CH505 gp120 proteins - 20 µg of CH505TF/GLA-SE at months 0, 2, 4, 8, and 12 - 100 µg of CH505TF/GLA-SE at months 0, 2, 4, 8, and 12 - 400 µg of CH505TF/GLA-SE at months 0, 2, 4, 8, and 12 - CH505TF/GLA-SE at month 0; CH505w53/GLA-SE at month 2; CH505w78/GLA-SE at months 4, 8, 12, and 16		[281]
Protein subunit			HVTN 137/ NCT04177355	I	2020-est. 2023	USA	105	IM administration of 100 µg BG505 SOSIP.664 gp140 at month 0, 2 admixed with - 1 µg 3M-052-AF adjuvanted with 500 µg Alum - 5 µg 3M-052-AF adjuvanted with 500 µg Alum IM administration of 100 µg BG505 SOSIP.664 gp140 at month 0, 2, 6 admixed with - 300 µg CpG 1018 adjuvanted with 500 µg Alum - 1 µg or 5 µg 3M-052-AF adjuvanted with 500 µg Alum GLA-LSQ (GLA 5 µg, and QS-21 2 µg) 500 µg Alum		[282]
Protein subunit			RV 546/ WRAIR 1920/ NCT04658667	I	2022-est. 2027	Thailand	120	Late boost regimen for patients who previously received a late boost of AIDSVAX®B/E with or without ALVAC in HVTN 306; Administration of 2 injections (IM) of IHV01 and A244/AHFG at a full (app. 300 µg) or fractional dose (app. 60 µg) with or without ALFQ adjuvant at day 0		[128,129]

Vaccine technology	Priming	Boosting	Vaccine trial/ Study ID	Study phase	Duration	Location	Group size	Vaccine regimen	Outcome	Literature
DNA vector, virus vector, protein subunit	DNA in combination with soluble protein subunits or DNA in combination with soluble protein subunits and Vaccinia virus vector		PV1/ NCT04066881	II	2020-est. 2024	Uganda	1668	DNA-HIV-PT123 HIV vaccine (three DNA plasmids that encode clade C ZM96 Gag, clade C ZM96 Env, and CN54 Pol-Nef) at different timepoints (IM) - plus adjuvanted AIDSVAX B/E (2v gp120) at weeks 0, 4, 24 and 48 - plus CN54gp140+MPLA-L at weeks 0 and 4, then MVA-CMDR (1 x10^8 pfu) and CN54gp140+MPLA-L at weeks 24 and 48 - plus CN54gp140+MPLA-L at weeks 0 and 4, then MVA-CMDR and CN54gp140+MPLA-L at weeks 24 and 48		[283]

*Abbreviations: 2v (bivalent), 3v (trivalent), Ad26 (adenovirus vector serotype 26), Ad35 (adenovirus vector serotype 35), Alum (aluminum hydroxide suspension), CCID50 (cell culture infectious dose 50 %), IM (intramuscularly), INT (intranasal), MVA (modified vaccinia Ankara), MVA-CMDR (modified vaccinia Ankara-Chiang Mai double recombinant), pfu (plaque forming units), rTV (replicating competent Tiantan vaccinia vector), SHIV (simian-human immunodeficiency virus), vp (viral particle)

11.2. DNA plasmid maps
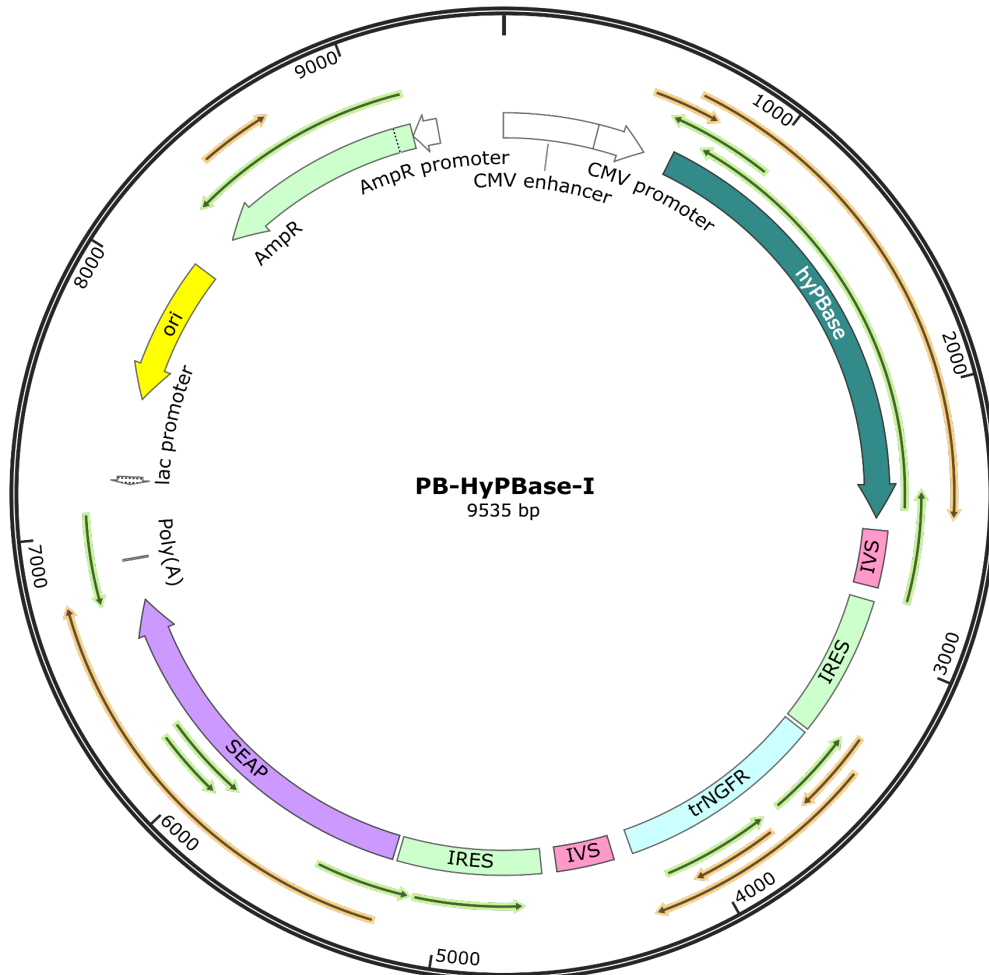
Figure 30. Plasmid map for PB-hyPBase-I. The DNA sequence for the transposase *hyPBase* [170] originated from the vector pCAG-hyPBase (Gene bank accession number: OL519599.1) and was codon optimized for expression in human and CHO cells, respectively. The expression of *hyPBase* was coupled to the expression of the reporter gene secreted alkaline phosphatase (*SEAP*). Open reading frames (ORFs) are indicated by orange arrows.

Figure 31. Plasmid map for PB-Mos1.Gag-IpW. The DNA sequence for *mos1.gag* was taken from the patent US 10,369,214 [14] and was codon optimized for expression in human and CHO cells, respectively. The expression of *mos1.gag* was coupled to the expression of the puromycin resistance gene (*Puro^R*). The expression cassette was flanked by *PiggyBac* derived ITRs. Open reading frames (ORFs) are indicated by orange arrows.
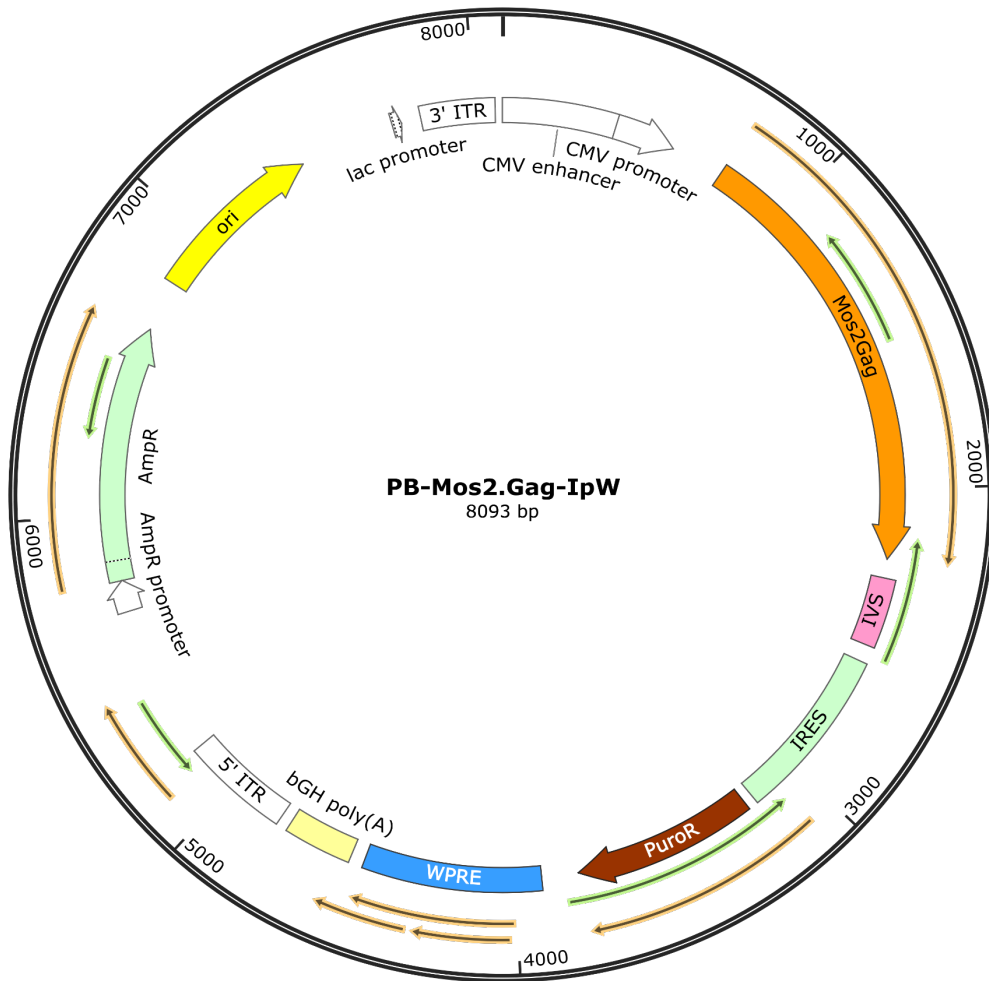
Figure 32. Plasmid map for PB-Mos2.Gag-IpW. The DNA sequence for *mos2.gag* was taken from the patent US 10,369,214 [14] and was codon optimized for expression in human and CHO cells, respectively. The expression of *mos2.gag* was coupled to the expression of the puromycin resistance gene (*Puro^R*). The expression cassette was flanked by *PiggyBac* derived ITRs. Open reading frames (ORFs) are indicated by orange arrows.
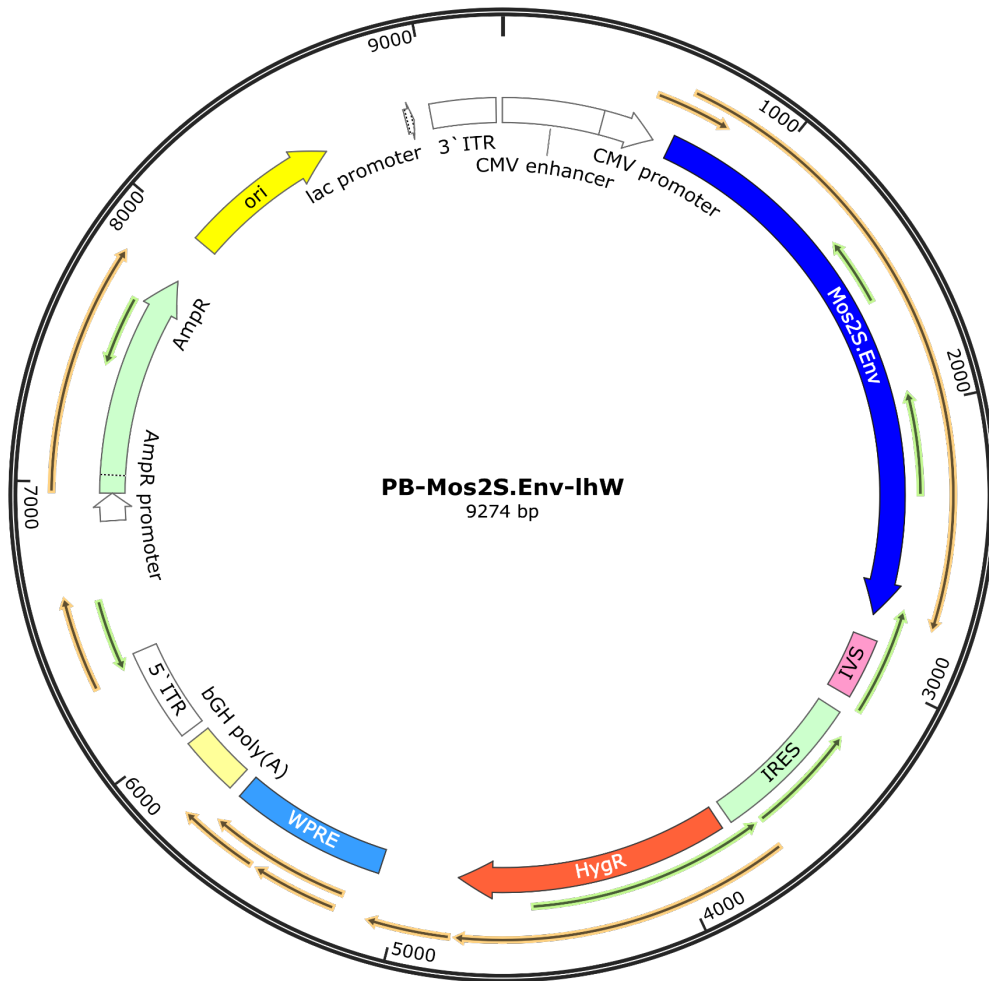
Figure 33. Plasmid map for PB-Mos2S.Env-IhW. The DNA sequence for *mos2s.env* was taken from the patent US 10,369,214 [14] and was codon optimized for expression in human and CHO cells, respectively. The expression of *mos2s.env* was coupled to the expression of the hygromycin resistance gene (*Hyg^R*). The expression cassette was flanked by *PiggyBac* derived ITRs. Open reading frames (ORFs) are indicated by orange arrows.
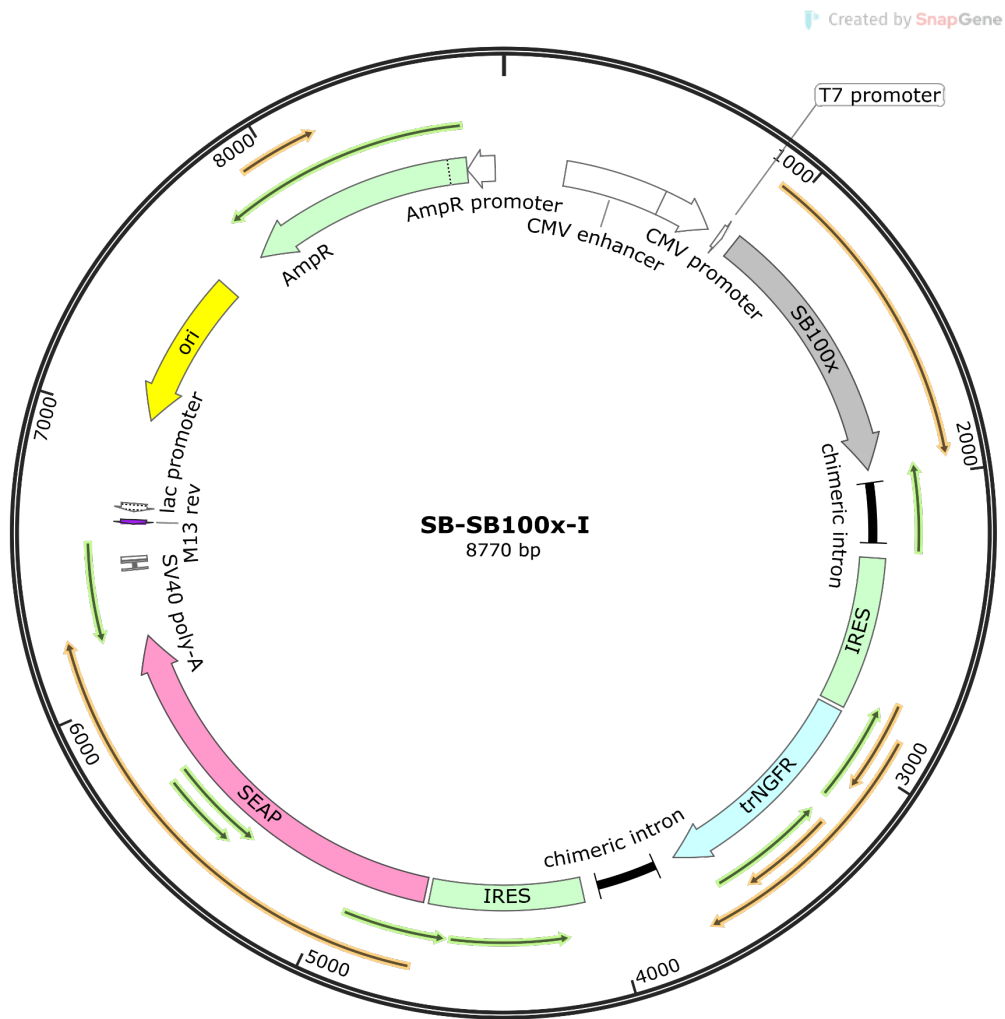
Figure 34. Plasmid map for SB-SB100x-I. This plasmid served for the expression of the transposase *SB100x* and was previously described by Berg *et al*. 2019 [261]. The expression of *SB100x* was coupled to the expression of the reporter gene secreted alkaline phosphatase (*SEAP*). Open reading frames (ORFs) are indicated by orange arrows.
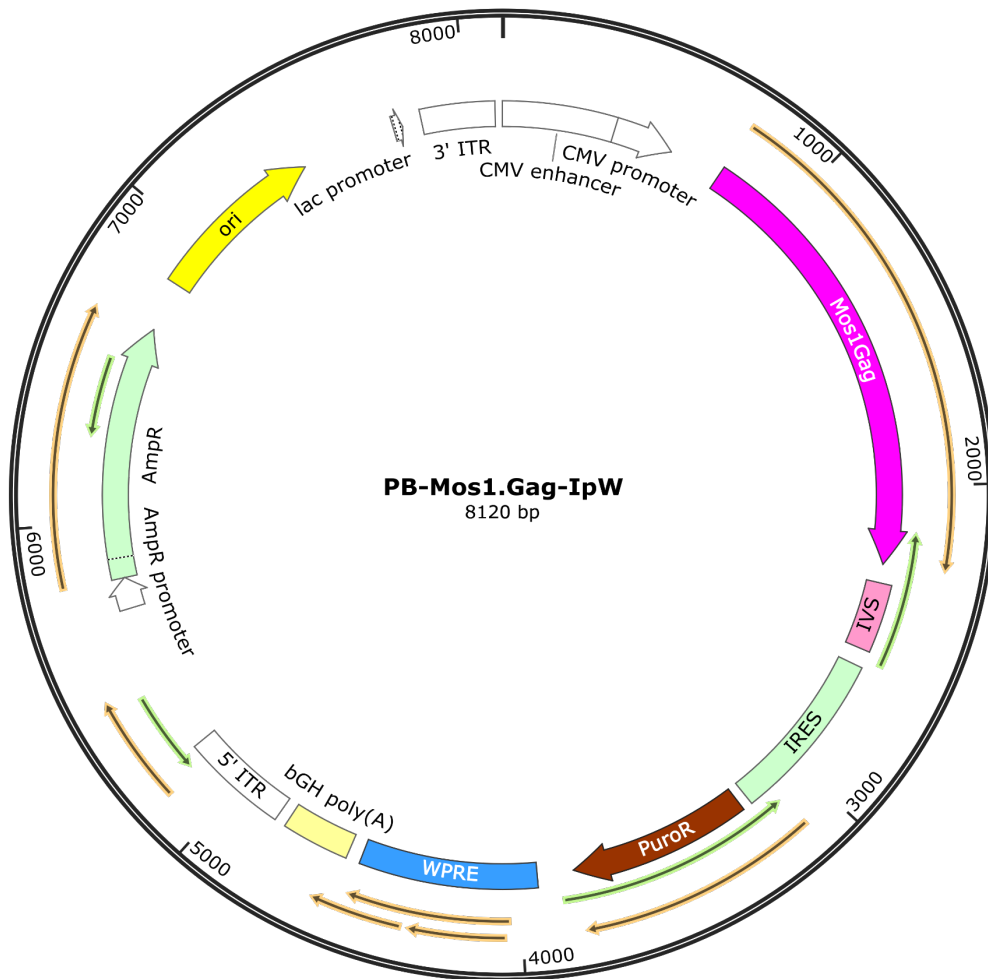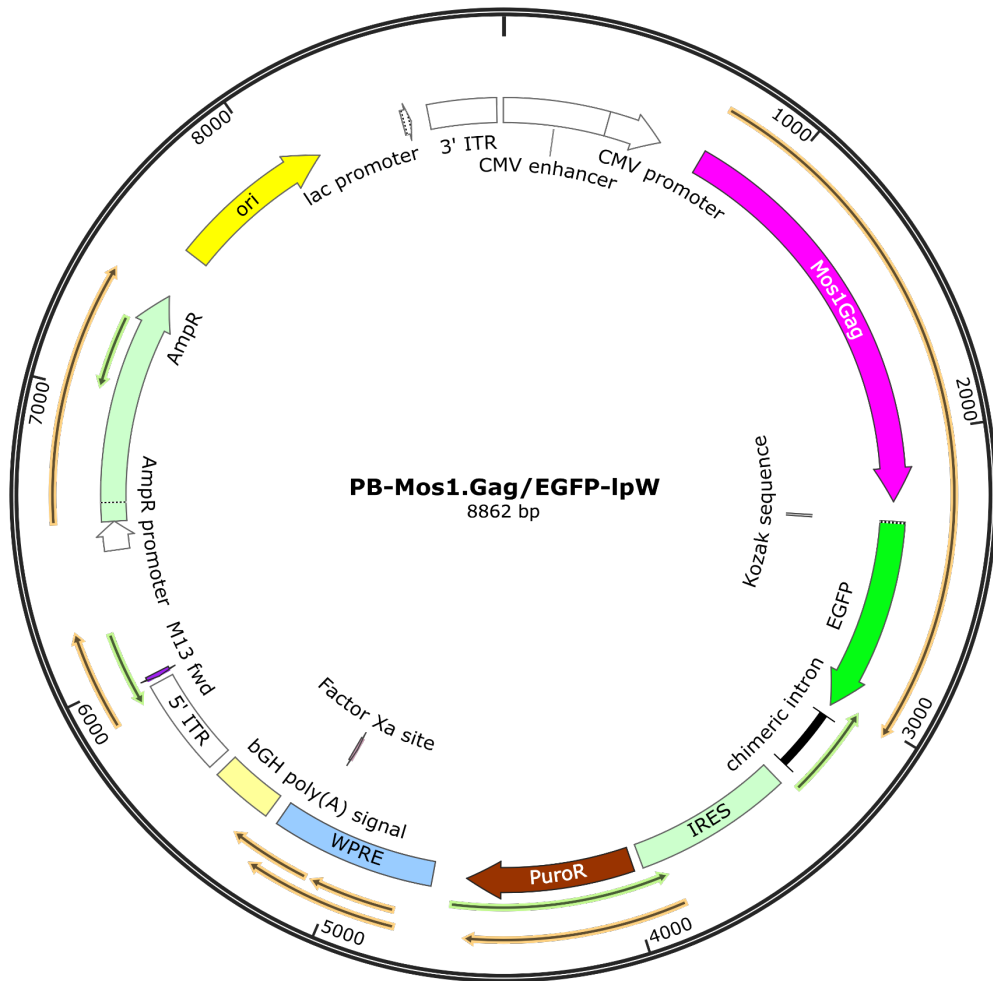
Figure 35. Plasmid map for PB-Mos1.Gag/EGFP-lpW. This plasmid served for the expression of the fusion gene *mos1.gag-egfp*. The expression of this fusion gene was coupled to the expression of the puromycin resistance gene (*Puro^R*). The expression cassette was flanked by *PiggyBac* derived ITRs. Open reading frames (ORFs) are indicated by orange arrows.

Figure 36. Plasmid map for SB-dTomato/PDGFR-β-TM-lnW. This plasmid served for the expression of the fusion gene *dTomato-pdgfr β tm*. The expression of this fusion gene was coupled to the expression of the neomycin resistance gene (*Neo*[R]). The expression cassette was flanked by *Sleeping Beauty* derived ITRs. Open reading frames (ORFs) are indicated by orange arrows.
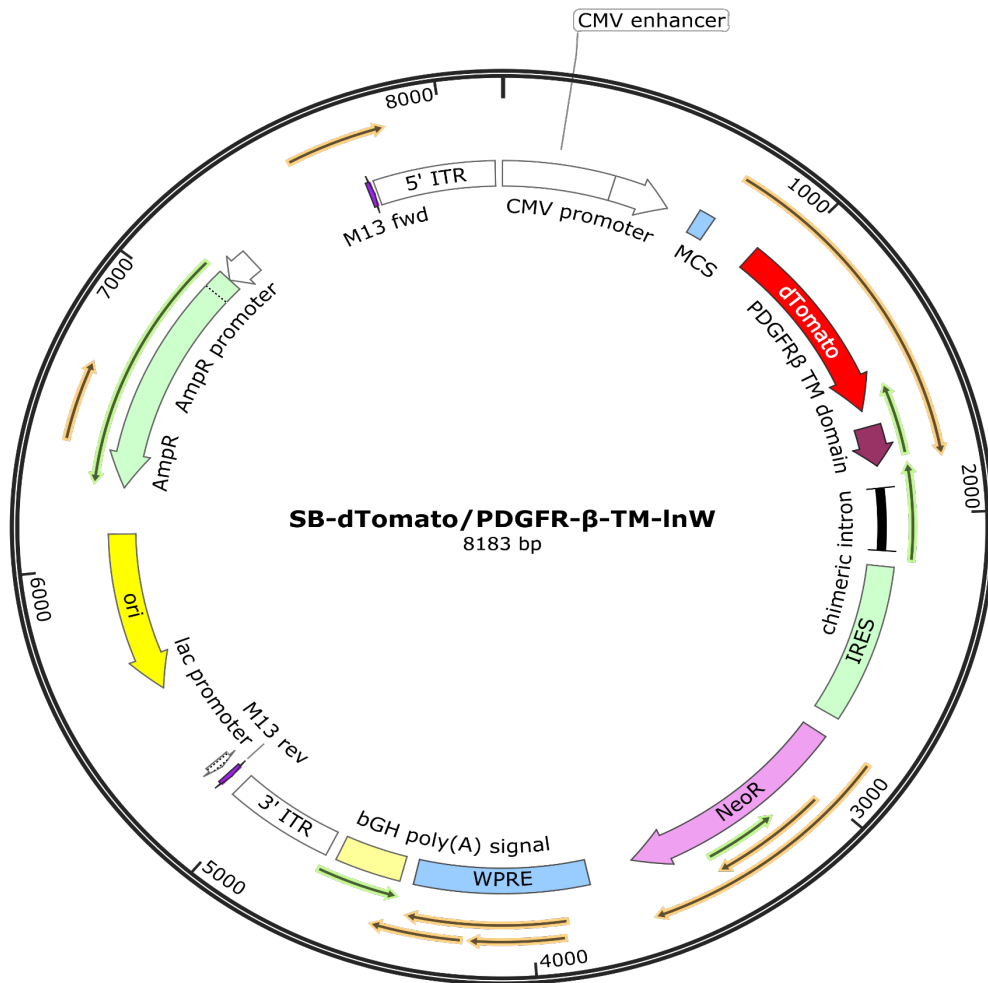
11.3. Nucleotide sequences

ATGGGGGAGTAGCCTGGACGACGAGCACATCCTGTCCGCACTGCTGCAGAGC
GACGACGAACTGGTGGGGGAAGATTCAGATTCAGAAGTGTCTGACCACGTG
AGCGAGGACGATGTGCAGTCTGACACCGAGGAGGCCTTCATCGATGAGGTG
CACGAGGTGCAGCCAACAAGCTCCGGCAGCGAGATCCTGGATGAGCAGAA
CGTGATCGAGCAGCCTGGCTCTAGCCTGGCTTCCAATCGGATCCTGACCCTG
CCACAGAGAACAATCCGCGGCAAGAATAAGCACTGCTGGTCCACCTCTAAG
CCTACACGGAGGAGCAGGGTGTCCGCCCTGAACATCGTGCGGTCCCAGAGG
GGCCCAACCAGAATGTGCCGCAATATCTACGACCCCCTGCTGTGCTTTAAGC
TGTTCTTTACCGATGAGATCATCAGCGAGATCGTGAAGTGGACAAACGCCG
AGATCTCCCTGAAGAGACGCGAGTCTATGACCAGCGCCACCTTCAGGGACA
CCAATGAGGATGAGATCTACGCCTTCTTTGGCATCCTGGTGATGACCGCTGT
GCGGAAGGACAACCACATGAGCACAGACGATCTGTTTGATAGGAGCCTGTC
CATGGTGTACGTGAGCGTGATGTCTCGGGACCGGTTCGATTTTCTGATCCGG
TGCCTGAGGATGGACGATAAGTCCATCCGGCCTACCCTGAGGGAGAATGAC
GTGTTCACACCAGTGAGAAAGATCTGGGATCTGTTTATCCACCAGTGTATCC
AGAACTACACCTGGAGCTCACCTGACAATTGATGAACAGCTGCTGGGAT
TCAGAGGCAGGTGCCCTTTTCGCGTGTACATCCCAAATAAGCCCTCTAAGTA
TGGCATCAAGATCCTGATGATGTGCGATAGCGGCACCAAGTACATGATCAA
CGGCATGCCATATCTGGGAAGAGGCACCCAGACCAACGGCGTGCCCCTGGG
AGAGTACTATGTGAAGGAGCTGTCCAAGCCTGTGCACGGCTCTTGCCGCAA
CATCACCTGTGACAATTGGTTCACATCTATCCCCCTGGCTAAGAACCTGCTG
CAGGAGCCTTATAAGCTGACCATCGTGGGCACAGTGAGAAGCAACAAGCGC
GAGATCCCCGAGGTGCTGAAGAATTCTAGAAGCCGCCCTGTGGGCACCTCC
ATGTTCTGCTTTGATGGCCCACTGACACTGGTGTCTTACAAGCCCAAGCCTG
CCAAGATGGTGTATCTGCTGTCCTCTTGTGACGAGGATGCTTCCATCAACGA
GTCTACCGGCAAGCCCCAGATGGTGATGTACTATAATCAGACCAAGGGCGG
CGTGGACACACTGGATCAGATGTGCAGCGTGATGACCTGTTCCCGGAAGAC
AAACAGGTGGCCTATGGCCCTGCTGTACGGCATGATCAACATCGCTTGCATC
AATTCTTTTATCATCTATAGCCACAACGTGAGCTCCAAGGGCGAGAAGGTG
CAGAGCAGAAAGAAGTTCATGCGCAATCTGTACATGGGCCTGACCTCTAGC
TTTATGCGGAAGAGGCTGGAGGCCCCTACACTGAAGAGATACCTGCGCGAC
AACATCTCCAATATCCTGCCTAAGGAGGTGCCAGGCACCAGCGACGATTCC
ACAGAGGAGCCAGTGATGAAGAAGCGGACCTACTGCACATATTGTCCCTCT
AAGATCCGGAGGAAGGCCTCCGCTTCTTGTAAGAAGTGTAAAAAGTGATT
TGTAGAGAGCATAATATCGACATGTGCCAGTCCTGTTTC

Figure 37. Coding sequence for *hyPBase* in 5'-to-3' direction. The nucleotide sequence for *hyPBase* [170] originated from the vector pCAG-hyPBase (Gene bank accession number: OL519599.1) and was codon optimized for expression in human and CHO cells.

ATGGGGGGCAAGAGCAAGCGTCCTGAGTGGCGGGGAACTGGACCGATGGGA
GAAGATTAGACTGCGACCTGGCGGCAAAAAGAAGTATCGCCTGAAGCACAT
CGTGTGGGCCAGCCGGGAGCTGGAGCGGTTCGCTGTGAACCCTGGCCTGCT
GGAGACATCCGAGGGATGCCGGCAGATCCTGGGACAGCTGCAGCCAAGCCT
GCAGACCGGATCCGAGGAGCTGCGCTCTCTGTACAATACAGTGGCCACCCT
GTATTGCGTGCACCAGCGGATCGAGATCAAGGACACAAAGGAGGCTCTGGA

GAAGATCGAGGAGGAGCAGAACAAGAGCAAGAAGAAGGCTCAGCAGGCCG
CTGCCGATACCGGCAATAGCTCCCAGGTGTCTCAGAACTACCCAATCGTGC
AGAATATCCAGGGCCAGATGGTGCACCAGGCTATCTCTCCCCGCACCCTGA
ACGCCTGGGTGAAGGTGGTGGAGGAGAAGGCTTTCAGCCCTGAAGTGATCC
CAATGTTTTCTGCTCTGAGCGAGGGCGCCACACCTCAGGACCTGAACACAA
TGCTGAATACCGTGGGAGGACACCAGGCTGCTATGCAGATGCTGAAGGAGA
CAATCAACGAGGAGGCTGCCGAGTGGGACAGGGTGCACCCAGTGCACGCTG
ACCCATCGCCCCTGGCCAGATGAGGGAGCCTAGGGGCTCTGACATCGCTG
GCACCACAAGCACACTGCAGGAGCAGATCGGCTGGATGACCAACAATCCCC
CTATCCCCGTGGGCGAGATCTACAAGCGGTGGATCATCCTGGGCCTGAACA
AGATCGTGAGGATGTATTCCCCCGTGAGCATCCTGGACATCAGACAGGGCC
CAAAGGAGCCCTTCCGGGACTACGTGGATAGGTTTTATAAGACACTGAGGG
CTGAGCAGGCCAGCCAGGACGTGAAGAATTGGATGACAGAGACACTGCTG
GTGCAGAACGCTAATCCTGATTGCAAGACCATCCTGAAGGCCCTGGGCCCA
GCTGCCACTGGAGGAGATGATGACCGCTTGTCAGGGCGTGGGCGGCCCA
GGACACAAAGCTAGGGTGCTGGCTGAGGCTATGAGCCAGGTGACAAACTCC
GCCACCATCATGATGCAGAGAGGCAACTTCAGAAATCAGCGCAAGACCGTG
AAGTGCTTTAACTGTGGCAAGGAGGGCCACATCGCTAAGAATTGCAGGGCT
CCAAGGAAGAAGGGATGCTGGAAGTGCGGCAAGGAAGGCCACCAGATGAA
GGACTGTACAGAGAGGCAGGCTAACTTCCTGGGCAAGATCTGGCCCTCCAA
TAAGGGCAGACCTGGCAACTTTCTGCAGAATAGGCCTGAGCCAACCGCTCC
ACCAGAGGAGTCCTTCAGATTTGGCGAGGAGACAACAACCCCATCTCAGAA
GCAGGAGCCCATCGATAAGAAATGTATCCCCTGGCAAGCCTGAAGAGTCT
GTTCGGAAACGACCCATCCTCCCAG

Figure 38. Coding sequence for Mos1.Gag in 5'-to-3' direction. The nucleotide sequence was taken from the patent US 10,369,214 [14] and was codon optimized for expression in human and CHO cells.

ATGGGAGCAAGGGCTTCTATTCTGAGGGGAGGAAAACTGGACAAGTGGGA
AAAAATCCGACTGCGACCTGGAGGGAAAAAACATTACATGCTGAAGCACCT
GGTGTGGGCCAGCAGGGAGCTGGAGAGATTCGCTCTGAACCCTGGCCTGCT
GGAGACAAGCGAGGGCTGCAAGCAGATCATCAAGCAGCTGCAGCCAGCCC
TGCAGACCGGCACAGAGGAGCTGCGCTCTCTGTTTAACACCGTGGCCACAC
TGTACTGCGTGCACGCTGAGATCGAGGTGCGGGACACCAAGGAGGCTCTGG
ATAAGATCGAGGAGGAGCAGAATAAGTCCCAGCAGAAGACACAGCAGGCC
AAGGAGGCTGACGGCAAGGTGTCTCAGAACTATCCAATCGTGCAGAATCTG
CAGGGCCAGATGGTGCACCAGCCAATCAGCCCCAGGACCCTGAACGCCTGG
GTGAAAGTGATCGAGGAGAAGGCTTTCTCTCCAGAAGTGATCCCCATGTTT
ACCGCCCTGAGCGAGGGAGCTACACCACAGGACCTGAACACCATGCTGAAT
ACAGTGGGCGGCCACCAGGCCGCTATGCAGATGCTGAAGGACACAATCAAT
GAGGAGGCCGCTGAGTGGGATAGACTGCACCCAGTGCACGCTGGACCTGTG
GCTCCAGGCCAGATGAGGGAGCCCAGGGGCAGCGACATCGCTGGCACCAC
ATCCAACCTGCAGGAGCAGATCGCTTGGATGACCTCCAATCCCCCTATCCCC
GTGGGCGACATCTACAAGAGGTGGATCATCCTGGGCCTGAACAAGATCGTG
AGAATGTATAGCCCTACATCCATCCTGGACATCAAGCAGGGCCCCAAGGAG
CCTTTCCGCGACTACGTGGATCGGTTCTTTAAGACCCTGAGGGCTGAGCAGG
CTACACAGGACGTGAAGAATTGGATGACCGATACACTGCTGGTGCAGAACG

CCAATCCCGACTGCAAGACCATCCTGAGGGCCCTGGGCCCTGGCGCTACCC
TGGAGGAGATGATGACAGCTTGTCAGGGCGTGGGCGGACCTTCTCACAAGG
CTAGAGTGCTGGCCGAGGCTATGTCTCAGACCAACAGCACAATCCTGATGC
AGAGGTCCAATTTCAAGGGCTCTAAGAGAATCGTGAAGTGCTTTAACTGTG
GCAAGGAGGGCCACATCGCCAGAAATTGCCGCGCTCCACGGAAGAAGGGC
TGCTGGAAGTGCGGCAAGGAAGGCCACCAGATGAAGGATTGTACCGAGCG
CCAGGCTAATTTTCTCGGCAAGATCTGGCCTTCCCACAAGGGCCGCCCAGGC
AATTTTCTGCAGTCTCGGCCTGAGCCAACAGCTCCACCAGCTGAGAGCTTCC
GGTTTGAGGAGACAACACCCGCCCCTAAGCAGGAGCCCAAAGATAGAGAG
CCACTGACAAGCCTGAGAAGCCTGTTCGGTAGCGACCCACTGAGCCAG

Figure 39. Coding sequence for Mos2.Gag in 5'-to-3' direction. The nucleotide sequence was taken from the patent US 10,369,214 [14] and was codon optimized for expression in human and CHO cells.

ATGAGGGTCCGGGGAATGCTGAGGAATTGGCAGCAGTGGTGGATTTGGTCT
TCTCTGGGCTTTTGGATGCTGATGATCTACTCCGTGATGGGCAACCTGTGGG
TGACCGTGTACTATGGCGTGCCAGTGTGGAAGGACGCCAAGACCACACTGT
TCTGCGCTAGCGATGCCAAGGCTTACGAGAAGGAGGTGCACAACGTGTGGG
CTACCCACGCTTGCGTGCCAACAGATCCAAATCCCCAGGAGATCGTGCTGG
GCAACGTGACCGAGAACTTCAACATGTGGAAGAACGACATGGTGGATCAGA
TGCACGAGGACATCATCAGCCTGTGGGATGCCTCCCTGGAGCCATGCGTGA
AGCTGACCCCCCTGTGCGTGACACTGAATTGTAGAAACGTGCGCAATGTGA
GCTCCAACGGCACCTACAATATCATCCACAACGAGACATATAAGGAGATGA
AGAATTGTTCCTTCAACGCTACAACCGTGGTGGAGGATAGAAAGCAGAAGG
TGCACGCTCTGTTTTATCGCCTGGACATCGTGCCCCTGGATGAGAACAATTC
TAGCGAGAAGTCCTCTGAGAATAGCTCCGAGTACTATAGACTGATCAATTG
CAACACCTCCGCCATCACACAGGCTTGTCCTAAGGTGTCTTTCGACCCTATC
CCAATCCACTACTGCGCCCCAGCTGGCTATGCCATCCTGAAGTGTAACAATA
AGACCTTTAACGGCACAGGCCCCTGCAACAACGTGAGCACCGTGCAGTGTA
CACACGGCATCAAGCCTGTGGTGTCTACCCAGCTGCTGCTGAATGGCAGCCT
GGCCGAGGAGGAGATCATCATCAGAAGCGAGAACCTGACCAACAATGCTA
AGACAATCATCGTGCACCTGAATGAGACAGTGAACATCACCTGCACACGCC
CAAACAATAACACAAGAAAGAGCATCCGCATCGGCCCTGGCCAGACCTTCT
ACGCCACAGGCGACATCATCGGCGACATCCGGCAGGCTCACTGTAATCTGT
CCAGGGATGGCTGGAACAAGACCCTGCAGGGCGTGAAGAAGAAGCTGGCC
GAGCACTTCCCTAATAAGACAATCAAGTTTGCTCCACACTCCGGCGGCGAC
CTGGAGATCACCACACACACCTTCAACTGCCGCGGCGAGTTCTTTTACTGTA
ACACATCTAATCTGTTTAACGAGAGCAATATCGAGCGGAATGACTCTATCAT
CACCCTGCCTTGCAGGATCAAGCAGATCATCAACATGTGGCAGGAAGTGGG
AAGGGCTATCTATGCTCCACCTATCGCCGGCAATATCACATGTAGAAGCAA
CATCACCGGCCTGCTGCTGACACGCGACGGAGGATCCAATAACGGCGTGCC
CAACGATACCGAGACATTCAGGCCTGGCGGCGGCGACATGCGGAATAACTG
GAGGAGCGAGCTGTACAAGTATAAGGTGGTGGAGGTGAAGCCACTGGGAG
TGGCTCCTACCGAGGCTAAGAGGAGGGTGGTGGAGAGGGAGAAGAGGGCT
GTGGGAATCGGAGCCGTGTTCCTGGGAATCCTGGGAGCTGCTGGATCCACC
ATGGGAGCTGCTTCTATCACCCTGACAGTGCAGGCTAGGCAGCTGCTGAGC
GGAATCGTGCAGCAGCAGTCCAACCTGCTGAGGGCCATCGAGGCTCAGCAG

CACATGCTGCAGCTGACCGTGTGGGGCATCAAGCAGCTGCAGACAAGAGTG
CTGGCCATCGAGAGATACCTGCAGGATCAGCAGCTGCTGGGCCTGTGGGGA
TGCTCCGGCAAGCTGATCTGTACCACAGCTGTGCCATGGAATACCTCTTGGA
GCAACAAGTCTCAGACCGACATCTGGGATAATATGACATGGATGCAGTGGG
ACAAGGAGATCGGCAACTACACAGGCGAGATCTATAGGCTGCTGGAGGAGT
CTCAGAATCAGCAGGAGAAGAACGAGAAGGACCTGCTGGCCCTGGATAGCT
GGAATAACCTGTGGAACTGGTTCTCCATCTCTAAGTGGCTGTATATCAAGAT
CTTTATCATGATCGTGGGCGGCCTGATCGGTCTGAGAATCATCTTTGCTGTG
CTGTCAATCGTGAATAGGGTGCGGCAGGGTTAT

Figure 40. Coding sequence for Mos2S.Env in 5'-to-3' direction. The nucleotide sequence was taken from the patent US 10,369,214 [14] and was codon optimized for expression in human and CHO cells.

ATGGGAAAGAGCAAAGAAATCTCACAGGACCTGAGGAAGAGGATCGTGGA
CCTGCACAAGAGCGGGAGCAGCCTGGGAGCAATCTCAAAGCGGCTGGCCGT
GCCCAGATCTAGCGTGCAGACAATCGTGAGGAAGTACAAGCACCACGGCAC
CACCCAGCCATCTTACAGATCCGGCAGAAGGAGAGTGCTGTCCCCTAGAGA
TGAGAGGACCCTGGTGCGGAAGGTGCAGATCAATCCTAGGACAACCGCCAA
GGACCTCGTGAAGATGCTGGAGGAGACAGGCACCAAGGTGTCTATCTCCAC
CGTGAAGAGAGTGCTGTACCGCCACAACCTGAAGGGCCACTCCGCCAGAAA
GAAGCCACTGCTGCAGAATAGGCACAAGAAGGCCAGACTGCGGTTTGCCAG
AGCCCACGGCGATAAGGACAGGACATTCTGGAGAAACGTGCTGTGGAGCG
ATGAGACCAAGATCGAGCTGTTCGGCCACAACGATCACAGATACGTGTGGA
GAAAGAAGGGCGAGGCCTGCAAGCCAAAGAACACCATCCCAACAGTGAAG
CACGGCGGCGGCAGCATCATGCTGTGGGGCTGTTTCGCCGCCGGCGGCACA
GGCGCCCTGCACAAGATCGATGGCATCATGGATGCCGTGCAGTATGTGGAC
ATCCTGAAGCAGCACCTGAAGACATCCGTGAGAAAGCTGAAGCTGGGCAGA
AAGTGGGTGTTCCAGCACGATAACGACCCAAAGCACACCAGCAAGCACGTG
CGGAAGTGGCTGAAGGACAACAAGGTGAAGGTGCTGGAGTGGCCTTCTCAG
AGCCCAGATCTGAATCCCATCGAGAATCTGTGGGCCGAGCTGAAGAAGAGA
GTGAGGGCCAGACGGCCTACAAACCTGACCCAGCTGCACCAGCTGTGCCAG
GAGGAGTGGGCCAAGATCCACCCAAACTACTGCGGCAAGCTGGTGGAGGG
CTATCCAAAAAGACTGACTCAGGTGAAGCAGTTCAAAGGAAACGCTACCAA
ATAC

Figure 41. Coding sequence for the transposase *Sleeping Beauty 100x* in 5'-to-3' direction. The cognate vector encompassing the *SB100x* expression cassette was already available in our group [261].

ATGGGGGGCAAGAGCAAGCGTCCTGAGTGGCGGGGAACTGGACCGATGGGA
GAAGATTAGACTGCGACCTGGCGGCAAAAAGAAGTATCGCCTGAAGCACAT
CGTGTGGGCCAGCCGGGAGCTGGAGCGGTTCGCTGTGAACCCTGGCCTGCT
GGAGACATCCGAGGGATGCCGGCAGATCCTGGGACAGCTGCAGCCAAGCCT
GCAGACCGGATCCGAGGAGCTGCGCTCTCTGTACAATACAGTGGCCACCCT
GTATTGCGTGCACCAGCGGATCGAGATCAAGGACACAAAGGAGGCTCTGGA
GAAGATCGAGGAGGAGCAGAACAAGAGCAAGAAGAAGGCTCAGCAGGCCG
CTGCCGATACCGGCAATAGCTCCCAGGTGTCTCAGAACTACCCAATCGTGC

AGAATATCCAGGGCCAGATGGTGCACCAGGCTATCTCTCCCCGCACCCTGA
ACGCCTGGGTGAAGGTGGTGGAGGAGAAGGCTTTCAGCCCTGAAGTGATCC
CAATGTTTTCTGCTCTGAGCGAGGGCGCCACACCTCAGGACCTGAACACAA
TGCTGAATACCGTGGGAGGACACCAGGCTGCTATGCAGATGCTGAAGGAGA
CAATCAACGAGGAGGCTGCCGAGTGGGACAGGGTGCACCCAGTGCACGCTG
GACCCATCGCCCCTGGCCAGATGAGGGAGCCTAGGGGCTCTGACATCGCTG
GCACCACAAGCACACTGCAGGAGCAGATCGGCTGGATGACCAACAATCCCC
CTATCCCCGTGGGCGAGATCTACAAGCGGTGGATCATCCTGGGCCTGAACA
AGATCGTGAGGATGTATTCCCCCGTGAGCATCCTGGACATCAGACAGGGCC
CAAAGGAGCCCTTCCGGGACTACGTGGATAGGTTTTATAAGACACTGAGGG
CTGAGCAGGCCAGCCAGGACGTGAAGAATTGGATGACAGAGACACTGCTG
GTGCAGAACGCTAATCCTGATTGCAAGACCATCCTGAAGGCCCTGGGCCCA
GCTGCCACACTGGAGGAGATGATGACCGCTTGTCAGGGCGTGGGCGGCCCA
GGACACAAAGCTAGGGTGCTGGCTGAGGCTATGAGCCAGGTGACAAACTCC
GCCACCATCATGATGCAGAGAGGCAACTTCAGAAATCAGCGCAAGACCGTG
AAGTGCTTTAACTGTGGCAAGGAGGGCCACATCGCTAAGAATTGCAGGGCT
CCAAGGAAGAAGGGATGCTGGAAGTGCGGCAAGGAAGGCCACCAGATGAA
GGACTGTACAGAGAGGCAGGCTAACTTCCTGGGCAAGATCTGGCCCTCCAA
TAAGGGCAGACCTGGCAACTTTCTGCAGAATAGGCCTGAGCCAACCGCTCC
ACCAGAGGAGTCCTTCAGATTTGGCGAGGAGACAACAACCCCATCTCAGAA
GCAGGAGCCCATCGATAAAGAAATGTATCCCCTGGCAAGCCTGAAGAGTCT
GTTCGGAAACGACCCATCCTCCCAGGGCGGGTCGACGAGCTCAGAATTCTG
CAGTCGACGGTACCGCGGGCCCGGGATCCACCGGCCGGTCGCCACCATGGT
GAGCAAGGGCGAGGAGCTGTTCACCGGGGTGGTGCCCATCCTGGTCGAGCT
GGACGGCGACGTAAACGGCCACAAGTTCAGCGTGTCCGGCGAGGGCGAGG
GCGATGCCACCTACGGCAAGCTGACCCTGAAGTTCATCTGCACCACCGGCA
AGCTGCCCGTGCCCTGGCCCACCCTCGTGACCACCCTGACCTACGGCGTGCA
GTGCTTCAGCCGCTACCCCGACCACATGAAGCAGCACGACTTCTTCAAGTCC
GCCATGCCCGAAGGCTACGTCCAGGAGCGCACCATCTTCTTCAAGGACGAC
GGCAACTACAAGACCCGCGCCGAGGTGAAGTTCGAGGGCGACACCCTGGTG
AACCGCATCGAGCTGAAGGGCATCGACTTCAAGGAGGACGGCAACATCCTG
GGGCACAAGCTGGAGTACAACTACAACAGCCACAACGTCTATATCATGGCC
GACAAGCAGAAGAACGGCATCAAGGTGAACTTCAAGATCCGCCACAACATC
GAGGACGGCAGCGTGCAGCTCGCCGACCACTACCAGCAGAACACCCCCATC
GGCGACGGCCCCGTGCTGCTGCCCGACAACCACTACCTGAGCACCCAGTCC
GCCCTGAGCAAAGACCCCAACGAGAAGCGCGATCACATGGTCCTGCTGGAG
TTCGTGACCGCCGCCGGGATCACTCTCGGCATGGACGAGCTGTACAAG

Figure 42. Coding sequence for the fusion protein Mos1.Gag-EGFP in 5'-to-3' direction.

ATGGAGACAGACACACTCCTGCTATGGGTACTGCTGCTCTGGGTTCCAGGTT
CCACTGGTGACTATCCATATGATGTTCCAGATTATGCTGGGGCCCAGCCGGC
CAGATCTGGCGGCGGCCTGAACGACATCTTCGAGGCCCAGAAGATCGAGTG
GCACGAGGGCGCGCCGATGGTGAGCAAGGGCGAGGAGGTCATCAAAGAGT
TCATGCGCTTCAAGGTGCGCATGGAGGGCTCCATGAACGGCCACGAGTTCG
AGATCGAGGGCGAGGGCGAGGGCGCCCCTACGAGGGCACCCAGACCGCC
AAGCTGAAGGTGACCAAGGGCGGCCCCCTGCCCTTCGCCTGGGACATCCTG

TCCCCCCAGTTCATGTACGGCTCCAAGGCGTACGTGAAGCACCCCGCCGAC
ATCCCCGATTACAAGAAGCTGTCCTTCCCCGAGGGCTTCAAGTGGGAGCGC
GTGATGAACTTCGAGGACGGCGGTCTGGTGACCGTGACCCAGGACTCCTCC
CTGCAGGACGGCACGCTGATCTACAAGGTGAAGATGCGCGGCACCAACTTC
CCCCCCGACGGCCCCGTAATGCAGAAGAAGACCATGGGCTGGGAGGCCTCC
ACCGAGCGCCTGTACCCCCGCGACGGCGTGCTGAAGGGCGAGATCCACCAG
GCCCTGAAGCTGAAGGACGGCGGCCACTACCTGGTGGAGTTCAAGACCATC
TACATGGCCAAGAAGCCCGTGCAACTGCCCGGCTACTACTACGTGGACACC
AAGCTGGACATCACCTCCCACAACGAGGACTACACCATCGTGGAACAGTAC
GAGCGCTCCGAGGGCCGCCACCACCTGTTCCTGTACGGCATGGACGAGCTG
TACAAGCGGCCGCGGCTGCAGGTCGACGAACAAAAACTCATCTCAGAAGAG
GATCTGAATGCTGTGGGCCAGGACACGCAGGAGGTCATCGTGGTGCCACAC
TCCTTGCCCTTTAAGGTGGTGGTGATCTCAGCCATCCTGGCCCTGGTGGTGC
TCACCATCATCTCCCTTATCATCCTCATCATGCTTTGGCAGAAGAAGCCACG
T

Figure 43. Coding sequence for the fusion protein dTomato-PDGFR β TM in 5'-to-3' direction. The nucleotide sequence encoding dTomato originated from the plasmid pLenti-V6.3 Ultra-Chili, which was a gift from Ewa Snaar-Jagalska (Addgene plasmid #106173; http://n2t.net/addgene:106173; RRID:Addgene_106173). The nucleotide sequence coding for PDGFR β TM originated from the plasmid pDisplay-AP-CFP-TM, which was a gift from Alice Ting (Addgene plasmid #20861; http://n2t.net/addgene:20861; RRID:Addgene_20861) [264].

12.   References

References

1.   Naseer, S.; Khalid, S.; Parveen, S.; Abbass, K.; Song, H.; Achim, M. V. COVID-19 outbreak: Impact on global economy. *Frontiers in Public Health* **2022**, *10*, 1009393, doi:10.3389/fpubh.2022.1009393.

2.   Watson, O. J.; Barnsley, G.; Toor, J.; Hogan, A. B.; Winskill, P.; Ghani, A. C. Global impact of the first year of COVID-19 vaccination: a mathematical modelling study. *The Lancet Infectious Diseases* **2022**, *22*, 1293–1302, doi:10.1016/S1473-3099(22)00320-6.

3.   Saleh, A.; Qamar, S.; Tekin, A.; Singh, R.; Kashyap, R. Vaccine Development Throughout History. *Cureus* **2021**, *13*, e16635, doi:10.7759/cureus.16635.

4.   Tannock, G. A.; Kim, H.; Xue, L. Why are vaccines against many human viral diseases still unavailable; an historic perspective? *J. Med. Virol.* **2020**, *92*, 129–138, doi:10.1002/jmv.25593.

5.   Cuevas, J. M.; Geller, R.; Garijo, R.; López-Aldeguer, J.; Sanjuán, R.; Rowland-Jones, S. L. Extremely High Mutation Rate of HIV-1 In Vivo. *PLOS Biology* **2015**, *13*, e1002251, doi:10.1371/journal.pbio.1002251.

6.   Barouch, D. H. Challenges in the development of an HIV-1 vaccine. *Nature* **2008**, *455*, 613–619, doi:10.1038/nature07352.

7.   Barton F. Haynes; Peter B. Gilbert; M. Juliana McElrath; Susan Zolla-Pazner; Georgia D Tomaras; S Munir Alam; David T Evans; David C Montefiori; Chitraporn Karnasuta; Ruengpueng Sutthent*; et al.* Immune-Correlates Analysis of an HIV-1 Vaccine Efficacy Trial. *New England Journal of Medicine* **2012**, *366*, 1275–1286, doi:10.1056/NEJMoa1113425.

8.   Alter, G.; Barouch, D. Immune Correlate-Guided HIV Vaccine Design. *Cell Host and Microbe* **2018**, *24*, 25–33, doi:10.1016/j.chom.2018.06.012.

9. Oxenius, A.; Price, D. A.; Hersberger, M.; Schlaepfer, E.; Weber, R.; Weber, M.; Kundig, T. M.; Böni, J.; Joller, H.; Phillips, R. E.*; et al.* HIV-Specific Cellular Immune Response Is Inversely Correlated with Disease Progression as Defined by Decline of CD4+ T Cells in Relation to HIV RNA Load. *The Journal of Infectious Diseases* **2004**, *189*, 1199–1208, doi:10.1086/382028.

10. Zolla-Pazner, S.; DeCamp, A.; Gilbert, P. B.; Williams, C.; Yates, N. L.; Williams, W. T.; Howington, R.; Fong, Y.; Morris, D. E.; Soderberg, K. A.*; et al.* Vaccine-Induced IgG Antibodies to V1V2 Regions of Multiple HIV-1 Subtypes Correlate with Decreased Risk of HIV-1 Infection. *PLoS ONE* **2014**, *9*, e87572, doi:10.1371/journal.pone.0087572.

11. Korber, B.; Fischer, W. T cell-based strategies for HIV-1 vaccines. *Human Vaccines & Immunotherapeutics* **2020**, *16*, 713–722, doi:10.1080/21645515.2019.1666957.

12. Santra, S.; Liao, H.-X.; Zhang, R.; Muldoon, M.; Watson, S.; Fischer, W.; Theiler, J.; Szinger, J.; Balachandran, H.; Buzby, A.*; et al.* Mosaic vaccines elicit CD8+ T lymphocyte responses that confer enhanced immune coverage of diverse HIV strains in monkeys. *Nature Medicine* **2010**, *16*, 324–328, doi:10.1038/nm.2108.

13. Barouch, D. H.; O'Brien, K. L.; Simmons, N. L.; King, S. L.; Abbink, P.; Maxfield, L. F.; Sun, Y.-H.; La Porte, A.; Riggs, A. M.; Lynch, D. M.*; et al.* Mosaic HIV-1 vaccines expand the breadth and depth of cellular immune responses in rhesus monkeys. *Nature Medicine* **2010**, *16*, 319–323, doi:10.1038/nm.2089.

14. Langedijk, J. P. M.; Van Manen, D.; Vellinga, J.; Wegmann, F.; Callendret, B. C. S.; Krarup, A.; Stitz, J. Synthetic human immunodeficiency virus (HIV) envelope antigen, vectors, and compositions thereof **2019**, *US 10,369,214*.

15. Fischer, W.; Perkins, S.; Theiler, J.; Bhattacharya, T.; Yusim, K.; Funkhouser, R.; Kuiken, C.; Haynes, B.; Letvin, N. L.; Walker, B. D.*; et al.* Polyvalent vaccines for optimal coverage of potential T-cell epitopes in global HIV-1 variants. *Nature Medicine* **2007**, *13*, 100–106, doi:10.1038/nm1461.

16. Gheysen, D.; Jacobs, E.; de Foresta, F.; Thiriart, C.; Francotte, M.; Thines, D.; De Wilde, M. Assembly and release of HIV-1 precursor Pr55gag virus-like particles from recombinant baculovirus-infected insect cells. *Cell* **1989**, *59*, 103–112, doi:10.1016/0092-8674(89)90873-8.

17. Lavado-García, J.; Jorge, I.; Boix-Besora, A.; Vázquez, J.; Gòdia, F.; Cervera, L. Characterization of HIV-1 virus-like particles and determination of Gag stoichiometry for different production platforms. *Biotechnology and Bioengineering* **2021**, *118*, 2660–2675, doi:10.1002/bit.27786.

18. Bachmann, M. F.; Jennings, G. T. Vaccine delivery: a matter of size, geometry, kinetics and molecular patterns. *Nature Reviews Immunology* **2010**, *10*, 787–796, doi:10.1038/nri2868.

19. Temchura, V.; Kalinin, S.; Nabi, G.; Tippler, B.; Niezold, T.; Überla, K. Divergence of Primary Cognate B- and T-Cell Proliferative Responses to Subcutaneous and Intravenous Immunization with Virus-Like Particles. *Viruses* **2014**, *6*, 3334–3347, doi:10.3390/v6083334.

20. Zhang, S.; Cubas, R.; Li, M.; Chen, C.; Yao, Q. Virus-like particle vaccine activates conventional B2 cells and promotes B cell differentiation to IgG2a producing plasma cells. *Molecular Immunology* **2009**, *46*, 1988–2001, doi:10.1016/j.molimm.2009.03.008.

21. Tsunetsugu-Yokota, Y.; Morikawa, Y.; Isogai, M.; Kawana-Tachikawa, A.; Odawara, T.; Nakamura, T.; Grassi, F.; Autran, B.; Iwamoto, A. Yeast-Derived Human Immunodeficiency Virus Type 1 p55 ^{gag} Virus-Like Particles Activate Dendritic Cells (DCs) and Induce Perforin Expression in Gag-Specific CD8 $^{+}$ T Cells by Cross-Presentation of DCs. *Journal of Virology* **2003**, *77*, 10250–10259, doi:10.1128/JVI.77.19.10250-10259.2003.

22. Deml, L.; Speth, C.; Dierich, M. P.; Wolf, H.; Wagner, R. Recombinant HIV-1 Pr55gag virus-like particles: potent stimulators of innate and acquired immune responses. *Molecular Immunology* **2005**, *42*, 259–277, doi:10.1016/j.molimm.2004.06.028.

23. Raposo, G.; Stoorvogel, W. Extracellular vesicles: Exosomes, microvesicles, and friends. *Journal of Cell Biology* **2013**, *200*, 373–383, doi:10.1083/jcb.201211138.

24. Steppert, P.; Burgstaller, D.; Klausberger, M.; Berger, E.; Pereira Aguilar, P.; Schneider, T. A.; Kramberger, P.; Tover, A.; Nöbauer, K.; Razzazi-Fazeli, E.*; et al.* Purification of HIV-1 gag virus-like particles and separation of other extracellular particles. *Journal of Chromatography A* **2016**, *1455*, 93–101, doi:10.1016/j.chroma.2016.05.053.

25. Reiter, K.; Pereira Aguilar, P.; Wetter, V.; Steppert, P.; Tover, A.; Jungbauer, A. Separation of virus-like particles and extracellular vesicles by flow-through and heparin affinity chromatography. *Journal of Chromatography A* **2019**, *1588*, 77–84, doi:10.1016/j.chroma.2018.12.035.

26. van Doorn, R. H. The epidemiology of emerging infectious diseases and pandemics **2021**, *49*, 659–662, doi:10.1016/j.mpmed.2021.07.011.

27. Woolhouse, M. E. J.; Brierley, L. Epidemiological characteristics of human-infective RNA viruses. *Scientific Data* **2018**, *5*, 180017, doi:10.1038/sdata.2018.17.

28. Cesarman, E.; Damania, B.; Krown, S. E.; Martin, J.; Bower, M.; Whitby, D. Kaposi sarcoma. *Nature Reviews Disease Primers* **2019**, *5*, 9, doi:10.1038/s41572-019-0060-9.

29. Angel A. Justiz Vaillant; Roopa Naik. *HIV-1 Associated Opportunistic Infections. StatPearls*. Available online: https://www.ncbi.nlm.nih.gov/books/NBK539787/ (accessed on 19 February 2023).

30. Gottlieb, M. S.; Schroff, R.; Schanker, H. M.; Weisman, J. D.; Fan, P. T.; Wolf, R. A.; Saxon, A. Pneumocystis carinii pneumonia and mucosal candidiasis in previously healthy homosexual men: evidence of a new acquired cellular immunodeficiency. *New England Journal of Medicine* **1981**, *305*, 1425–1431, doi:10.1056/NEJM198112103052401.

31. HIV.gov. *A Timeline of HIV and AIDS*. Available online: https://www.hiv.gov/hiv-basics/overview/history/hiv-and-aids-timeline#year-1981 (accessed on 19 February 2023).

32. Barré-Sinoussi, F.; Chermann, J. C.; Rey, F.; Nugeyre, M. T.; Chamaret, S.; Gruest, J.; Dauguet, C.; Axler-Blin, C.; Vézinet-Brun, F.; Rouzioux, C.*; et al.* Isolation of a T-Lymphotropic Retrovirus from a Patient at Risk for Acquired Immune Deficiency Syndrome (AIDS). *Science* **1983**, *220*, 868–871, doi:10.1126/science.6189183.

33. Di Marzo Veronese, F.; Copeland, T. D.; DeVico, A. L.; Rahman, R.; Oroszlan, S.; Gallo, R. C.; Sarngadharan, M. G. Characterization of highly immunogenic p66/p51 as the reverse transcriptase of HTLV-III/LAV. *Science* **1986**, *231*, 1289–1291, doi:10.1126/science.2418504.

34. van Heuvel, Y.; Schatz, S.; Rosengarten, J. F.; Stitz, J. Infectious RNA: Human Immunodeficiency Virus (HIV) Biology, Therapeutic Intervention, and the Quest for a Vaccine. *Toxins* **2022**, *14*, 138, doi:10.3390/toxins14020138.

35. Hu, W.-S.; Hughes, S. H. HIV-1 Reverse Transcription. *Cold Spring Harbor Perspectives in Medicine* **2012**, *2*, a006882-a006882, doi:10.1101/cshperspect.a006882.

36. Marintcheva, B. Viral Tools for In Vitro Manipulations of Nucleic Acids. *Harnessing the Power of Viruses* **2018**, doi:10.1016/B978-0-12-810514-6.00002-7.

37. Woolhouse, M. E. J.; Adair, K.; Brierley, L.; Atlas, R. M.; Maloy, S. RNA Viruses: A Case Study of the Biology of Emerging Infectious Diseases. *Microbiology Spectrum* **2013**, *1*, doi:10.1128/microbiolspec.OH-0001-2012.

38. World Health Organization. Zoonoses. Available online: https://www.who.int/news-room/fact-sheets/detail/zoonoses (accessed on 19 February 2023).

39. Sharp, P. M.; Hahn, B. H. Origins of HIV and the AIDS Pandemic. *Cold Spring Harbor Perspectives in Medicine* **2011**, *1*, a006841-a006841, doi:10.1101/cshperspect.a006841.

40. Giovanetti, M.; Ciccozzi, M.; Parolin, C.; Borsetti, A. Molecular Epidemiology of HIV-1 in African Countries: A Comprehensive Overview. *Pathogens* **2020**, *9*, 1072, doi:10.3390/pathogens9121072.

41. Peeters, M.; Gueye, A.; Mboup, S.; Bibollet-Ruche, F.; Ekaza, E.; Mulanga, C.; Ouedrago, R.; Gandji, R.; Mpele, P.; Dibanga, G.*; et al.* Geographical distribution of HIV-1 group O viruses in Africa. *AIDS* **1997**, *11*, 493–498, doi:10.1097/00002030-199704000-00013.

42. Simon, F.; Mauclère, P.; Roques, P.; Loussert-Ajaka, I.; Müller-Trutwin, M. C.; Saragosti, S.; Georges-Courbot, M. C.; Barré-Sinoussi, F.; Brun-Vézinet, F. Identification of a new human immunodeficiency virus type 1 distinct from group M and group O. *Nature Medicine* **1998**, *4*, 1032–1037, doi:10.1038/2017.

43. Ayouba, A.; Souquières, S.; Njinku, B.; Martin, P. M. V.; Müller-Trutwin, M. C.; Roques, P.; Barré-Sinoussi, F.; Mauclère, P.; Simon, F.; Nerrienet, E. HIV-1 group N among HIV-1-seropositive individuals in Cameroon. *AIDS* **2000**, *14*, 2623–2625, doi:10.1097/00002030-200011100-00033.

44. Yamaguchi, J.; Coffey, R.; Vallari, A.; Ngansop, C.; Mbanya, D.; Ndembi, N.; Kaptué, L.; Gürtler, L. G.; Bodelle, P.; Schochetman, G.*; et al.* Identification of HIV Type 1 Group N Infections in a Husband and Wife in Cameroon: Viral Genome Sequences Provide Evidence for Horizontal Transmission. *AIDS Research and Human Retroviruses* **2006**, *22*, 83–92, doi:10.1089/aid.2006.22.83.

45. Plantier, J.-C.; Leoz, M.; Dickerson, J. E.; De Oliveira, F.; Cordonnier, F.; Lemée, V.; Damond, F.; Robertson, D. L.; Simon, F. A new human immunodeficiency virus derived from gorillas. *Nature Medicine* **2009**, *15*, 871–872, doi:10.1038/nm.2016.

46. Vallari, A.; Holzmayer, V.; Harris, B.; Yamaguchi, J.; Ngansop, C.; Makamche, F.; Mbanya, D.; Kaptué, L.; Ndembi, N.; Gürtler, L.*; et al.* Confirmation of Putative HIV-1 Group P in Cameroon. *Journal of Virology* **2011**, *85*, 1403–1407, doi:10.1128/JVI.02005-10.

47. Gallo, R. C.; Montagnier, L. The chronology of AIDS research. *Nature* **1987**, *326*, 435–436, doi:10.1038/326435a0.

48. Ratner, L.; Haseltine, W.; Patarca, R.; Livak, K. J.; Starcich, B.; Josephs, S. F.; Doran, E. R.; Rafalski, J. A.; Whitehorn, E. A.; Baumeister, K. Complete nucleotide sequence of the AIDS virus, HTLV-III. *Nature* **1985**, *313*, 277–284, doi:10.1038/313277a0.

49. Wain-Hobson, S.; Sonigo, P.; Danos, O.; Cole, S.; Alizon, M. Nucleotide sequence of the AIDS virus, LAV. *Cell* **1985**, *40*, 9–17, doi:10.1016/0092-8674(85)90303-4.

50. Coffin, J.M.; Hughes, S.H.; Varmus, H.E.; editors. *Retroviruses;* Cold Spring Harbor (NY): Cold Spring Harbor Laboratory Press, 1997. Available online: https://www.ncbi.nlm.nih.gov/books/NBK19464/ (accessed on 21 February 2023).

51. Cervera, L.; Gòdia, F.; Tarrés-Freixas, F.; Aguilar-Gurrieri, C.; Carrillo, J.; Blanco, J.; Gutiérrez-Granados, S. Production of HIV-1-based virus-like particles for vaccination: achievements and limits. *Applied Microbiology and Biotechnology* **2019**, *103*, 7367–7384, doi:10.1007/s00253-019-10038-3.

52. Lever, A.; Gottlinger, H.; Haseltine, W.; Sodroski, J. Identification of a sequence required for efficient packaging of human immunodeficiency virus type 1 RNA into virions. *Journal of Virology* **1989**, *63*, 4085–4087, doi:10.1128/jvi.63.9.4085-4087.1989.

53. Peng, C.; Ho, B. K.; Chang, T. W.; Chang, N. T. Role of human immunodeficiency virus type 1-specific protease in core protein maturation and viral infectivity. *Journal of Virology* **1989**, *63*, 2550–2556, doi:10.1128/jvi.63.6.2550-2556.1989.

54. Bryant, M.; Ratner, L. Myristoylation-dependent replication and assembly of human immunodeficiency virus 1. *Proceedings of the National Academy of Sciences* **1990**, *87*, 523–527, doi:10.1073/pnas.87.2.523.

55. Bell, N. M.; Lever, A. . M. HIV Gag polyprotein: processing and early viral particle assembly. *Trends in Microbiology* **2013**, *21*, 136–144, doi:10.1016/j.tim.2012.11.006.

56. Müller, B.; Kräusslich, H.-G. HIV-1 Maturation. *Encyclopedia of AIDS* **2013**, doi:10.1007/978-1-4614-9610-6_59-1.

57. Veronese, F. D.; Copeland, T. D.; Oroszlan, S.; Gallo, R. C.; Sarngadharan, M. G. Biochemical and immunological analysis of human immunodeficiency virus gag gene products p17 and p24. *Journal of Virology* **1988**, *62*, 795–801, doi:10.1128/jvi.62.3.795-801.1988.

58. Mervis, R. J.; Ahmad, N.; Lillehoj, E. P.; Raum, M. G.; Salazar, F. H.; Chan, H. W.; Venkatesan, S. The gag gene products of human immunodeficiency virus type 1: alignment within the gag open reading frame, identification of posttranslational modifications, and evidence for alternative gag precursors. *Journal of Virology* **1988**, *62*, 3993–4002, doi:10.1128/JVI.62.11.3993-4002.1988.

59. Hill, M.; Tachedjian, G.; Mak, J. The packaging and maturation of the HIV-1 Pol proteins. *Current HIV Research* **2005**, *3*, 73–85, doi:10.2174/1570162052772942.

60. Moulard, M.; Decroly, E. Maturation of HIV envelope glycoprotein precursors by cellular endoproteases. *Biochimica et Biophysica Acta (BBA) - Reviews on Biomembranes* **2000**, *1469*, 121–132, doi:10.1016/S0304-4157(00)00014-9.

61. Allan, J. S.; Coligan, J. E.; Barin, F.; McLane, M. F.; Sodroski, J. G.; Rosen, C. A.; Haseltine, W. A.; Lee, T. H.; Essex, M. Major glycoprotein antigens that induce antibodies in AIDS patients are encoded by HTLV-III. *Science* **1985**, *228*, 1091–1094, doi:10.1126/science.2986290.

62. Veronese, F. D.; DeVico, A. L.; Copeland, T. D.; Oroszlan, S.; Gallo, R. C.; Sarngadharan, M. G. Characterization of gp41 as the transmembrane protein coded

by the HTLV-III/LAV envelope gene. *Science* **1985**, *229*, 1402–1405, doi:10.1126/science.2994223.

63. Checkley, M. A.; Luttge, B. G.; Freed, E. O. HIV-1 Envelope Glycoprotein Biosynthesis, Trafficking, and Incorporation. *Journal of Molecular Biology* **2011**, *410*, 582–608, doi:10.1016/j.jmb.2011.04.042.

64. Gallaher, W. R.; Ball, J. M.; Garry, R. F.; Griffin, M. C.; Montalero, R. C. A General Model for the Transmembrane Proteins of HIV and Other Retroviruses. *AIDS Research and Human Retroviruses* **1989**, *5*, 431–440, doi:10.1089/aid.1989.5.431.

65. Rossi, E.; Meuser, M. E.; Cunanan, C. J.; Cocklin, S. Structure, Function, and Interactions of the HIV-1 Capsid Protein. *Life* **2021**, *11*, 100, doi:10.3390/life11020100.

66. *"HIV-1 Genome and Structure", by BioRender.com (2023)*. Available online: https://app.biorender.com/biorender-templates (accessed on 21 February 2023).

67. Gallo, S. A.; Finnegan, C. M.; Viard, M.; Raviv, Y.; Dimitrov, A.; Rawat, S. S.; Puri, A.; Durell, S.; Blumenthal, R. The HIV Env-mediated fusion reaction. *Biochimica et Biophysica Acta (BBA) - Biomembranes* **2003**, *1614*, 36–50, doi:10.1016/S0005-2736(03)00161-5.

68. Berger, E. A.; Farber, J. M.; Murphy, P. M. Chemokine receptors as HIV-1 coreceptors: Roles in Viral Entry, Tropism, and Disease. *Annual Review of Immunology* **1999**, *17*, 657–700, doi:10.1146/annurev.immunol.17.1.657.

69. Zila, V.; Margiotta, E.; Turoňová, B.; Müller, T. G.; Zimmerli, C. E.; Mattei, S.; Allegretti, M.; Börner, K.; Rada, J.; Müller, B.*; et al.* Cone-shaped HIV-1 capsids are transported through intact nuclear pores. *Cell* **2021**, *184*, 1032-1046.e18, doi:10.1016/j.cell.2021.01.025.

70. Dharan, A.; Bachmann, N.; Talley, S.; Zwikelmaier, V.; Campbell, E. M. Nuclear pore blockade reveals that HIV-1 completes reverse transcription and uncoating in

the nucleus. *Nature Microbiology* **2020**, *5*, 1088–1095, doi:10.1038/s41564-020-0735-8.

71. Burdick, R. C.; Li, C.; Munshi, M. H.; Rawson, J. M. O.; Nagashima, K.; Hu, W.-S.; Pathak, V. K. HIV-1 uncoats in the nucleus near sites of integration. *Proceedings of the National Academy of Sciences* **2020**, *117*, 5486–5493, doi:10.1073/pnas.1920631117.

72. Craigie, R.; Bushman, F. D. HIV DNA Integration. *Cold Spring Harbor Perspectives in Medicine* **2012**, *2*, a006890-a006890, doi:10.1101/cshperspect.a006890.

73. Chiu, T.; Davies, D. Structure and Function of HIV-1 Integrase. *Current Topics in Medicinal Chemistry* **2004**, *4*, 965–977, doi:10.2174/1568026043388547.

74. Beilhartz, G. L.; Götte, M. HIV-1 Ribonuclease H: Structure, Catalytic Mechanism and Inhibitors. *Viruses* **2010**, *2*, 900–926, doi:10.3390/v2040900.

75. Shukla, A.; Ramirez, N.-G. P.; D'Orso, I. HIV-1 Proviral Transcription and Latency in the New Era. *Viruses* **2020**, *12*, 555, doi:10.3390/v12050555.

76. Ruelas, D. S.; Greene, W. C. An Integrated Overview of HIV-1 Latency. *Cell* **2013**, *155*, 519–529, doi:10.1016/j.cell.2013.09.044.

77. Chavez, L.; Calvanese, V.; Verdin, E.; Emerman, M. HIV Latency Is Established Directly and Early in Both Resting and Activated Primary CD4 T Cells. *PLoS Pathogens* **2015**, *11*, e1004955, doi:10.1371/journal.ppat.1004955.

78. *"HIV Replication Cycle", by BioRender.com (2023)*. Available online: https://app.biorender.com/biorender-templates (accessed on 21 February 2023).

79. Emery, A.; Swanstrom, R. HIV-1: To Splice or Not to Splice, That Is the Question. *Viruses* **2021**, *13*, 181, doi:10.3390/v13020181.

80. Dutilleul, A.; Rodari, A.; Van Lint, C. Depicting HIV-1 Transcriptional Mechanisms: A Summary of What We Know. *Viruses* **2020**, *12*, 1385, doi:10.3390/v12121385.

81. Geyer, H.; Holschbach, C.; Hunsmann, G.; Schneider, J. Carbohydrates of human immunodeficiency virus. Structures of oligosaccharides linked to the envelope glycoprotein 120. *The Journal of biological chemistry* **1988**, *263*, 11760–11767.

82. McCune, J. M.; Rabin, L. B.; Feinberg, M. B.; Lieberman, M.; Kosek, J. C.; Reyes, G. R.; Weissman, I. L. Endoproteolytic cleavage of gp160 is required for the activation of human immunodeficiency virus. *Cell* **1988**, *53*, 55–67, doi:10.1016/0092-8674(88)90487-4.

83. Ghanam, R. H.; Samal, A. B.; Fernandez, T. F.; Saad, J. S. Role of the HIV-1 Matrix Protein in Gag Intracellular Trafficking and Targeting to the Plasma Membrane for Virus Assembly. *Frontiers in Microbiology* **2012**, *3*, 55, doi:10.3389/fmicb.2012.00055.

84. Brügger, B.; Glass, B.; Haberkant, P.; Leibrecht, I.; Wieland, F. T.; Kräusslich, H.-G. The HIV lipidome: a raft with an unusual composition. *Proceedings of the National Academy of Sciences* **2006**, *103*, 2641–2646, doi:10.1073/pnas.0511136103.

85. Shaw, G. M.; Hunter, E. HIV Transmission. *Cold Spring Harbor Perspectives in Medicine* **2012**, *2*, a006965-a006965, doi:10.1101/cshperspect.a006965.

86. *Drug Abuse and HIV Research Report Series*. Available online: https://nida.nih.gov/publications/research-reports/hivaids/who-risk-hiv-infection-which-populations-are-most-affected.

87. Deeks, S. G.; Overbaugh, J.; Phillips, A.; Buchbinder, S. HIV infection. *Nature Reviews Disease Primers* **2015**, *1*, 15035, doi:10.1038/nrdp.2015.35.

88. Moir, S.; Chun, T.-W.; Fauci, A. S. Pathogenic Mechanisms of HIV Disease. *Annual Review of Pathology: Mechanisms of Disease* **2011**, *6*, 223–248, doi:10.1146/annurev-pathol-011110-130254.

89. Poorolajal, J.; Hooshmand, E.; Mahjub, H.; Esmailnasab, N.; Jenabi, E. Survival rate of AIDS disease and mortality in HIV-infected patients: a meta-analysis. *Public Health* **2016**, *139*, 3–12, doi:10.1016/j.puhe.2016.05.004.

90. Rosendahl Huber, S.; van Beek, J.; de Jonge, J.; Luytjes, W.; van Baarle, D. T Cell Responses to Viral Infections - Opportunities for Peptide Vaccination. *Frontiers in Immunology* **2014**, *5*, doi:10.3389/fimmu.2014.00171.

91. Perez, C. L.; Milush, J. M.; Buggert, M.; Eriksson, E. M.; Larsen, M. V.; Liegler, T.; Hartogensis, W.; Bacchetti, P.; Lund, O.; Hecht, F. M.*; et al.* Targeting of Conserved Gag-Epitopes in Early HIV Infection Is Associated with Lower Plasma Viral Load and Slower CD4+ T Cell Depletion. *AIDS Research and Human Retroviruses* **2013**, *29*, 602–612, doi:10.1089/aid.2012.0171.

92. Deeks, S. G.; Walker, B. D. Human Immunodeficiency Virus Controllers: Mechanisms of Durable Virus Control in the Absence of Antiretroviral Therapy. *Immunity* **2007**, *27*, 406–416, doi:10.1016/j.immuni.2007.08.010.

93. Munro, J. B.; Gorman, J.; Ma, X.; Zhou, Z.; Arthos, J.; Burton, D. R.; Koff, W. C.; Courter, J. R.; Smith, A. B.; Kwong, P. D.*; et al.* Conformational dynamics of single HIV-1 envelope trimers on the surface of native virions. *Science* **2014**, *346*, 759–763, doi:10.1126/science.1254426.

94. Griffith, S. A.; McCoy, L. E. To bnAb or Not to bnAb: Defining Broadly Neutralising Antibodies Against HIV-1. *Frontiers in Immunology* **2021**, *12*, 1–16, doi:10.3389/fimmu.2021.708227.

95. Mascola, J. R.; Montefiori, D. C. The Role of Antibodies in HIV Vaccines. *Annual Review of Immunology* **2010**, *28*, 413–444, doi:10.1146/annurev-immunol-030409-101256.

96. Doores, K. J. The HIV glycan shield as a target for broadly neutralizing antibodies. *FEBS Journal* **2015**, *282*, 4679–4691, doi:10.1111/febs.13530.

97. Corti, D.; Lanzavecchia, A. Broadly Neutralizing Antiviral Antibodies. *Annual Review of Immunology* **2013**, *31*, 705–742, doi:10.1146/annurev-immunol-032712-095916.

98. van Gils, M. J.; Sanders, R. W. Broadly neutralizing antibodies against HIV-1: Templates for a vaccine. *Virology* **2013**, *435*, 46–56, doi:10.1016/j.virol.2012.10.004.

99. Binley, J. M.; Lybarger, E. A.; Crooks, E. T.; Seaman, M. S.; Gray, E.; Davis, K. L.; Decker, J. M.; Wycuff, D.; Harris, L.; Hawkins, N.*; et al.* Profiling the Specificity of Neutralizing Antibodies in a Large Panel of Plasmas from Patients Chronically Infected with Human Immunodeficiency Virus Type 1 Subtypes B and C. *Journal of Virology* **2008**, *82*, 11651–11668, doi:10.1128/JVI.01762-08.

100. Subbaraman, H.; Schanz, M.; Trkola, A. Broadly neutralizing antibodies: What is needed to move from a rare event in HIV-1 infection to vaccine efficacy? *Retrovirology* **2018**, *15*, 52, doi:10.1186/s12977-018-0433-2.

101. Forsythe, S. S.; McGreevey, W.; Whiteside, A.; Shah, M.; Cohen, J.; Hecht, R.; Bollinger, L. A.; Kinghorn, A. Twenty Years Of Antiretroviral Therapy For People Living With HIV: Global Costs, Health Achievements, Economic Benefits. *Health affairs (Project Hope)* **2019**, *38*, 1163–1172, doi:10.1377/hlthaff.2018.05391.

102. U.S. Department of Health & Human Services. *FDA-Approved HIV Medicines*, 2021. Available online: https://hivinfo.nih.gov/understanding-hiv/fact-sheets/fda-approved-hiv-medicines (accessed on 21 February 2023).

103. Panel on Antiretroviral Guidelines for Adults and Adolescents. Guidelines for the Use of Antiretroviral Agents in Adults and Adolescents with HIV (2021). Available online: https://clinicalinfo.hiv.gov/sites/default/files/guidelines/documents/adult-adolescent-arv/guidelines-adult-adolescent-arv.pdf (accessed on 21 February 2023).

104. Volberding, P. A.; Deeks, S. G. Antiretroviral therapy and management of HIV infection. *The Lancet* **2010**, *376*, 49–62, doi:10.1016/S0140-6736(10)60676-9.

105. Cunha, R. F.; Simões, S.; Carvalheiro, M.; Azevedo Pereira, J. M.; Costa, Q.; Ascenso, A. Novel Antiretroviral Therapeutic Strategies for HIV. *Molecules* **2021**, *26*, 5305, doi:10.3390/molecules26175305.

106. Pennings, P. S. HIV drug resistance: problems and perspectives. *Infectious Disease Reports* **2013**, *5*, e5, doi:10.4081/idr.2013.s1.e5.

107. Mohri, H.; Singh, M. K.; Ching, W. T.; Ho, D. D. Quantitation of zidovudine-resistant human immunodeficiency virus type 1 in the blood of treated and untreated patients. *Proceedings of the National Academy of Sciences* **1993**, *90*, 25–29, doi:10.1073/pnas.90.1.25.

108. Cohen, M. S.; Chen, Y. Q.; McCauley, M.; Gamble, T.; Hosseinipour, M. C.; Kumarasamy, N.; Hakim, J. G.; Kumwenda, J.; Grinsztejn, B.; Pilotto, J. H.*; et al.* Antiretroviral Therapy for the Prevention of HIV-1 Transmission. *New England Journal of Medicine* **2016**, *375*, 830–839, doi:10.1056/NEJMoa1600693.

109. Eakle, R.; Venter, F.; Rees, H. Pre-exposure prophylaxis (PrEP) in an era of stalled HIV prevention: Can it change the game? *Retrovirology* **2018**, *15*, 29, doi:10.1186/s12977-018-0408-3.

110. Blair, H. A. Cabotegravir Extended-Release Injectable Suspension: A Review in HIV-1 Pre-Exposure Prophylaxis. *Drugs* **2022**, *82*, 1489–1498, doi:10.1007/s40265-022-01791-3.

111. Rey, D. Post-exposure prophylaxis for HIV infection. *Expert Review of Anti-infective Therapy* **2011**, *9*, 431–442, doi:10.1586/eri.11.20.

112. Davey, R. T.; Bhat, N.; Yoder, C.; Chun, T.-W.; Metcalf, J. A.; Dewar, R.; Natarajan, V.; Lempicki, R. A.; Adelsberger, J. W.; Miller, K. D.*; et al.* HIV-1 and T cell dynamics after interruption of highly active antiretroviral therapy (HAART) in patients with a history of sustained viral suppression. *Proceedings of the*

National Academy of Sciences **1999**, *96*, 15109–15114, doi:10.1073/pnas.96.26.15109.

113. World Health Organization. *Data on the HIV response.* Available online: https://www.who.int/data/gho/data/themes/hiv-aids/data-on-the-hiv-aids-response (accessed on 21 February 2023).

114. Trovato, M.; D'Apice, L.; Prisco, A.; De Berardinis, P. HIV Vaccination: A Roadmap among Advancements and Concerns. *International Journal of Molecular Sciences* **2018**, *19*, 1241, doi:10.3390/ijms19041241.

115. Rao, M.; Peachman, K.; Kim, J.; Gao, G.; Alving, C.; Michael, N.; Rao, V. HIV-1 Variable Loop 2 and its Importance in HIV-1 Infection and Vaccine Development. *Current HIV Research* **2013**, *11*, 427–438, doi:10.2174/1570162X113116660064.

116. Burton, D. R.; Hangartner, L. Broadly Neutralizing Antibodies to HIV and Their Role in Vaccine Design. *Annual Review of Immunology* **2016**, *34*, 635–659, doi:10.1146/annurev-immunol-041015-055515.

117. Wibmer, C. K.; Moore, P. L.; Morris, L. HIV broadly neutralizing antibody targets. *Current Opinion in HIV and AIDS* **2015**, *10*, 135–143, doi:10.1097/COH.0000000000000153.

118. De Rose, R.; Kent, S. J.; Ranasinghe, C. Prime-Boost Vaccination: Impact on the HIV-1 Vaccine Field. *Novel Approaches and Strategies for Biologics, Vaccines and Cancer Therapies* **2015**, doi:10.1016/B978-0-12-416603-5/00012-2.

119. D'Souza, M. P.; Yang, O. O. Adenovirus vectors as HIV-1 vaccines. *AIDS* **2015**, *29*, 395–400, doi:10.1097/QAD.0000000000000548.

120. Gómez, C. E.; Perdiguero, B.; García-Arriaza, J.; Esteban, M. Poxvirus vectors as HIV/AIDS vaccines in humans. *Human Vaccines & Immunotherapeutics* **2012**, *8*, 1192–1207, doi:10.4161/hv.20778.

121. Rezaei, T.; Khalili, S.; Baradaran, B.; Mosafer, J.; Rezaei, S.; Mokhtarzadeh, A.; de la Guardia, M. Recent advances on HIV DNA vaccines development: Stepwise

improvements to clinical trials. *Journal of Controlled Release* **2019**, *316*, 116–137, doi:10.1016/j.jconrel.2019.10.045.

122. Mu, Z.; Haynes, B. F.; Cain, D. W. HIV mRNA Vaccines—Progress and Future Paths. *Vaccines* **2021**, *9*, 134, doi:10.3390/vaccines9020134.

123. Derking, R.; Sanders, R. W. Structure-guided envelope trimer design in HIV-1 vaccine development: a narrative review. *Journal of the International AIDS Society* **2021**, *24*, 25797, doi:10.1002/jia2.25797.

124. Bontempo, A.; Garcia, M. M.; Rivera, N.; Cayabyab, M. J. A Systematic Approach to HIV-1 Vaccine Immunogen Selection. *AIDS Research and Human Retroviruses* **2020**, *36*, 762–770, doi:10.1089/aid.2019.0239.

125. Chen, C.-W.; Saubi, N.; Joseph-Munné, J. Design Concepts of Virus-Like Particle-Based HIV-1 Vaccines. *Frontiers in Immunology* **2020**, *11*, 1–8, doi:10.3389/fimmu.2020.573157.

126. Rerks-Ngarm, S.; Pitisuttithum, P.; Nitayaphan, S.; Kaewkungwal, J.; Chiu, J.; Paris, R.; Premsri, N.; Namwat, C.; de Souza, M.; Adams, E.*; et al.* Vaccination with ALVAC and AIDSVAX to Prevent HIV-1 Infection in Thailand. *New England Journal of Medicine* **2009**, *361*, 2209–2220, doi:10.1056/NEJMoa0908492.

127. Pitisuttithum, P.; Rerks-Ngarm, S.; Bussaratid, V.; Dhitavat, J.; Maekanantawat, W.; Pungpak, S.; Suntharasamai, P.; Vanijanonta, S.; Nitayapan, S.; Kaewkungwal, J.*; et al.* Safety and Reactogenicity of Canarypox ALVAC-HIV (vCP1521) and HIV-1 gp120 AIDSVAX B/E Vaccination in an Efficacy Trial in Thailand. *PLoS ONE* **2011**, *6*, e27837, doi:10.1371/journal.pone.0027837.

128. Rerks-Ngarm, S.; Pitisuttithum, P.; Excler, J.-L.; Nitayaphan, S.; Kaewkungwal, J.; Premsri, N.; Kunasol, P.; Karasavvas, N.; Schuetz, A.; Ngauy, V.*; et al.* Randomized, Double-Blind Evaluation of Late Boost Strategies for HIV-Uninfected Vaccine Recipients in the RV144 HIV Vaccine Efficacy Trial. *The Journal of Infectious Diseases* **2017**, *215*, 1255–1263, doi:10.1093/infdis/jix099.

129. Pitisuttithum, P.; Nitayaphan, S.; Chariyalertsak, S.; Kaewkungwal, J.; Dawson, P.; Dhitavat, J.; Phonrat, B.; Akapirat, S.; Karasavvas, N.; Wieczorek, L.*; et al.* Late boosting of the RV144 regimen with AIDSVAX B/E and ALVAC-HIV in HIV-uninfected Thai volunteers: a double-blind, randomised controlled trial. *The Lancet HIV* **2020**, *7*, e238-e248, doi:10.1016/S2352-3018(19)30406-0.

130. Gray, G. E.; Bekker, L.-G.; Laher, F.; Malahleha, M.; Allen, M.; Moodie, Z.; Grunenberg, N.; Huang, Y.; Grove, D.; Prigmore, B.*; et al.* Vaccine Efficacy of ALVAC-HIV and Bivalent Subtype C gp120–MF59 in Adults. *New England Journal of Medicine* **2021**, *384*, 1089–1100, doi:10.1056/NEJMoa2031499.

131. Baden, L. R.; Stieh, D. J.; Sarnecki, M.; Walsh, S. R.; Tomaras, G. D.; Kublin, J. G.; McElrath, M. J.; Alter, G.; Ferrari, G.; Montefiori, D.*; et al.* Safety and immunogenicity of two heterologous HIV vaccine regimens in healthy, HIV-uninfected adults (TRAVERSE): a randomised, parallel-group, placebo-controlled, double-blind, phase 1/2a study. *The Lancet HIV* **2020**, *7*, e688-e698, doi:10.1016/S2352-3018(20)30229-0.

132. *Johnson & Johnson and Global Partners Announce Results from Phase 2b Imbokodo HIV Vaccine Clinical Trial in Young Women in Sub-Saharan Africa.* Available online: https://www.jnj.com/johnson-johnson-and-global-partners-announce-results-from-phase-2b-imbokodo-hiv-vaccine-clinical-trial-in-young-women-in-sub-saharan-africa (accessed on 21 February 2023).

133. *Janssen and Global Partners to Discontinue Phase 3 Mosaico HIV Vaccine Clinical Trial.* Available online: https://www.jnj.com/janssen-and-global-partners-to-discontinue-phase-3-mosaico-hiv-vaccine-clinical-trial (accessed on 21 February 2023).

134. Hogan, M. J.; Pardi, N. mRNA Vaccines in the COVID-19 Pandemic and Beyond. *Annual Review of Medicine* **2022**, *73*, 17–39, doi:10.1146/annurev-med-042420-112725.

135. Pardi, N.; Labranche, C. C.; Ferrari, G.; Cain, D. W.; Tombácz, I.; Parks, R. J.; Muramatsu, H.; Mui, B. L.; Tam, Y. K.; Karikó, K.*; et al.* Characterization of HIV-

1 Nucleoside-Modified mRNA Vaccines in Rabbits and Rhesus Macaques. *Molecular Therapy - Nucleic Acids* **2019**, *15*, 36–47, doi:10.1016/j.omtn.2019.03.003.

136. Moyo, N.; Vogel, A. B.; Buus, S.; Erbar, S.; Wee, E. G.; Sahin, U.; Hanke, T. Efficient Induction of T Cells against Conserved HIV-1 Regions by Mosaic Vaccines Delivered as Self-Amplifying mRNA. *Molecular Therapy - Methods and Clinical Development* **2019**, *12*, 32–46, doi:10.1016/j.omtm.2018.10.010.

137. Zhang, P.; Narayanan, E.; Liu, Q.; Tsybovsky, Y.; Boswell, K.; Ding, S.; Hu, Z.; Follmann, D.; Lin, Y.; Miao, H.*; et al.* A multiclade env–gag VLP mRNA vaccine elicits tier-2 HIV-1-neutralizing antibodies and reduces the risk of heterologous SHIV infection in macaques. *Nature Medicine* **2021**, *27*, 2234–2245, doi:10.1038/s41591-021-01574-5.

138. Zhao, C.; Ao, Z.; Yao, X. Current Advances in Virus-Like Particles as a Vaccination Approach against HIV Infection. *Vaccines* **2016**, *4*, 2, doi:10.3390/vaccines4010002.

139. Bachmann, M. F.; Hoffmann Rohrer, U.; Kündig, T. M.; Bürki, K.; Hengartner, H.; Zinkernagel, R. M. The Influence of Antigen Organization on B Cell Responsiveness. *Science* **1993**, *262*, 1448–1451, doi:10.1126/science.8248784.

140. McBurney, S. P.; Young, K. R.; Ross, T. M. Membrane embedded HIV-1 envelope on the surface of a virus-like particle elicits broader immune responses than soluble envelopes. *Virology* **2007**, *358*, 334–346, doi:10.1016/j.virol.2006.08.032.

141. Chua, A. J.; Vituret, C.; Tan, M. L.; Gonzalez, G.; Boulanger, P.; Ng, M.-L.; Hong, S.-S. A novel platform for virus-like particle-display of flaviviral envelope domain III: induction of Dengue and West Nile virus neutralizing antibodies. *Virology Journal* **2013**, *10*, 129, doi:10.1186/1743-422X-10-129.

142. Fontana, D.; Garay, E.; Cervera, L.; Kratje, R.; Prieto, C.; Gòdia, F. Chimeric VLPs Based on HIV-1 Gag and a Fusion Rabies Glycoprotein Induce Specific

Antibodies against Rabies and Foot-and-Mouth Disease Virus. *Vaccines* **2021**, *9*, 251, doi:10.3390/vaccines9030251.

143. Boix-Besora, A.; Lorenzo, E.; Lavado-García, J.; Gòdia, F.; Cervera, L. Optimization, Production, Purification and Characterization of HIV-1 GAG-Based Virus-like Particles Functionalized with SARS-CoV-2. *Vaccines* **2022**, *10*, 250, doi:10.3390/vaccines10020250.

144. Martins, S. A.; Santos, J.; Silva, R. D. M.; Rosa, C.; Cabo Verde, S.; Correia, J. D. G.; Melo, R. How promising are HIV-1-based virus-like particles for medical applications. *Frontiers in Cellular and Infection Microbiology* **2022**, *12*, doi:10.3389/fcimb.2022.997875.

145. Nooraei, S.; Bahrulolum, H.; Hoseini, Z. S.; Katalani, C.; Hajizade, A.; Easton, A. J.; Ahmadian, G. Virus-like particles: preparation, immunogenicity and their roles as nanovaccines and drug nanocarriers. *Journal of Nanobiotechnology* **2021**, *19*, 59, doi:10.1186/s12951-021-00806-7.

146. Kirnbauer, R.; Booy, F.; Cheng, N.; Lowy, D. R.; Schiller, J. T. Papillomavirus L1 major capsid protein self-assembles into virus-like particles that are highly immunogenic. *Proceedings of the National Academy of Sciences* **1992**, *89*, 12180–12184, doi:10.1073/pnas.89.24.12180.

147. Noad, R.; Roy, P. Virus-like particles as immunogens. *Trends in Microbiology* **2003**, *11*, 438–444, doi:10.1016/S0966-842X(03)00208-7.

148. Thrane, S.; Aves, K.-L.; Uddbäck, I. E. M.; Janitzek, C. M.; Han, J.; Yang, Y. R.; Ward, A. B.; Theander, T. G.; Nielsen, M. A.; Salanti, A.*; et al.* A Vaccine Displaying a Trimeric Influenza-A HA Stem Protein on Capsid-Like Particles Elicits Potent and Long-Lasting Protection in Mice. *Vaccines* **2020**, *8*, doi:10.3390/vaccines8030389.

149. Andersson, A.-M.; Schwerdtfeger, M.; Holst, P. Virus-Like-Vaccines against HIV. *Vaccines* **2018**, *6*, 10, doi:10.3390/vaccines6010010.

150. Tong, T.; Crooks, E. T.; Osawa, K.; Binley, J. M. HIV-1 Virus-Like Particles Bearing Pure Env Trimers Expose Neutralizing Epitopes but Occlude Nonneutralizing Epitopes. *Journal of Virology* **2012**, *86*, 3574–3587, doi:10.1128/JVI.06938-11.

151. Stano, A.; Leaman, D. P.; Kim, A. S.; Zhang, L.; Autin, L.; Ingale, J.; Gift, S. K.; Truong, J.; Wyatt, R. T.; Olson, A. J.*; et al.* Dense Array of Spikes on HIV-1 Virion Particles. *Journal of Virology* **2017**, *91*, doi:10.1128/JVI.00415-17.

152. Zhu, P.; Liu, J.; Bess, J.; Chertova, E.; Lifson, J. D.; Grisé, H.; Ofek, G. A.; Taylor, K. A.; Roux, K. H. Distribution and three-dimensional structure of AIDS virus envelope spikes. *Nature* **2006**, *441*, 847–852, doi:10.1038/nature04817.

153. Burnie, J.; Guzzo, C. The incorporation of host proteins into the external HIV-1 envelope. *Viruses* **2019**, *11*, 1–25, doi:10.3390/v11010085.

154. Martin, S. J.; Vyakarnam, A.; Cheingsong-Popov, R.; Callow, D.; Jones, K. L.; Senior, J. M.; Adams, S. E.; Kingsman, A. J.; Matear, P.; Gotch, F. M. Immunization of human HIV-seronegative volunteers with recombinant p17/p24:Ty virus-like particles elicits HIV-1 p24-specific cellular and humoral immune responses. *AIDS* **1993**, *7*, 1315–1323.

155. Weber, J.; Cheinsong-Popov, R.; Callow, D.; Adams, S.; Patou, G.; Hodgkin, K.; Martin, S.; Gotch, F.; Kingsman, A. Immunogenicity of the yeast recombinant p17 p24:Ty virus-like particles (p24-VLP) in healthy volunteers. *Vaccine* **1995**, *13*, 831–834, doi:10.1016/0264-410X(94)00061-Q.

156. Buonaguro, L.; Visciano, M. L.; Tornesello, M. L.; Tagliamonte, M.; Biryahwaho, B.; Buonaguro, F. M. Induction of Systemic and Mucosal Cross-Clade Neutralizing Antibodies in BALB/c Mice Immunized with Human Immunodeficiency Virus Type 1 Clade A Virus-Like Particles Administered by Different Routes of Inoculation. *Journal of Virology* **2005**, *79*, 7059–7067, doi:10.1128/JVI.79.11.7059-7067.2005.

157. Crooks, E. T.; Tong, T.; Chakrabarti, B.; Narayan, K.; Georgiev, I. S.; Menis, S.; Huang, X.; Kulp, D.; Osawa, K.; Muranaka, J.*; et al.* Vaccine-Elicited Tier 2 HIV-1 Neutralizing Antibodies Bind to Quaternary Epitopes Involving Glycan-Deficient Patches Proximal to the CD4 Binding Site. *PLoS Pathogens* **2015**, *11*, e1004932, doi:10.1371/journal.ppat.1004932.

158. Chang, M. O.; Suzuki, T.; Suzuki, H.; Takaku, H. HIV-1 Gag-Virus-Like Particles Induce Natural Killer Cell Immune Responses via Activation and Maturation of Dendritic Cells. *Journal of Innate Immunity* **2012**, *4*, 187–200, doi:10.1159/000329226.

159. Gonelli, C. A.; King, H. A. D.; Mackenzie, C.; Sonza, S.; Center, R. J.; Purcell, D. F. J. Immunogenicity of HIV-1-Based Virus-Like Particles with Increased Incorporation and Stability of Membrane-Bound Env. *Vaccines* **2021**, *9*, 239, doi:10.3390/vaccines9030239.

160. Walsh, G. Biopharmaceutical benchmarks 2018. *Nature Biotechnology* **2018**, *36*, 1136–1145, doi:10.1038/nbt.4305.

161. Walsh, G.; Walsh, E. Biopharmaceutical benchmarks 2022. *Nature Biotechnology* **2022**, *40*, 1722–1760, doi:10.1038/s41587-022-01582-x.

162. Berg, K.; Schäfer, V. N.; Tschorn, N.; Stitz, J.; Zielonka, S.; Krah, S. Advanced Establishment of Stable Recombinant Human Suspension Cell Lines Using Genotype–Phenotype Coupling Transposon Vectors. *Methods in Molecular Biology* **2020**, *2070*, doi:10.1007/978-1-4939-9853-1_20.

163. Baldi, L.; Hacker, D. L.; Adam, M.; Wurm, F. M. Recombinant protein production by large-scale transient gene expression in mammalian cells: state of the art and future perspectives. *Biotechnology Letters* **2007**, *29*, 677–684, doi:10.1007/s10529-006-9297-y.

164. Tschorn, N.; Berg, K.; Stitz, J. Transposon vector-mediated stable gene transfer for the accelerated establishment of recombinant mammalian cell pools allowing for

high-yield production of biologics. *Biotechnology Letters* **2020**, *42*, 1103–1112, doi:10.1007/s10529-020-02889-y.

165. Chen, Z.-Y.; He, C.-Y.; Ehrhardt, A.; Kay, M. A. Minicircle DNA vectors devoid of bacterial DNA result in persistent and high-level transgene expression in vivo. *Molecular Therapy* **2003**, *8*, 495–500, doi:10.1016/s1525-0016(03)00168-0.

166. Schmieder, V.; Fieder, J.; Drerup, R.; Gutierrez, E. A.; Guelch, C.; Stolzenberger, J.; Stumbaum, M.; Mueller, V. S.; Higel, F.; Bergbauer, M.*; et al.* Towards maximum acceleration of monoclonal antibody development: Leveraging transposase-mediated cell line generation to enable GMP manufacturing within 3 months using a stable pool. *Journal of Biotechnology* **2022**, *349*, 53–64, doi:10.1016/j.jbiotec.2022.03.010.

167. Ivics, Z.; Hackett, P. B.; Plasterk, R. H.; Izsvák, Z. Molecular Reconstruction of Sleeping Beauty, a Tc1-like Transposon from Fish, and Its Transposition in Human Cells. *Cell* **1997**, *91*, 501–510, doi:10.1016/S0092-8674(00)80436-5.

168. Koga, A.; Suzuki, M.; Inagaki, H.; Bessho, Y.; Hori, H. Transposable element in fish. *Nature* **1996**, *383*, 30, doi:10.1038/383030a0.

169. Fraser, M. J.; Clszczon, T.; Elick, T.; Bauser, C. Precise excision of TTAA-specific lepidopteran transposons piggyBac (IFP2) and tagalong (TFP3) from the baculovirus genome in cell lines from two species of Lepidoptera. *Insect Molecular Biology* **1996**, *5*, 141–151, doi:10.1111/j.1365-2583.1996.tb00048.x.

170. Yusa, K.; Zhou, L.; Li, M. A.; Bradley, A.; Craig, N. L. A hyperactive piggyBac transposase for mammalian applications. *Proceedings of the National Academy of Sciences* **2011**, *108*, 1531–1536, doi:10.1073/pnas.1008322108.

171. Wen, W.; Song, S.; Han, Y.; Chen, H.; Liu, X.; Qian, Q. An efficient Screening System in Yeast to Select a Hyperactive piggyBac Transposase for Mammalian Applications. *International Journal of Molecular Sciences* **2020**, *21*, 3064, doi:10.3390/ijms21093064.

172. Cadiñanos, J.; Bradley, A. Generation of an inducible and optimized piggyBac transposon system. *Nucleic Acids Research* **2007**, *35*, e87, doi:10.1093/nar/gkm446.

173. Voigt, F.; Wiedemann, L.; Zuliani, C.; Querques, I.; Sebe, A.; Mátés, L.; Izsvák, Z.; Ivics, Z.; Barabas, O. Sleeping Beauty transposase structure allows rational design of hyperactive variants for genetic engineering. *Nature Communications* **2016**, *7*, doi:10.1038/ncomms11126.

174. Mátés, L.; Chuah, M. K. L.; Belay, E.; Jerchow, B.; Manoj, N.; Acosta-Sanchez, A.; Grzela, D. P.; Schmitt, A.; Becker, K.; Matrai, J.*; et al.* Molecular evolution of a novel hyperactive Sleeping Beauty transposase enables robust stable gene transfer in vertebrates. *Nature Genetics* **2009**, *41*, 753–761, doi:10.1038/ng.343.

175. Grabundzija, I.; Irgang, M.; Mátés, L.; Belay, E.; Matrai, J.; Gogol-Döring, A.; Kawakami, K.; Chen, W.; Ruiz, P.; Chuah, M. K.*; et al.* Comparative analysis of transposable element vector systems in human cells. *Molecular Therapy* **2010**, *18*, 1200–1209, doi:10.1038/mt.2010.47.

176. Ding, S.; Wu, X.; Li, G.; Han, M.; Zhuang, Y.; Xu, T. Efficient Transposition of the piggyBac (PB) Transposon in Mammalian Cells and Mice. *Cell* **2005**, *122*, 473–483, doi:10.1016/j.cell.2005.07.013.

177. Sandoval-Villegas, N.; Nurieva, W.; Amberger, M.; Ivics, Z. Contemporary Transposon Tools: A Review and Guide through Mechanisms and Applications of Sleeping Beauty, piggyBac and Tol2 for Genome Engineering. *International Journal of Molecular Sciences* **2021**, *22*, 5084, doi:10.3390/ijms22105084.

178. Lynch, A. G.; Tanzer, F.; Fraser, M. J.; Shephard, E. G.; Williamson, A.-L.; Rybicki, E. P. Use of the piggyBac transposon to create HIV-1 gag transgenic insect cell lines for continuous VLP production. *BMC Biotechnology* **2010**, *10*, 30, doi:10.1186/1472-6750-10-30.

179. Johnson, E. T.; Dowd, P. F. A non-autonomous insect piggyBac transposable element is mobile in tobacco. *Mol. Genet. Genomics* **2014**, *289*, 895–902, doi:10.1007/s00438-014-0860-2.

180. Wilson, M. H.; Coates, C. J.; George, A. L. PiggyBac transposon-mediated gene transfer in human cells. *Molecular Therapy* **2007**, *15*, 139–145, doi:10.1038/sj.mt.6300028.

181. WHO. *HIV/AIDS*, 2021. Available online: https://www.who.int/news-room/fact-sheets/detail/hiv-aids (accessed on 20 February 2023).

182. Ng'uni, T.; Chasara, C.; Ndhlovu, Z. M. Major Scientific Hurdles in HIV Vaccine Development: Historical Perspective and Future Directions. *Frontiers in Immunology* **2020**, *11*, doi:10.3389/fimmu.2020.590780.

183. Korber, B. T.; Letvin, N. L.; Haynes, B. F. T-Cell Vaccine Strategies for Human Immunodeficiency Virus, the Virus with a Thousand Faces. *Journal of Virology* **2009**, *83*, 8300–8314, doi:10.1128/JVI.00114-09.

184. Bellier, B.; Dalba, C.; Clerc, B.; Desjardins, D.; Drury, R.; Cosset, F.-L.; Collins, M.; Klatzmann, D. DNA vaccines encoding retrovirus-based virus-like particles induce efficient immune responses without adjuvant. *Vaccine* **2006**, *24*, 2643–2655, doi:10.1016/j.vaccine.2005.11.034.

185. Goepfert, P. A.; Elizaga, M. L.; Seaton, K.; Tomaras, G. D.; Montefiori, D. C.; Sato, A.; Hural, J.; DeRosa, S. C.; Kalams, S. A.; McElrath, M. J.*; et al.* Specificity and 6-Month Durability of Immune Responses Induced by DNA and Recombinant Modified Vaccinia Ankara Vaccines Expressing HIV-1 Virus-Like Particles. *The Journal of Infectious Diseases* **2014**, *210*, 99–110, doi:10.1093/infdis/jiu003.

186. Perdiguero, B.; Sánchez-Corzo, C.; Sorzano, C.; Saiz, L.; Mediavilla, P.; Esteban, M.; Gómez, C. A Novel MVA-Based HIV Vaccine Candidate (MVA-gp145-GPN) Co-Expressing Clade C Membrane-Bound Trimeric gp145 Env and Gag-Induced Virus-Like Particles (VLPs) Triggered Broad and Multifunctional HIV-1-Specific T Cell and Antibody Responses. *Viruses* **2019**, *11*, 160, doi:10.3390/v11020160.

187. Rosengarten, J. F.; Schatz, S.; Stitz, J. Detection of Neutralization-sensitive Epitopes in Antigens Displayed on Virus-Like Particle (VLP)-Based Vaccines Using a Capture Assay. *Journal of Visualized Experiments* **2022**, *2022*, doi:10.3791/63137.

188. Rosengarten, J. F.; Schatz, S.; Wolf, T.; Barbe, S.; Stitz, J. Components of a HIV-1 vaccine mediate virus-like particle (VLP)-formation and display of envelope proteins exposing broadly neutralizing epitopes. *Virology* **2022**, *568*, 41–48, doi:10.1016/j.virol.2022.01.008.

189. Jaffray, A.; Shephard, E.; Van Harmelen, J.; Williamson, C.; Williamson, A.-L.; Rybicki, E. P. Human immunodeficiency virus type 1 subtype C Gag virus-like particle boost substantially improves the immune response to a subtype C gag DNA vaccine in mice. *Journal of General Virology* **2004**, *85*, 409–413, doi:10.1099/vir.0.19396-0.

190. Wright, E. R.; Schooler, J. B.; Ding, H. J.; Kieffer, C.; Fillmore, C.; Sundquist, W. I.; Jensen, G. J. Electron cryotomography of immature HIV-1 virions reveals the structure of the CA and SP1 Gag shells. *The EMBO Journal* **2007**, *26*, 2218–2226, doi:10.1038/sj.emboj.7601664.

191. Saha, I.; Saffarian, S. Dynamics of the HIV Gag Lattice Detected by Localization Correlation Analysis and Time-Lapse iPALM. *Biophysical Journal* **2020**, *119*, 581–592, doi:10.1016/j.bpj.2020.06.023.

192. Sanders, R. W.; Moore, J. P. Native-like Env trimers as a platform for HIV-1 vaccine design. *Immunological Reviews* **2017**, *275*, 161–182, doi:10.1111/imr.12481.

193. Sanders, R. W.; van Gils, M. J.; Derking, R.; Sok, D.; Ketas, T. J.; Burger, J. A.; Ozorowski, G.; Cupo, A.; Simonich, C.; Goo, L.*; et al.* HIV-1 neutralizing antibodies induced by native-like envelope trimers. *Science* **2015**, *349*, doi:10.1126/science.aac4223.

194. Buchacher, A.; Predl, R.; Strutzenberger, K.; Steinfelllner, W.; Trkola, A.; Purtscher, M.; Gruber, G.; Tauer, C.; Steindl, F.; Jungbauer, A.*; et al.* Generation of Human Monoclonal Antibodies against HIV-1 Proteins; Electrofusion and Epstein-Barr Virus Transformation for Peripheral Blood Lymphocyte Immortalization. *AIDS Research and Human Retroviruses* **1994**, *10*, 359–369, doi:10.1089/aid.1994.10.359.

195. Walker, L. M.; Phogat, S. K.; Chan-Hui, P.-Y.; Wagner, D.; Phung, P.; Goss, J. L.; Wrin, T.; Simek, M. D.; Fling, S.; Mitcham, J. L.*; et al.* Broad and Potent Neutralizing Antibodies from an African Donor Reveal a New HIV-1 Vaccine Target. *Science* **2009**, *326*, 285–289, doi:10.1126/science.1178746.

196. Davenport, T. M.; Friend, D.; Ellingson, K.; Xu, H.; Caldwell, Z.; Sellhorn, G.; Kraft, Z.; Strong, R. K.; Stamatatos, L. Binding Interactions between Soluble HIV Envelope Glycoproteins and Quaternary-Structure-Specific Monoclonal Antibodies PG9 and PG16. *Journal of Virology* **2011**, *85*, 7095–7107, doi:10.1128/JVI.00411-11.

197. McLellan, J. S.; Pancera, M.; Carrico, C.; Gorman, J.; Julien, J.-P.; Khayat, R.; Louder, R.; Pejchal, R.; Sastry, M.; Dai, K.*; et al.* Structure of HIV-1 gp120 V1/V2 domain with broadly neutralizing antibody PG9. *Nature* **2011**, *480*, 336–343, doi:10.1038/nature10696.

198. Gorny, M. K.; Conley, A. J.; Karwowska, S.; Buchbinder, A.; Xu, J. Y.; Emini, E. A.; Koenig, S.; Zolla-Pazner, S. Neutralization of diverse human immunodeficiency virus type 1 variants by an anti-V3 human monoclonal antibody. *Journal of Virology* **1992**, *66*, 7538–7542, doi:10.1128/jvi.66.12.7538-7542.1992.

199. Trkola, A.; Purtscher, M.; Muster, T.; Ballaun, C.; Buchacher, A.; Sullivan, N.; Srinivasan, K.; Sodroski, J.; Moore, J. P.; Katinger, H. Human monoclonal antibody 2G12 defines a distinctive neutralization epitope on the gp120 glycoprotein of human immunodeficiency virus type 1. *Journal of Virology* **1996**, *70*, 1100–1108, doi:10.1128/jvi.70.2.1100-1108.1996.

200. Scanlan, C. N.; Pantophlet, R.; Wormald, M. R.; Saphire, E. O.; Stanfield, R.; Wilson, I. A.; Katinger, H.; Dwek, R. A.; Rudd, P. M.; Burton, D. R. The Broadly Neutralizing Anti-Human Immunodeficiency Virus Type 1 Antibody 2G12 Recognizes a Cluster of α1→2 Mannose Residues on the Outer Face of gp120. *Journal of Virology* **2002**, *76*, 7306–7321, doi:10.1128/JVI.76.14.7306-7321.2002.

201. Yang, Z.; Dam, K.-M. A.; Bridges, M. D.; Hoffmann, M. A. G.; DeLaitsch, A. T.; Gristick, H. B.; Escolano, A.; Gautam, R.; Martin, M. A.; Nussenzweig, M. C.*; et al.* Neutralizing antibodies induced in immunized macaques recognize the CD4-binding site on an occluded-open HIV-1 envelope trimer. *Nature Communications* **2022**, *13*, 732, doi:10.1038/s41467-022-28424-3.

202. UCSF Chimera: An Extensible Molecular Modeling System. Available online: https://www.cgl.ucsf.edu/chimera/download.html (accessed on 5 February 2023).

203. Chapman, R.; Jongwe, T. I.; Douglass, N.; Chege, G.; Williamson, A.-L.; Wang, S. Heterologous prime-boost vaccination with DNA and MVA vaccines, expressing HIV-1 subtype C mosaic Gag virus-like particles, is highly immunogenic in mice. *PLoS ONE* **2017**, *12*, e0173352, doi:10.1371/journal.pone.0173352.

204. Hogan, M. J.; Conde-Motter, A.; Jordan, A. P.; Yang, L.; Cleveland, B.; Guo, W.; Romano, J.; Ni, H.; Pardi, N.; Labranche, C. C.*; et al.* Increased surface expression of HIV-1 envelope is associated with improved antibody response in vaccinia prime/protein boost immunization. *Virology* **2018**, *514*, 106–117, doi:10.1016/j.virol.2017.10.013.

205. Castillo-Menendez, L. R.; Witt, K.; Espy, N.; Princiotto, A.; Madani, N.; Pacheco, B.; Finzi, A.; Sodroski, J.; Silvestri, G. Comparison of Uncleaved and Mature Human Immunodeficiency Virus Membrane Envelope Glycoprotein Trimers. *Journal of Virology* **2018**, *92*, doi:10.1128/JVI.00277-18.

206. Moore, P. L.; Crooks, E. T.; Porter, L.; Zhu, P.; Cayanan, C. S.; Grise, H.; Corcoran, P.; Zwick, M. B.; Franti, M.; Morris, L.*; et al.* Nature of Nonfunctional Envelope Proteins on the Surface of Human Immunodeficiency Virus Type 1. *Journal of Virology* **2006**, *80*, 2515–2528, doi:10.1128/JVI.80.5.2515-2528.2006.

207. Li, Y.; O'Dell, S.; Wilson, R.; Wu, X.; Schmidt, S. D.; Hogerkorp, C.-M.; Louder, M. K.; Longo, N. S.; Poulsen, C.; Guenaga, J.*; et al.* HIV-1 Neutralizing Antibodies Display Dual Recognition of the Primary and Coreceptor Binding Sites and Preferential Binding to Fully Cleaved Envelope Glycoproteins. *Journal of Virology* **2012**, *86*, 11231–11241, doi:10.1128/JVI.01543-12.

208. Ringe, R. P.; Sanders, R. W.; Yasmeen, A.; Kim, H. J.; Lee, J. H.; Cupo, A.; Korzun, J.; Derking, R.; van Montfort, T.; Julien, J.-P.*; et al.* Cleavage strongly influences whether soluble HIV-1 envelope glycoprotein trimers adopt a native-like conformation. *Proceedings of the National Academy of Sciences* **2013**, *110*, 18256–18261, doi:10.1073/pnas.1314351110.

209. Lee, J. H.; Ozorowski, G.; Ward, A. B. Cryo-EM structure of a native, fully glycosylated, cleaved HIV-1 envelope trimer. *Science* **2016**, *351*, 1043–1048, doi:10.1126/science.aad2450.

210. Zhu, P.; Chertova, E.; Bess, J.; Lifson, J. D.; Arthur, L. O.; Liu, J.; Taylor, K. A.; Roux, K. H. Electron tomography analysis of envelope glycoprotein trimers on HIV and simian immunodeficiency virus virions. *Proceedings of the National Academy of Sciences* **2003**, *100*, 15812–15817, doi:10.1073/pnas.2634931100.

211. Harris, A.; Borgnia, M. J.; Shi, D.; Bartesaghi, A.; He, H.; Pejchal, R.; Kang, Y.; Depetris, R.; Marozsan, A. J.; Sanders, R. W.*; et al.* Trimeric HIV-1 glycoprotein gp140 immunogens and native HIV-1 envelope glycoproteins display the same closed and open quaternary molecular architectures. *Proceedings of the National Academy of Sciences* **2011**, *108*, 11440–11445, doi:10.1073/pnas.1101414108.

212. Frimpong, K.; Spector, S. A. Cotransduction of nondividing cells using lentiviral vectors. *Gene Therapy* **2000**, *7*, 1562–1569, doi:10.1038/sj.gt.3301283.

213. Abad, J. L.; Serrano, F.; San Román, A. L.; Delgado, R.; Bernad, A.; González, M. A. Single-step, multiple retroviral transduction of human T cells. *The Journal of Gene Medicine* **2002**, *4*, 27–37, doi:10.1002/jgm.242.

214. van Etten, B.; ten Hagen, T. L. M.; de Vries, M. R.; Ambagtsheer, G.; Huet, T.; Eggermont, A. M. M. Prerequisites for effective adenovirus mediated gene therapy of colorectal liver metastases in the rat using an intracellular neutralizing antibody fragment to p21-Ras. *British Journal of Cancer* **2002**, *86*, 436–442, doi:10.1038/sj.bjc.6600089.

215. Mei, L.; Jin, X.; Song, C.; Wang, M.; Levy, R. J. Immobilization of gene vectors on polyurethane surfaces using a monoclonal antibody for localized gene delivery. *The Journal of Gene Medicine* **2006**, *8*, 690–698, doi:10.1002/jgm.912.

216. Mitrofanova, E.; Unfer, R.; Vahanian, N.; Link, C. Rat sodium iodide symporter allows using lower dose of 131I for cancer therapy. *Gene Therapy* **2006**, *13*, 1052–1056, doi:10.1038/sj.gt.3302758.

217. A Study of Heterologous Vaccine Regimen of Adenovirus Serotype 26 Mosaic4 Human Immunodeficiency Virus(Ad26.Mos4.HIV), Adjuvanted Clade C gp140 and Mosaic gp140 to Prevent HIV-1 Infection Among Cis-gender Men and Transgender Individuals Who Have Sex With Cis-gender Men and/or Transgender Individuals (MOSAICO): NCT03964415. Available online: https://clinicaltrials.gov/ct2/show/NCT03964415 (accessed on 4 February 2023).

218. Ellenberger, D.; Wyatt, L.; Li, B.; Buge, S.; Lanier, N.; Rodriguez, I. V.; Sariol, C. A.; Martinez, M.; Monsour, M.; Vogt, J.*; et al.* Comparative immunogenicity in rhesus monkeys of multi-protein HIV-1 (CRF02_AG) DNA/MVA vaccines expressing mature and immature VLPs. *Virology* **2005**, *340*, 21–32, doi:10.1016/j.virol.2005.06.014.

219. Iyer, S. S.; Gangadhara, S.; Victor, B.; Shen, X.; Chen, X.; Nabi, R.; Kasturi, S. P.; Sabula, M. J.; Labranche, C. C.; Reddy, P. B. J.*; et al.* Virus-Like Particles Displaying Trimeric Simian Immunodeficiency Virus (SIV) Envelope gp160 Enhance the Breadth of DNA/Modified Vaccinia Virus Ankara SIV Vaccine-Induced Antibody Responses in Rhesus Macaques. *Journal of Virology* **2016**, *90*, 8842–8854, doi:10.1128/JVI.01163-16.

220. Desjardins, D.; Huret, C.; Dalba, C.; Kreppel, F.; Kochanek, S.; Cosset, F.-L.; Tangy, F.; Klatzmann, D.; Bellier, B. Recombinant retrovirus-like particle forming DNA vaccines in prime-boost immunization and their use for hepatitis C virus vaccine development. *The Journal of Gene Medicine* **2009**, *11*, 313–325, doi:10.1002/jgm.1307.

221. Tschorn, N.; van Heuvel, Y.; Stitz, J. Transgene Expression and Transposition Efficiency of Two-Component Sleeping Beauty Transposon Vector Systems Utilizing Plasmid or mRNA Encoding the Transposase. *Molecular Biotechnology* **2022**, doi:10.1007/s12033-022-00642-6.

222. Wilber, A.; Frandsen, J. L.; Geurts, J. L.; Largaespada, D. A.; Hackett, P. B.; McIvor, R. S. RNA as a source of transposase for Sleeping Beauty-mediated gene insertion and expression in somatic cells and tissues. *Molecular Therapy* **2006**, *13*, 625–630, doi:10.1016/j.ymthe.2005.10.014.

223. Bire, S.; Gosset, D.; Jégot, G.; Midoux, P.; Pichon, C.; Rouleux-Bonnin, F. Exogenous mRNA delivery and bioavailability in gene transfer mediated by piggyBac transposition. *BMC Biotechnology* **2013**, *13*, 75, doi:10.1186/1472-6750-13-75.

224. Helgers, H.; Hengelbrock, A.; Schmidt, A.; Rosengarten, J.; Stitz, J.; Strube, J. Process Design and Optimization towards Digital Twins for HIV-Gag VLP Production in HEK293 Cells, including Purification. *Processes* **2022**, *10*, 419, doi:10.3390/pr10020419.

225. Hengelbrock, A.; Helgers, H.; Schmidt, A.; Vetter, F. L.; Juckers, A.; Rosengarten, J. F.; Stitz, J.; Strube, J. Digital Twin for HIV-Gag VLP Production in HEK293 Cells. *Processes* **2022**, *10*, doi:10.3390/pr10050866.

226. Helgers, H.; Hengelbrock, A.; Rosengarten, J. F.; Stitz, J.; Schmidt, A.; Strube, J. Towards Autonomous Process Control—Digital Twin for HIV-Gag VLP Production in HEK293 Cells Using a Dynamic Metabolic Model. *Processes* **2022**, *10*, 2015, doi:10.3390/pr10102015.

227. Shapiro, S. Z. Clinical development of candidate HIV vaccines: different problems for different vaccines. *AIDS Research and Human Retroviruses* **2014**, *30*, 325–329, doi:10.1089/aid.2013.0114.

228. Fruth, U. Considerations regarding efficacy endpoints in HIV vaccine trials: executive summary and recommendations of an expert consultation jointly organized by WHO, UNAIDS and ANRS in support of the Global HIV Vaccine Enterprise. *Vaccine* **2009**, *27*, 1989–1996, doi:10.1016/j.vaccine.2008.12.029.

229. Mellors, J. W.; Rinaldo, C. R.; Gupta, P.; White, R. M.; Todd, J. A.; Kingsley, L. A. Prognosis in HIV-1 infection predicted by the quantity of virus in plasma. *Science* **1996**, *272*, 1167–1170, doi:10.1126/science.272.5265.1167.

230. Wolf, F. de; Spijkerman, I.; Schellekens, P. T.; Langendam, M.; Kuiken, C.; Bakker, M.; Roos, M.; Coutinho, R.; Miedema, F.; Goudsmit, J. AIDS prognosis based on HIV-1 RNA, CD4+ T-cell count and function: markers with reciprocal predictive value over time after seroconversion. *AIDS* **1997**, *11*, 1799–1806, doi:10.1097/00002030-199715000-00003.

231. Quinn, T. C.; Wawer, M. J.; Sewankambo, N.; Serwadda, D.; Li, C.; Wabwire-Mangen, F.; Meehan, M. O.; Lutalo, T.; Gray, R. H. Viral load and heterosexual transmission of human immunodeficiency virus type 1. Rakai Project Study Group. *New England Journal of Medicine* **2000**, *342*, 921–929, doi:10.1056/NEJM200003303421303.

232. Wolf, M. W.; Reichl, U. Downstream processing of cell culture-derived virus particles. *Expert Review of Vaccines* **2011**, *10*, 1451–1475, doi:10.1586/erv.11.111.

233. Cruz, P. E.; Peixoto, C. C.; Devos, K.; Moreira, J. L.; Saman, E.; Carrondo, M. J. Characterization and downstream processing of HIV-1 core and virus-like-particles produced in serum free medium. *Enzyme and Microbial Technology* **2000**, *26*, 61–70, doi:10.1016/S0141-0229(99)00128-3.

234. Théry, C.; Regnault, A.; Garin, J.; Wolfers, J.; Zitvogel, L.; Ricciardi-Castagnoli, P.; Raposo, G.; Amigorena, S. Molecular Characterization of Dendritic Cell-

Derived Exosomes. *Journal of Cell Biology* **1999**, *147*, 599–610, doi:10.1083/jcb.147.3.599.

235. Lavado-García, J.; González-Domínguez, I.; Cervera, L.; Jorge, I.; Vázquez, J.; Gòdia, F. Molecular Characterization of the Coproduced Extracellular Vesicles in HEK293 during Virus-Like Particle Production. *Journal of Proteome Research* **2020**, *19*, 4516–4532, doi:10.1021/acs.jproteome.0c00581.

236. Martin-Jaular, L.; Nevo, N.; Schessner, J. P.; Tkach, M.; Jouve, M.; Dingli, F.; Loew, D.; Witwer, K. W.; Ostrowski, M.; Borner, G. H. H.*; et al.* Unbiased proteomic profiling of host cell extracellular vesicle composition and dynamics upon HIV-1 infection. *The EMBO Journal* **2021**, *40*, e105492, doi:10.15252/embj.2020105492.

237. Wolf, T.; Rosengarten, J.; Härtel, I.; Stitz, J.; Barbe, S. A Hydrodynamic Approach to the Study of HIV Virus-Like Particle (VLP) Tangential Flow Filtration. *Membranes* **2022**, *12*, 1248, doi:10.3390/membranes12121248.

238. Moreira, A. S.; Cavaco, D. G.; Faria, T. Q.; Alves, P. M.; Carrondo, M. J. T.; Peixoto, C. Advances in Lentivirus Purification. *Biotechnology Journal* **2021**, *16*, e2000019, doi:10.1002/biot.202000019.

239. Negrete, A.; Pai, A.; Shiloach, J. Use of hollow fiber tangential flow filtration for the recovery and concentration of HIV virus-like particles produced in insect cells. *Journal of Virological Methods* **2014**, *195*, 240–246, doi:10.1016/j.jviromet.2013.10.017.

240. Valkama, A. J.; Oruetxebarria, I.; Lipponen, E. M.; Leinonen, H. M.; Käyhty, P.; Hynynen, H.; Turkki, V.; Malinen, J.; Miinalainen, T.; Heikura, T.*; et al.* Development of Large-Scale Downstream Processing for Lentiviral Vectors. *Molecular Therapy - Methods and Clinical Development* **2020**, *17*, 717–730, doi:10.1016/j.omtm.2020.03.025.

241. Gutiérrez-Granados, S.; Cervera, L.; Gòdia, F.; Carrillo, J.; Segura, M. M. Development and validation of a quantitation assay for fluorescently tagged HIV-1

virus-like particles. *Journal of Virological Methods* **2013**, *193*, 85–95, doi:10.1016/j.jviromet.2013.05.010.

242. Pereira Aguilar, P.; González-Domínguez, I.; Schneider, T. A.; Gòdia, F.; Cervera, L.; Jungbauer, A. At-line multi-angle light scattering detector for faster process development in enveloped virus-like particle purification. *Journal of Separation Science* **2019**, *42*, 2640–2649, doi:10.1002/jssc.201900441.

243. Katharina Helena Morawitz. Charakterisierung von Fluoreszenz-Fusionsproteinen: Bachelorarbeit; Technische Hochschule Köln, 2021.

244. Cervera, L.; Gutiérrez-Granados, S.; Martínez, M.; Blanco, J.; Gòdia, F.; Segura, M. M. Generation of HIV-1 Gag VLPs by transient transfection of HEK 293 suspension cell cultures using an optimized animal-derived component free medium. *Journal of Biotechnology* **2013**, *166*, 152–165, doi:10.1016/j.jbiotec.2013.05.001.

245. Fuenmayor, J.; Gòdia, F.; Cervera, L. Production of virus-like particles for vaccines. *New Biotechnology* **2017**, *39*, 174–180, doi:10.1016/j.nbt.2017.07.010.

246. González-Domínguez, I.; Puente-Massaguer, E.; Cervera, L.; Gòdia, F. Quality Assessment of Virus-Like Particles at Single Particle Level: A Comparative Study. *Viruses* **2020**, *12*, 223, doi:10.3390/v12020223.

247. Schneider, I. C.; Hartmann, J.; Braun, G.; Stitz, J.; Klamp, T.; Bihi, M.; Sahin, U.; Buchholz, C. J. Displaying Tetra-Membrane Spanning Claudins on Enveloped Virus-Like Particles for Cancer Immunotherapy. *Biotechnology Journal* **2018**, *13*, 1700345, doi:10.1002/biot.201700345.

248. Nikles, D.; Bach, P.; Boller, K.; Merten, C. A.; Montrasio, F.; Heppner, F. L.; Aguzzi, A.; Cichutek, K.; Kalinke, U.; Buchholz, C. J. Circumventing Tolerance to the Prion Protein (PrP): Vaccination with PrP-Displaying Retrovirus Particles Induces Humoral Immune Responses against the Native Form of Cellular PrP. *Journal of Virology* **2005**, *79*, 4033–4042, doi:10.1128/JVI.79.7.4033-4042.2005.

249. Montero, M.; Gulzar, N.; Klaric, K.-A.; Donald, J. E.; Lepik, C.; Wu, S.; Tsai, S.; Julien, J.-P.; Hessell, A. J.; Wang, S.*; et al.* Neutralizing epitopes in the membrane-proximal external region of HIV-1 gp41 are influenced by the transmembrane domain and the plasma membrane. *Journal of Virology* **2012**, *86*, 2930–2941, doi:10.1128/JVI.06349-11.

250. Bednarska, J.; Pelchen-Matthews, A.; Novak, P.; Burden, J. J.; Summers, P. A.; Kuimova, M. K.; Korchev, Y.; Marsh, M.; Shevchuk, A. Rapid formation of human immunodeficiency virus-like particles. *Proceedings of the National Academy of Sciences* **2020**, *117*, 21637–21646, doi:10.1073/pnas.2008156117.

251. *National Library of Medicine (US), National Center for Biotechnology Information; [1988]*. Available online: https://www.ncbi.nlm.nih.gov/ (accessed on 21 February 2023).

252. *Basic Local Alignment Search Tool (BLAST)*. Available online: https://blast.ncbi.nlm.nih.gov/Blast.cgi (accessed on 21 February 2023).

253. *Expert Protein Analysis System (Expasy)*. Available online: http://www.expasy.org (accessed on 21 February 2023).

254. Gasteiger, E. ExPASy: the proteomics server for in-depth protein knowledge and analysis. *Nucleic Acids Research* **2003**, *31*, 3784–3788, doi:10.1093/nar/gkg563.

255. *Snapgene software*. Available online: www.snapgene.com (accessed on 21 February 2023).

256. *Oligo Calculator version 3.27*. Available online: http://biotools.nubic.northwestern.edu/OligoCalc.html (accessed on 21 July 2023).

257. Schindelin, J.; Arganda-Carreras, I.; Frise, E.; Kaynig, V.; Longair, M.; Pietzsch, T.; Preibisch, S.; Rueden, C.; Saalfeld, S.; Schmid, B.*; et al.* Fiji: an open-source platform for biological-image analysis. *Nature Methods* **2012**, *9*, 676–682, doi:10.1038/nmeth.2019.

258. *Microsoft Excel*. Available online: https://office.microsoft.com/excel (accessed on 21 February 2023).

259. *Microsoft Word*. Available online: https://office.microsoft.com/word (accessed on 21 February 2023).

260. Citavi. Available online: https://www.citavi.com/de (accessed on 4 February 2023).

261. Berg, K.; Schäfer, V. N.; Bartnicki, N.; Eggenschwiler, R.; Cantz, T.; Stitz, J. Rapid establishment of stable retroviral packaging cells and recombinant susceptible target cell lines employing novel transposon vectors derived from Sleeping Beauty. *Virology* **2019**, *531*, 40–47, doi:10.1016/j.virol.2019.02.014.

262. Weltner, J.; Balboa, D.; Katayama, S.; Bespalov, M.; Krjutškov, K.; Jouhilahti, E.-M.; Trokovic, R.; Kere, J.; Otonkoski, T. Human pluripotent reprogramming with CRISPR activators. *Nature Communications* **2018**, *9*, 2643, doi:10.1038/s41467-018-05067-x.

263. Gibson, D. G.; Young, L.; Chuang, R.-Y.; Venter, J. C.; Hutchison, C. A.; Smith, H. O. Enzymatic assembly of DNA molecules up to several hundred kilobases. *Nature Methods* **2009**, *6*, 343–345, doi:10.1038/nmeth.1318.

264. Howarth, M.; Takao, K.; Hayashi, Y.; Ting, A. Y. Targeting quantum dots to surface proteins in living cells with biotin ligase. *Proceedings of the National Academy of Sciences* **2005**, *102*, 7583–7588, doi:10.1073/pnas.0503125102.

265. Liu, H.; Naismith, J. H. An efficient one-step site-directed deletion, insertion, single and multiple-site plasmid mutagenesis protocol. *BMC Biotechnology* **2008**, *8*, 91, doi:10.1186/1472-6750-8-91.

266. Protocol for preparation of chemically competent E. coli cells (rubidium chloride). Available online: http://coleman-lab.org/wp-content/uploads/2021/04/Preparation-of-chemically-competent-E.coli_.pdf (accessed on 4 February 2023).

267. Bertani, G. Studies on lysogenesis. I. The mode of phage liberation by lysogenic Escherichia coli. *Journal of Bacteriology* **1951**, 293–300, doi:10.1128/jb.62.3.293-300.1951.

268. Lynch, A.; Meyers, A. E.; Williamson, A.-L.; Rybicki, E. P. Stability studies of HIV-1 Pr55gag virus-like particles made in insect cells after storage in various formulation media. *Virology Journal* **2012**, *9*, 210, doi:10.1186/1743-422X-9-210.

269. Baden, L. R.; Karita, E.; Mutua, G.; Bekker, L.-G.; Gray, G.; Page-Shipp, L.; Walsh, S. R.; Nyombayire, J.; Anzala, O.; Roux, S.*; et al.* Assessment of the Safety and Immunogenicity of 2 Novel Vaccine Platforms for HIV-1 Prevention. *Annals of Internal Medicine* **2016**, *164*, 313, doi:10.7326/M15-0880.

270. Easterhoff, D.; Moody, M. A.; Fera, D.; Cheng, H.; Ackerman, M.; Wiehe, K.; Saunders, K. O.; Pollara, J.; Vandergrift, N.; Parks, R.*; et al.* Boosting of HIV envelope CD4 binding site antibodies with long variable heavy third complementarity determining region in the randomized double blind RV305 HIV-1 vaccine trial. *PLoS Pathogens* **2017**, *13*, e1006182, doi:10.1371/journal.ppat.1006182.

271. Rerks-Ngarm, S.; Paris, R. M.; Chunsutthiwat, S.; Premsri, N.; Namwat, C.; Bowonwatanuwong, C.; Li, S. S.; Kaewkungkal, J.; Trichavaroj, R.; Churikanont, N.*; et al.* Extended evaluation of the virologic, immunologic, and clinical course of volunteers who acquired HIV-1 infection in a phase III vaccine trial of ALVAC-HIV and AIDSVAX B/E. *Journal of Infectious Diseases* **2013**, *207*, 1195–1205, doi:10.1093/infdis/jis478.

272. Zhao, L. P.; Fiore-Gartland, A.; Carpp, L. N.; Cohen, K. W.; Rouphael, N.; Fleurs, L.; Dintwe, O.; Zhao, M.; Moodie, Z.; Fong, Y.*; et al.* Landscapes of binding antibody and T-cell responses to pox-protein HIV vaccines in Thais and South Africans. *PLoS ONE* **2020**, *15*, e0226803, doi:10.1371/journal.pone.0226803.

273. Lazarus, E. M.; Otwombe, K.; Adonis, T.; Sebastian, E.; Gray, G.; Grunenberg, N.; Roux, S.; Churchyard, G.; Innes, C.; Laher, F.*; et al.* Uptake of Genital Mucosal

Sampling in HVTN 097, a Phase 1b HIV Vaccine Trial in South Africa. *PLoS ONE* **2014**, *9*, e112303, doi:10.1371/journal.pone.0112303.

274. Bekker, L.-G.; Moodie, Z.; Grunenberg, N.; Laher, F.; Tomaras, G. D.; Cohen, K. W.; Allen, M.; Malahleha, M.; Mngadi, K.; Daniels, B.*; et al.* Subtype C ALVAC-HIV and bivalent subtype C gp120/MF59 HIV-1 vaccine in low-risk, HIV-uninfected, South African adults: a phase 1/2 trial. *The Lancet HIV* **2018**, *5*, e366-e378, doi:10.1016/S2352-3018(18)30071-7.

275. Laher, F.; Moodie, Z.; Cohen, K. W.; Grunenberg, N.; Bekker, L.-G.; Allen, M.; Frahm, N.; Yates, N. L.; Morris, L.; Malahleha, M.*; et al.* Safety and immune responses after a 12-month booster in healthy HIV-uninfected adults in HVTN 100 in South Africa: A randomized double-blind placebo-controlled trial of ALVAC-HIV (vCP2438) and bivalent subtype C gp120/MF59 vaccines. *PLoS medicine* **2020**, *17*, e1003038, doi:10.1371/journal.pmed.1003038.

276. Hanass-Hancock, J.; Carpenter, B.; Reddy, T.; Nzuza, A.; Gaffoor, Z.; Goga, A.; Andrasik, M. Participants' characteristics and motivations to screen for HIV vaccine and monoclonal antibody trials in KwaZulu-Natal, South Africa. *Trials* **2021**, *22*, 897, doi:10.1186/s13063-021-05792-7.

277. Barouch, D. H.; Tomaka, F. L.; Wegmann, F.; Stieh, D. J.; Alter, G.; Robb, M. L.; Michael, N. L.; Peter, L.; Nkolola, J. P.; Borducchi, E. N.*; et al.* Evaluation of a mosaic HIV-1 vaccine in a multicentre, randomised, double-blind, placebo-controlled, phase 1/2a clinical trial (APPROACH) and in rhesus monkeys (NHP 13-19). *The Lancet* **2018**, *392*, 232–243, doi:10.1016/S0140-6736(18)31364-3.

278. Moodie, Z.; Dintwe, O.; Sawant, S.; Grove, D.; Huang, Y.; Janes, H.; Heptinstall, J.; Omar, F. L.; Cohen, K.; Rosa, S. C. de*; et al.* Analysis of the HIV Vaccine Trials Network 702 Phase 2b-3 HIV-1 Vaccine Trial in South Africa Assessing RV144 Antibody and T-Cell Correlates of HIV-1 Acquisition Risk. *Journal of Infectious Diseases* **2022**, *226*, 246–257, doi:10.1093/infdis/jiac260.

279. Campion, S. L.; Brenna, E.; Thomson, E.; Fischer, W.; Ladell, K.; McLaren, J. E.; Price, D. A.; Frahm, N.; McElrath, J. M.; Cohen, K. W.*; et al.* Preexisting memory

CD4+ T cells contribute to the primary response in an HIV-1 vaccine trial. *Journal of Clinical Investigation* **2021**, *131*, doi:10.1172/JCI150823.

280. Shao, Y.; Li, T.; Wolf, H.; Liu, Y.; Wang, H.; Zhu, H.; Lv, W.; Lin, W.; Chen, J.; Liang, H.*; et al.* P14-15 LB. The safety and immunogenicity of HIV-1 vaccines based on DNA and replication competent vaccinia vector in phase I clinical trial. *Retrovirology* **2009**, *6*, P404, doi:10.1186/1742-4690-6-S3-P404.

281. Wolfe, L. S.; Smedley, J. G.; Bubna, N.; Hussain, A.; Harper, R.; Mostafa, S. Development of a platform-based approach for the clinical production of HIV gp120 envelope glycoprotein vaccine candidates. *Vaccine* **2021**, *39*, 3852–3861, doi:10.1016/j.vaccine.2021.05.073.

282. Kasturi, S. P.; Rasheed, M. A. U.; Havenar-Daughton, C.; Pham, M.; Legere, T.; Sher, Z. J.; Kovalenkov, Y.; Gumber, S.; Huang, J. Y.; Gottardo, R.*; et al.* 3M-052, a synthetic TLR-7/8 agonist, induces durable HIV-1 envelope–specific plasma cells and humoral immunity in nonhuman primates. *Science Immunology* **2020**, *5*, doi:10.1126/sciimmunol.abb1025.

283. Chimukuche, R. S.; Kawuma, R.; Mahapa, N.; Mkhwanazi, S.; Singh, N.; Siva, S.; Ruzagira, E.; Seeley, J. Examining oral pre-exposure prophylaxis (PrEP) literacy among participants in an HIV vaccine trial preparedness cohort study. *BMC Health Serv. Res.* **2022**, *22*, 1336, doi:10.1186/s12913-022-08730-8.

13. Acknowledgments

Some time has passed since I began the study of biology in my native town Cologne. After living in different cities, visiting different schools and universities, I have met numerous people of which some have become true and beloved friends. Now, here comes my chance to thank them officially for the support during this time.

First, I want to express my deepest gratitude to my mentor Prof. Dr. Jörn Stitz for giving me the opportunity to conduct my research studies in his laboratory. I am very thankful for the constructive supervision of my project and his untiring efforts to provide his students a pleasant working atmosphere. My motivation was strongly encouraged by his faith in me and his support to realize my scientific ideas independently. This gave me the chance to mature as a person and as a scientist in an environment that provided fun at work.

My special thanks go to Prof. Dr. Thomas Scheper, Prof. Dr. Cornelia Lee-Thedieck and apl. Prof. Dr. Sascha Beutel from the Leibniz University for agreeing to supervise me during my cooperative doctorate, the great support as well as for reading and evaluating my thesis.

I also thank the collaborators of the Sartorius AG for the scientific exchange during my project and for giving me the opportunity to participate in a practical training to gain insights into the large-scale VLP downstream bioprocessing. Many thanks go to Prof. Dr.-Ing. Jochen Strube and his working group from the TU Clausthal for upscaling experiments.

I am thankful for the excellent sample preparation and technical support by Beatrix Martiny, Dr. Christian Jüngst and Dr. Astrid Schauss at the CECAD Cologne Imaging Facility that enabled the microscopic-analysis of virus-like particles and cells.

I'd like to give my cordial thanks to my lab colleagues Natalie, Stefanie and Yasemin for technical and emotional support during my PhD project. I really enjoyed the time and our teamwork in the lab.

To all my friends I want to express my most heartfelt thanks. Thank you for the long-lasting friendships and for doing numerous fun activities over the past years. All of you have enriched my life in a certain way.

The person, who has influenced my life probably the most, is David. Thank you, for your unconditional support. I appreciate your confidence in me and your endless humor, which sweetens the good times and makes the challenging times more manageable. I am looking forward to our future as a little family.

My heartfelt thanks go to my mother, who passed away much too early. Your unconditional support made me to the person I am.

Finally, I´d like to mention all feline friends I was lucky to have as a cuddle companion during this time †Toni, †Beebo and †Pum Pum.

14. Curriculum Vitae

Education

2020 - 2023	Cooperative doctorate in biology at the Cologne University of Applied Sciences and the Gottfried Wilhelm Leibniz University Hannover
2018 - 2019	Training in a patent law firm (without a degree)
2015 - 2018	Doctorate in chemistry at the Heinrich Heine University Düsseldorf (without a degree)
2015	Master thesis at the Radboud University Nimwegen
2013 - 2015	Master studies in microbiology at the Rhenish Friedrich Wilhelm University of Bonn
2010 - 2013	Bachelor studies in biology at the University of Cologne
2010	High-school diploma

15.   List of Publications

Jamila Franca Rosengarten (70 %); Stefanie Schatz; Tobias Wolf; Stephan Barbe; Jörn Stitz. Components of a HIV-1 vaccine mediate virus-like particle (VLP)-formation and display of envelope proteins exposing broadly neutralizing epitopes. *Virology* **2022** *568*, p. 41–48. doi: 10.1016/j.virol.2022.01.008.

Jamila Franca Rosengarten (47.5 %)*; Stefanie Schatz*; Jörn Stitz. Detection of Neutralization-sensitive Epitopes in Antigens Displayed on Virus-Like Particle (VLP)-Based Vaccines Using a Capture Assay. *Journal of Visualized Experiments* **2022** *180*. doi: 10.3791/63137.

Yasemin van Heuvel; Stefanie Schatz; **Jamila Franca Rosengarten (12.5 %)**; Jörn Stitz. Infectious RNA: Human Immunodeficiency Virus (HIV) Biology, Therapeutic Intervention, and the Quest for a Vaccine. *Toxins* **2022** *14,* 2, p. 138. doi: 10.3390/toxins14020138.

Tobias Wolf; **Jamila Rosengarten (10 %)**; Ina Härtel; Jörn Stitz; Stéphan Barbe. A Hydrodynamic Approach to the Study of HIV Virus-Like Particle (VLP) Tangential Flow Filtration. *Membranes* **2022** *12*, 12, p. 1248. https://doi.org/10.3390/membranes12121248.

Heribert Helgers; Alina Hengelbrock; Axel Schmidt; **Jamila Rosengarten (5 %)**; Jörn Stitz; Jochen Strube. Process Design and Optimization towards Digital Twins for HIV-Gag VLP Production in HEK293 Cells, including Purification. *Processes* **2022** *10*, 2, p. 419. https://doi.org/10.3390/pr10020419.

Alina Hengelbrock; Heribert Helgers; Axel Schmidt; Florian Lukas Vetter; Alex Juckers; **Jamila Franca Rosengarten (5 %)**; Jörn Stitz; Jochen Strube. Digital Twin for HIV-Gag VLP Production in HEK293 Cells. *Processes* **2022** *10*, 5. https://doi.org/10.3390/pr10050866.

Heribert Helgers; Alina Hengelbrock; **Jamila Franca Rosengarten (5 %)**; Jörn Stitz; Axel Schmidt; Jochen Strube. Towards Autonomous Process Control-Digital Twin for HIV-Gag VLP Production in HEK293 Cells Using a Dynamic Metabolic Model. *Processes* **2022** *10*, 10, p. 2015. https://doi.org/10.3390/pr10102015.

*Shared first authorship: Conceptualization, methodology, formal analysis, data curation, writing – original draft, preparation, visualization.